



TECHNICKÁ UNIVERZITA V LIBERCI
Fakulta strojní



Experimental Investigations of Fans for Personal Protective Equipment

Diplomová práce

Studijní program: N2301 – Mechanical Engineering
Studijní obor: 2302T010 – Machines and Equipment Design
Autor práce: **Gafaru Moro**
Vedoucí práce: doc. Ing. Václav Dvořák, Ph.D.





TECHNICAL UNIVERSITY OF LIBEREC
Faculty of Mechanical Engineering ■

Experimental Investigations of Fans for Personal Protective Equipment

Master thesis

Study programme: N2301 – Mechanical Engineering
Study branch: 2302T010 – Machines and Equipment Design
Author: **Gafaru Moro**
Supervisor: doc. Ing. Václav Dvořák, Ph.D.





Zadání diplomové práce

Experimental Investigations of Fans for Personal Protective Equipment

Jméno a příjmení: **Gafaru Moro**
Osobní číslo: S17000374
Studijní program: N2301 Mechanical Engineering
Studijní obor: Machines and Equipment Design
Zadávající katedra: Department of Power Engineering Equipment
Akademický rok: **2018/2019**

Zásady pro vypracování:

1. Perform a literature search on ventilators, fan design methods, methodologies of static pressure measurement and mass flow measurement.
2. Design a test stand for experimental investigation of fans in the laboratories.
3. Measure the fan characteristics of at least 20 wheels (mass flow dependence on the backpressure) for different fan motor speed.
4. Calculate flow through the fan and compare various wheels, use dimensionless numbers.
5. Analyse results, compare different wheels, compare results with 1D theory.
6. Formulate the conclusions.
7. In the list of used literature, specify at least 10 sources.

Rozsah grafických prací: 10 stran
Rozsah pracovní zprávy: 50 stran
Forma zpracování práce: printed
Jazyk zpracování práce: English



Seznam odborné literatury:

[1] BLAIER, Frank P. *Fan Handbook: Selection, Application and Design* McGraw-Hill Education. 1998. ISBN 978-0070059337.

[2] GINGERY, David J. *How To Design & Build Centrifugal Fans For the Home Shop*. David J. Gibgery publishing, LLC, 1987, ISBN 978-1-878087-40-9.

Vedoucí práce: doc. Ing. Václav Dvořák, Ph.D.
Department of Power Engineering Equipment
Datum zadání práce: 1 November 2018
Předpokládaný termín odevzdání: 30 April 2020


prof. Dr. Ing. Petr Lenfeld
Dean

Liberec 1 February 2019




doc. Ing. Václav Dvořák, Ph.D.
Head of Department

Declaration

I hereby certify I have been informed that my master thesis is fully governed by Act No. 121/2000 Coll., the Copyright Act, in particular Article 60 – School Work.

I acknowledge that the Technical University of Liberec (TUL) does not infringe my copyrights by using my master thesis for the TUL's internal purposes.

I am aware of my obligation to inform the TUL on having used or granted license to use the results of my master thesis; in such a case the TUL may require reimbursement of the costs incurred for creating the result up to their actual amount.

I have written my master thesis myself using the literature listed below and consulting it with my thesis supervisor and my tutor.

At the same time, I honestly declare that the texts of the printed version of my master thesis and of the electronic version uploaded into the IS STAG are identical.

29. 4. 2019


Gafaru Moro

Abstract

The need to meet certain specified requirements of fan operation has resulted in many researchers in the field of fan design to explore different design methods. This work focuses on the investigation of different fan design parameters that affect the performance of fans used in powered air-purifying respirator type. To ascertain the performance of fans in practical situations, a fan test stand was designed and manufactured. The test stand was used to experimentally measure aerodynamic parameters of the fan which include backpressure, and mass flow rate. Furthermore, experimental results were compared with theoretical 1-D model formulated by Euler, however, with losses accounted for. The parameters that were considered were mainly focused on the design of impellers with straight blades and backward curved blades. The effects of the design parameters on fan performance including blade inlet and outlet angles, blade number, rotation speed of fan, roughness of blades, and mutual position of impellers and shaft are discussed. Comparisons of performance curves using dimensionless quantities revealed that an increase in the outlet blade angle from 20° to 50° resulted in higher flow. Optimum number of blade required for this design was also investigated for impellers with 8, 12 and 16 number of blades. The effect of blade roughness, and improper assembly due to mutual position of impeller and shaft had little effect on performance. The fan operating point was observed at pressure and flow coefficients of 0.35 and 0.12, respectively when the fan was tested with a combined ABEP-R filter. In addition, impellers with backward curved blades were modified to have short blades, high number of blades, and varying blade pitch angles. The effects of these modifications on fan performance are discussed.

Keywords: Air-purifying respirator, dimensionless quantities, Backpressure, test stand

Acknowledgment

First of all, I am very grateful to my supervisor Ing. Václav Dvořák of the Department of Power Engineering Equipment at Technical University of Liberec for his support and patience throughout this thesis work. His guidance and advice pointed me to the right direction when I seemed lost. I would also like to say a big thanks to my Ing. Jan Kracík, and Anas Elbarghthi for assisting me with acquisition of experimental data and result analysis. I am also grateful to the Fan Department of ZVVZ group for taking their time off their busy schedules to assist me with my research on fan laboratory set-up. Ms. Myka Mae Campo Duran, your support on the laboratory test stand model is much appreciated.

I wish to extend my gratitude to Ministries of Youth and Sport of the Czech Republic, and committees involved in the selection process for the Czech Government Scholarship for giving me the opportunity to further my education. I am indebted to your investment.

In Ghana, I wish to thank Dr. Elsie Effah Kaufmann for keeping me motivated and helping me shape my educational life. And finally, I would like to thank my family, especially my grandmother, for always keeping me inspired. I dedicate this work to my mother Ramatu Moro, your prayers keeps moving me above greater heights. To all those who were supportive during my study but whose names were not mentioned, I want you to know that your efforts are much appreciated and your kindness will forever be remembered.

Table of Contents

1	Introduction	11
2	Literature Review	12
2.1	Ventilation System	12
2.1.1	Classification of Ventilation Systems	13
2.2	Fan Design Considerations	15
2.2.1	Fan Types	15
2.2.2	System Resistance and Fan Performance	16
2.2.3	Pressure and Shaft Power	17
2.2.4	Efficiency	18
2.3	One-dimensional Analysis of Centrifugal Fan	19
2.3.1	Derivation of Euler Equation	19
2.4	Centrifugal Fan Design Considerations	22
2.4.1	Impeller Design Considerations	23
2.4.2	Fan Casing Design Considerations	25
2.4.3	Motor Design Considerations	26
2.5	Measurement of Aerodynamic Parameters	27
2.5.1	Static Pressure Measurement	27
2.5.2	Methodologies of Mass Flow Measurement	29
3	Test Stand Design	37
3.1	Details of Design	37
3.1.1	Fan Attachment Section	37
3.1.2	Upstream and Downstream Duct	37
3.1.3	Test Section	37
3.1.4	Backpressure Control	38
3.2	Proposed Design	38
3.3	Design Evaluation	39
4	Experimental Setup	44
4.1	Set-up Description	44
4.2	Experimented Impellers	44

4.2.1	Impellers without Modification	45
4.2.2	Modified Impellers with Backward Curved Blades.....	48
4.3	Representation of Results.....	51
5	Analytical solution – One dimensional	53
5.1	Deviation from the Linear Relation	53
5.1.1	Inter-Blade Circulation Loss.....	53
5.1.2	Impeller Loss	54
5.1.3	Outlet Pressure Loss	54
5.1.4	Inlet Loss.....	56
5.1.5	Internal Volumetric Leakage	57
6	Results and Discussion	59
6.1	Manufactured Parts and Assembly.....	59
6.2	Experimental and Analytical Results	62
6.2.1	Results for Testing of Test Stand and Fan.....	62
6.2.2	Results for Impellers with Straights Blades.....	66
6.2.3	Results for Impellers with Backward Curved Blades.....	70
6.2.4	Results for Modified Backward Curved Impellers	74
7	Conclusion.....	78
8	Reference.....	80

Nomenclature

A	Cross-sectional area	$[m^2]$
c	Fan absolute velocity	$[m/s]$
C	Coefficient of discharge	[1]
C_p	Constant pressure specific heat capacity	$[J/kg/K]$
d	Inner diameter of orifice	$[m]$
D	Inner diameter of pipe	$[m]$
e, E	Orifice plate thickness	$[m]$
k	Pressure loss coefficient	[1]
l_s	Orifice depth	$[m]$
l_1, l_2	Pressure tapping space	$[m^2]$
q_m	Mass flow rate	$[kg/s]$
p	Pressure	$[Pa]$
p_v	Dynamic pressure	$[Pa]$
$p_{th\infty}$	Theoretical pressure	$[Pa]$
Q_L	Leakage volume flow	$[m^3/s]$
r	Effective radius	$[m]$
R_a	Surface roughness	$[\mu m]$
Re	Reynolds number	[1]
T	Temperature	$[K]$
u	Fan peripheral speed	$[m/s]$
v	Velocity	$[m/s]$
w	Fan relative velocity	$[m/s]$
W	Work	$[J]$
y	Impeller position on shaft	$[mm]$
z	Number of blades	[1]
α	Orifice plate bevel angle	$[^\circ]$
β	Orifice to pipe diameter ratio	[1]

β_1	Blade inlet angle	[°]
β_2	Blade outlet angle	[°]
β_s	Swirl angle	[°]
ε	Expansibility factor	[1]
λ	Friction coefficient	[1]
ρ	Density	[kg/m ³]
τ_w	Shear stress on wall	[Pa]
φ	Flow coefficient	[1]
ψ	Pressure coefficient	[1]
ω	Angular velocity	[rev/min]

Subscript

$()_a$	Test stand upstream conditions
$()_b$	Test stand downstream conditions
$()_c$	Inter-blade circulation loss conditions
$()_{imp}$	Impeller loss conditions
$()_{in}$	Inlet loss conditions
$()_{out}$	Outlet loss conditions
$()_s$	Static conditions
$()_T$	Total conditions
$()_v$	Dynamic conditions
$()_1$	Fan inlet conditions
$()_2$	Fan outlet conditions
$()_{atm}$	Atmospheric conditions

Superscript

$()'$	Slip component
-------	----------------

1 Introduction

Mechanical Ventilators employ the use of fans and blowers to replace contaminated air with fresh air, and therefore, minimize the buildup of substances that contaminate the air such as smoke, flammable vapour and foul air in a closed space or building. For industrial applications, controlling contaminants and ensuring the safety of the workers may require the use of personal protective equipment such as face mask respirators if general purpose ventilators are insufficient to provide good indoor air quality. For proper functioning of respirators such as the powered-air-purifying respirators, it is necessary to identify the right design methods as well as ensure that components such as fans and filters meet their application requirements. Filters play a very significant role in ensuring quality indoor air by removing particles that pollute the air before it is supplied. However, they are not discussed in this work. It is required that fans such as centrifugal fans used in ventilation systems, operate at specific conditions for proper movement of contaminated air through filters.

However, it is almost impossible to design a fan that meets design requirements by mere calculations. Hence, experimental and numerical 3-D analyses are usually employed by researchers and designers for fan design. Researchers and designers make use of fan test stands in order to experimentally analyse the performance of fans. Therefore, designing a fan test stand will aid in measuring the main parameters for fan air movement such as static pressure and mass flow rate. Consequently, this will lead to designing fans that meet their application requirements, and hence ensuring that fans produced are economical and reliable. In addition, workers are guaranteed the comfort, and are protected from respiratory related problems that arise from improperly designed respirator systems.

2 Literature Review

2.1 Ventilation System

Ventilation is the supply of fresh air to a given space in order to prevent the buildup of air pollutants. Air pollutants may contain hazardous substances such as smoke, flammable vapour, foul air and dust that can cause diseases that are usually related to respiratory infections [1], [2]. For industrial application, ventilation systems are used for steady supply of fresh air that is circulated within the working space in order to remove unpleasant air [3]. Even with ventilation systems, the air pollutants within the working environment cannot be entirely removed but can be minimized to a harmless level [4]. Generally, the performance of ventilators is assessed based on the ability to remove pollutants to an acceptable level. Therefore, it is critical to examine the components of ventilation systems based on how effective their role is to remove air pollutants from the work place environment.

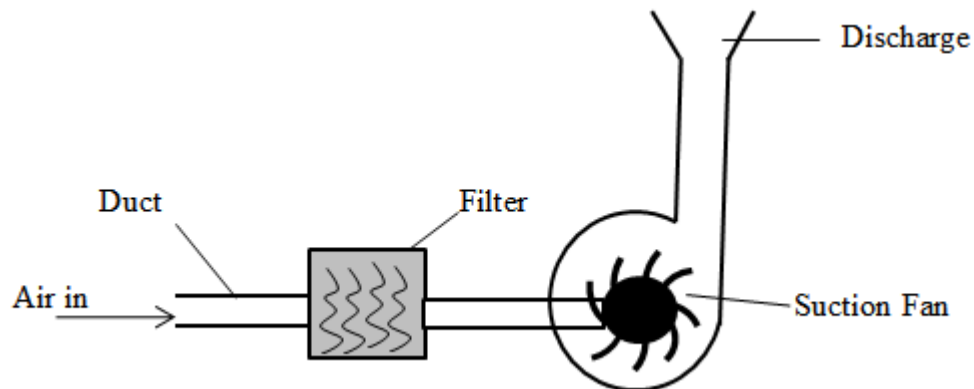


Figure 2.1: Schematic of air-purifying ventilator system.

Components such as fans and filters are very important in ensuring clean air environment. Filters ensure the adequate supply of indoor air quality for users in a building by removing particles that pollute the air before air is inhaled. Fans on the other hand ensure that the right volume of air is transported in the ducts in direct air supply or air exhaust systems. The movement of air with the aid of fan in ventilation systems is due to the pressure rise between the fan inlet and outlet vent. A schematic of a simple air supply ventilation system is shown in Figure 2.1 above.

2.1.1 Classification of Ventilation Systems

The need to ensure the effective reduction of substances that contaminates the air in homes and industries have resulted in the various designs of ventilation systems. Ventilation systems may be broadly classified into two main types; Natural and Mechanical Ventilation. Natural ventilation is characterized by air movement without fans, and hence, relies on the temperature difference between two media, and wind to enhance air movement [5]. In fact, if there is no temperature difference between the two media, the wind will serve as the only driving force for ventilation. However, when these two phenomena are not enough to circulate air, mechanical ventilation is employed. Mechanical Ventilation is characterized by the use of powered fans or blowers to provide fresh air in a given space. In addition, Mechanical Ventilators are designed to provide a continuous supply of fresh air, minimize the occurrence of fire outbreak, maintain temperature and humidity as well as reduce airborne contaminants.

Mechanical ventilators that are used in the industries may be classified into two main types; supply ventilation system and exhaust ventilation system [2]. The supply system ensures that contamination-free air is supplied to the working area. The temperature of the supplied air is usually maintained to a specific range in order to provide comfort in the ventilated space. The supply system is usually designed to have components such as air filters, ducts temperature regulation mechanisms.

On the other hand, exhaust system is designed purposely for the removal of contaminant from the work space. Based on the process of removal of contaminants, the local exhaust ventilation system may be divided into general exhaust system and local exhaust system [5]. The general exhaust system can be used in different modes such as temperature regulation mode and dilution mode. For ventilation systems working in temperature regulation mode, the air is heated and supplied. For dilution mode, the outdoor is used to dilute the contaminated air in order to reduce its concentration to an acceptable level, after which it is discharged into the atmosphere. Local exhaust system operate such that the exhaust is positioned near the source where contaminants are generated. This system usually has smaller air flow through hence the cost for heating the air is lesser compared with general exhaust systems.

However, if these engineering systems are ineffective in controlling contaminants and ensuring the safety of workers, personal protective equipment may be the only solution. Generally, respirators are classified into two types, air-purifying respirator which functions is to protect the user by filtering particles that pollute the air before it is inhaled, and air-supplying respirator which is aimed at supplying the user with contamination-free air from another source.

Air-purifying respirators, depending on the application, are designed to either function without a power source or with a power source. For non-powered air-purifying ventilators, contaminated air is breathed through filters. However, the powered air-purifying respirator supplies air by forcing contaminated air through a filtering mechanism. The filtering mechanism employed in this type of respirator is similar to negative-pressure respirators [6]. These filters are usually assembled with the fan. The fan is powered by a battery pack motor that is usually mounted on a belt pack. This orientation might change depending on the design of the air-purifying ventilation system or the application.

The main advantage of the air-pressure respirator is that it puts the face piece under positive pressure so that any leakage is outward from the face-piece [7]. Also, it ensures the safety of workers by filtering contaminated air before it is inhaled. However, one major setback that arises from the use of air-respirators, is the inability to produce and supply oxygen, therefore, making their use in oxygen deficient spaces impossible.

For proper functioning of air-purifying respirators, it is necessary to identify the right design methods as well as ensure that components such as fans and filters meet the application requirements. For instance, the flow rate of the air from the fan is significant in ensuring the effectiveness of air filtering. Richardson et al. [8], in their work, identified the relationship between air flow rate and particle penetration through filters. It was observed that high airflow rate leads to an increase in the penetration of particles through respirators. Therefore, it is ideal to select the right working flow rate in order to ensure that the wearer of the respirator is not exposed to health hazards.

2.2 Fan Design Considerations

2.2.1 Fan Types

Fans play an important role in ensuring the proper functioning of powered air-purifying respirators. There are different types of fans used in ventilation systems. Tito Mwinka [9] in his paper, stated that most commonly used fans in ventilation systems can be grouped into two categories; axial and centrifugal fan. An Axial fan is characterized by airflow within the fan impeller parallel to the fan shaft. They are usually preferred in application where low pressure and high volume flow are required. Axial fans may be grouped into: the propeller fan type, two-stage axial-flow fan, tube axial fans, and vane axial fans [10].

Generally, Centrifugal fans are characterized by trapping of air in vanes of the impeller or the rotor and subsequent throwing of air radially due to centrifugal force. They are usually employed in applications where there is the need for the fan to generate high pressure flow. Based on the blade geometry, centrifugal fans can be grouped into three types; radial, forward curved and backward curved fans. These classifications are based on the outlet blade angle, β_2 , that is, the angle the blade makes with the tangential to the outlet radius as shown in Figure 2.2 below.

Radial fans are fans having their blade tips or even whole blades to be radial. They operate under very high pressure compared with forward curved blades. They are used in industrial application where large particles of gas solids are required. Forward curved blades are relatively large number of shallow blades curved forward in the direction of rotation. They operate at a relatively moderate pressure compared with the radial fan, and it is characterised by a higher efficiency than radial fans. It is usually used in clean dust air systems. Also, the power rises continuously for a wide volume flow rate. For backward curved blades, the blades are curved backward to the direction of fan rotation. It is characterised by moderate volume flow, moderate pressure and high efficiency. In fact, amongst the three types of the centrifugal fan blades discussed, backward curved blades have the highest efficiency. Also a discontinuous rise in power is observed at high volume flow rate.

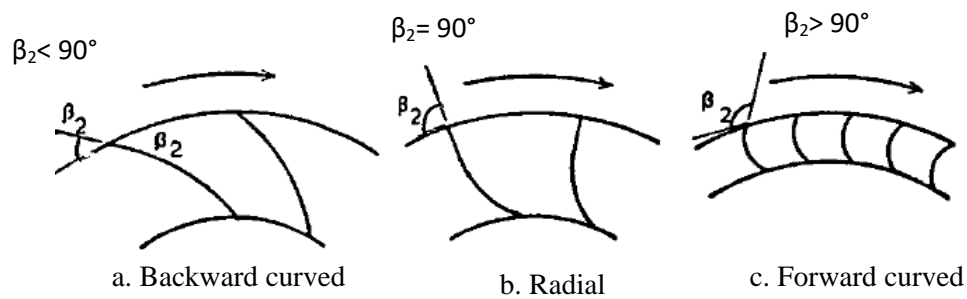


Figure 2.2: Centrifugal fan blade forms.

D. J. Gingery [11] in his book, concluded that the best choice of fan operating in a duct air system is centrifugal fans due to its ability to generate pressure. For the purpose of this work, centrifugal fans are considered.

2.2.2 System Resistance and Fan Performance

Fans operate such that the energy received by its rotating shaft is transmitted to air as a result of blade movements. This pressure enables the fan to develop pressure that moves gases against some resistance. Usually, these resistances affect the static pressure of the gas or air, and are caused by components in the fan system such as ducts, elbows and dampers. The variations in static pressure p_s , depend on the volume flow rate, Q , of air moving through the system such that the volume of air discharged across an orifice is proportional to the square root of pressure drop [12], that is, $\Delta p_s \propto Q^2$.

Figure 2.3 below, shows that the relationship between pressure and volume flow rate of fan operating in a system with some resistance. This is very significant in fan design because the air flow due to the fan operation can be determined, however, the system resistance must be computed first. Consideration of requirements from client and manufacturer during fan design is important to achieving the right fan design for a specific application. It is beneficial to consider the fan curves during fan design in order to obtain optimum performance. Fan curves demonstrate how fans operate under certain specified conditions.

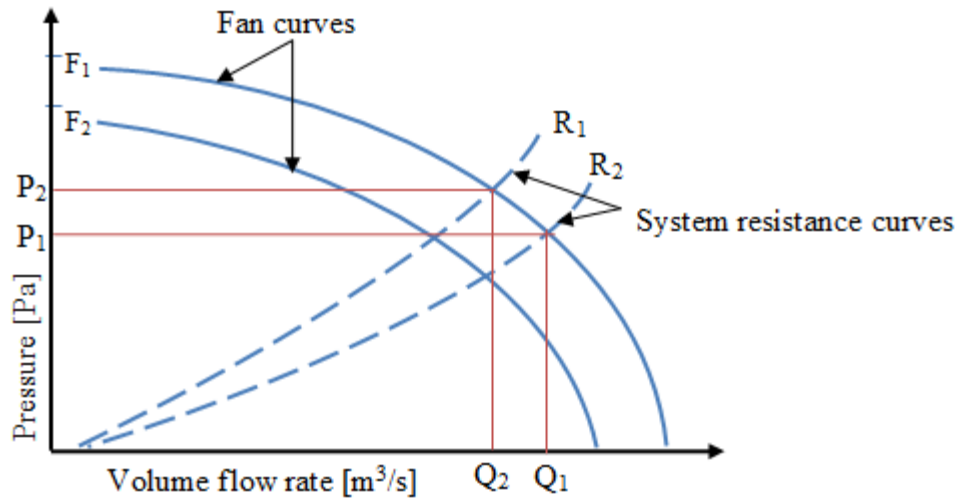


Figure 2.3: Effects of system characteristics on fan performance [13].

The resistance under which fans operate determines the operating point on a fan performance curve. From Figure 2.3 above, if the fan is operating at F_1 , it will operate along the F_1 performance curve. Therefore, system resistance curve, R_1 , means the fan operates at flow, Q_2 , against pressure P_2 . For centrifugal fans the various constructions of the fan blades affects the power of the fan at the expense of the flow rate.

2.2.3 Pressure and Shaft Power

In designing of centrifugal fans, care must be taken to regions below and higher than design points. For backward-curved fans, the design and off-design points have the most stable operation conditions. In addition, the power requirement for backward curved fans will decrease at higher flow rate regimes, usually above design point. However, there is continuous rise in power for both radial and forward curved blades. This is demonstrated in Figure 2.4 below.

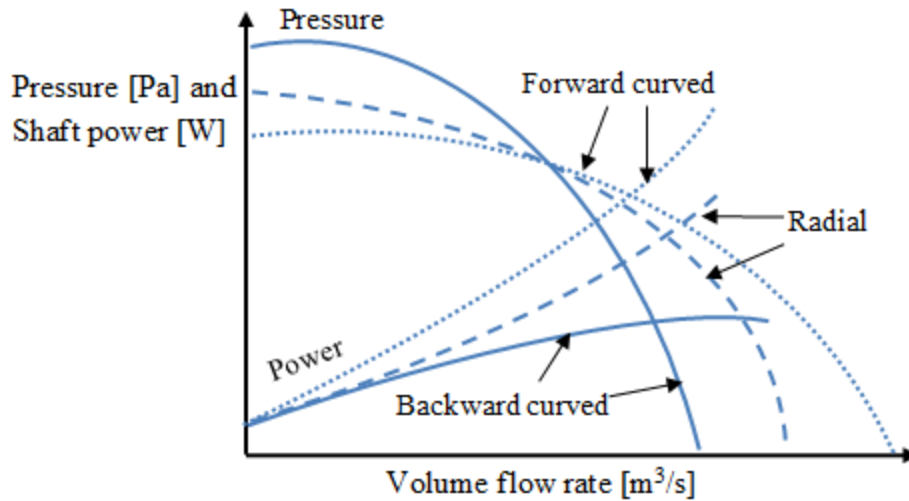


Figure 2.4: Comparing the types of centrifugal fans based on pressure and shaft power [12].

2.2.4 Efficiency

The type of blade construction affects the efficiency of centrifugal fans. In Figure 2.5 below, it can be observed that as flow rate increases, the efficiency of all the type of fans increases to peak efficiency and they begin to decrease with flow rate. Forward curved blades have the least efficiency. Radial and Forward curved blades, compared with backward curved fans, are less efficient because of continuous increase in power as flow rate increase. This is demonstrated in Figure 2.4. Also, because their power rises continuously with flow, they are characterised by higher operative cost irrespective of their low start-up cost [13]. Peak efficiencies of radial blades are relatively lower than backward curved blade [14].

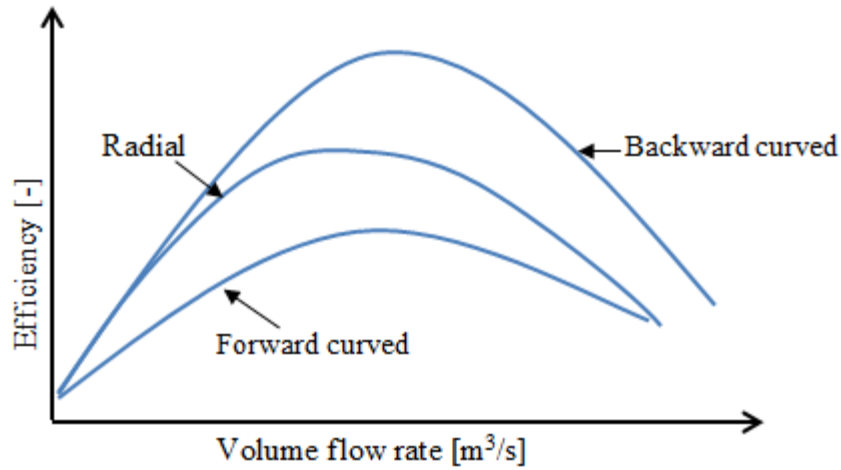


Figure 2.5: Efficiency of centrifugal fans [13].

2.3 One-dimensional Analysis of Centrifugal Fan

2.3.1 Derivation of Euler Equation

Considering the velocity triangle in Figure 2.6 below demonstrating a flow path by a selected blade, the relationship between the peripheral speeds u_1 and u_2 , relative velocities of the fluid relative to the blade w_1 and w_2 , and the absolute velocities c_1 and c_2 can be expressed in terms of the pressure generated by the fan. From Figure 2.6 below, the following deductions can be made;

The mass flow rate at the inlet of the impeller eye is equal to the mass flow rate leaving the outlet of the impeller.

From Continuity equation,

$$d\dot{m}_1 = d\dot{m}_2 = d\dot{m} = d\dot{V}\rho, \quad (2.1)$$

where $d\dot{V}$ is the elementary volumetric flow rate.

The moment of momentum equation can also be derived in terms of the components of the absolute velocities and the radius. This is given as;

$$d\dot{m}_2 c_{2u} r_2 = d\dot{m}_2 c_{2u} r_2 = dM, \quad (2.2)$$

Expressing in terms of elementary power dP

$$\rho d\dot{V} \omega c_{2u} r_2 = \rho d\dot{V} \omega c_{1u} r_1 = dM\omega = dP, \quad (2.3)$$

Assuming an incompressible fluid, the total power of a fan can be expressed as:

$$P = \Delta p \dot{V}, \quad (2.4)$$

where Δp is the transport fan pressure.

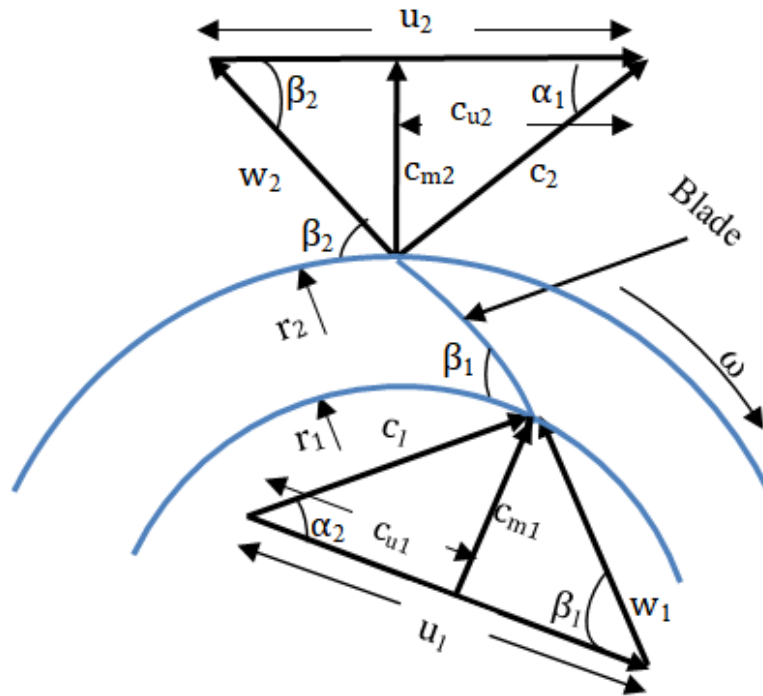


Figure 2.6: Velocity diagram for centrifugal fan

By comparing equation (2.3) and equation (2.4) the moment of momentum is modified as:

$$\rho \dot{V} c_{2u} u_2 = \rho \dot{V} c_{1u} u_1 = \Delta p \dot{V}, \quad (2.5)$$

By considering that the impeller consists of infinite number of blades, the Euler equation for theoretical transport pressure for centrifugal fan can be expressed as:

$$\Delta P_{th} = \rho (c_{2u} u_2 - c_{1u} u_1). \quad (2.6)$$

Considering the trigonometric dependencies, the Euler equation for fan in equation (2.6) can be modified by expressing the relative velocity in terms of trigonometry relations.

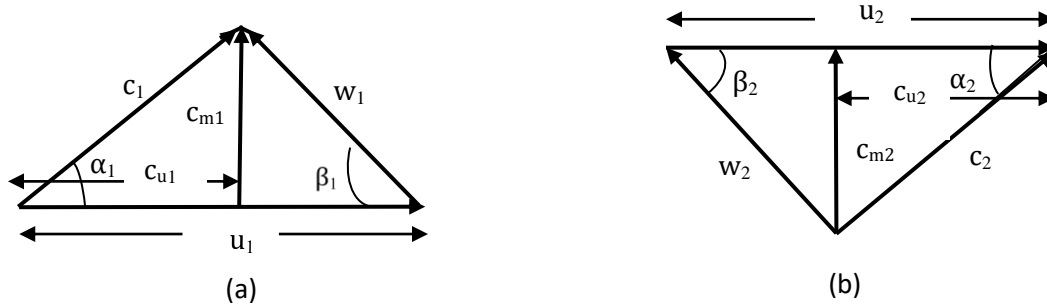


Figure 2.7: (a) Velocity triangle at fan inlet, (b) Velocity triangle at fan outlet

By expressing the relative, absolute and blade velocity in terms of cosine gives;

The outlet relative velocity;

$$w_2^2 = u_2^2 + c_2^2 - 2u_2c_2 \cos \alpha_2, \quad (2.7)$$

whiles the inlet relative velocity becomes;

$$w_1^2 = u_1^2 + c_1^2 - 2u_1c_1 \cos \alpha_1 \quad (2.8)$$

The product on the right hand side can be adjusted as

$$c_2 \cos \alpha_2 = c_{2u} \quad (2.9)$$

$$c_1 \cos \alpha_1 = c_{1u} \quad (2.10)$$

By substituting the relations in equation (2.7) and (2.8) into equation (2.6) results into the new Euler equation for centrifugal fans which can be derived as;

$$P_{th\infty} = \frac{\rho}{2} [(c_2^2 - c_1^2) + (w_1^2 - w_2^2) + (u_2^2 - u_1^2)] \quad (2.11)$$

For radial impellers, $c_{1u} = 0$, since $\alpha_1 = 90^\circ$.

Work transported by the impeller to the fluid can be calculated from the equation below

$$W_{\infty} = \frac{\Delta p_{th\infty}}{\rho} = u_2 c_{2u} \quad (2.12)$$

$$W_{\infty} = \frac{\Delta p_{th\infty}}{\rho} = u_2 \left(1 - \frac{c_{2m}}{u_2} \cot g \beta_2 \right) \quad (2.13)$$

The increase in pressure inside the impellers is given by the theoretical Euler line equation;

$$\Delta p_{th\infty} = \rho \frac{u_2^2}{2} \left(1 - \left(\frac{c_{2m}}{u_2} \cot g \beta_2 \right)^2 \right), \quad (2.14)$$

where c_{m2} can be obtained from the relation below

$$Q = \pi d_1 b_1 c_{m1} = \pi d_2 b_2 c_{m2} \quad (2.15)$$

The resulting equation gives the linear relations for radial curved, backward curved and forward curved fans represented in Figure 2.8 below.

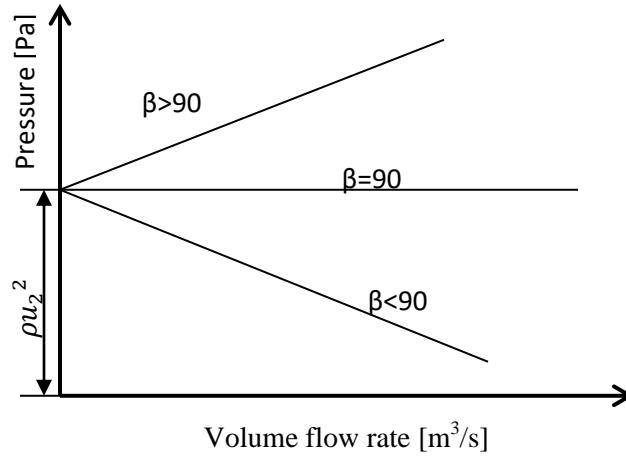


Figure 2.8: Ideal case.

2.4 Centrifugal Fan Design Considerations

Fans move air in sufficient quantity to significant design factor. They are designed to supply air to a space by using the kinetic energy of its impeller to move volume of air against the resistance within the system in which they operate [15]. Therefore, it is important to design fans to move sufficient volume of air at optimum pressure in order to overcome resistance within the duct system [14]. In the designing of fans, it is necessary to identify various features of the fan that

have a direct effect on fan efficiency, performance and noise. The considerations for the design of fan can be grouped into three: the impeller design considerations, fan casing design considerations, and the fan motor considerations [9]. For the impeller design, parameters such as impeller width, blade number and blade diameter, eye diameter, inlet and outlet blade angles are assessed. These parameters are known to affect performance and energy consumptions of turbomachines [16]. Parameters such as cut-off clearance, case dimensions and cut-off radius are also considered for fan casing design. For the motor design, the speeds of rotation of the shaft as well as impeller positioning on shaft dimensions are discussed.

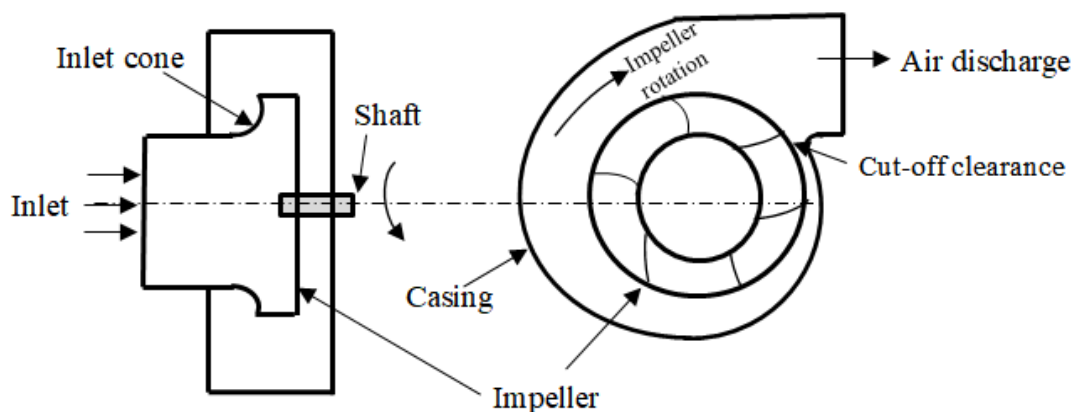


Figure 2.9: Schematic diagram of centrifugal fan.

2.4.1 Impeller Design Considerations

2.4.1.1 Inlet and Outlet Blade Angle

The design of centrifugal fans for a practical application is quite difficult than just for analysis purposes, especially the impeller. For a more efficient fan, the blade angle chosen for the blade construction must ensure less flow separation throughout the entire area of the impeller. To enhance laminar flow during the fan operation, the angle of the blades should be designed such that the area between blades is kept constant. An increase in fan performance was reported by Chen-Kang Huang and Mu-En Hsieh [17] when outlet angle was increased from 40° to 50° . An increase in inlet angle causes an increase in shaft power which results in an increase in pressure at high flow rate [18]. Figure 2.10 below shows the how angles of the blades are measured.

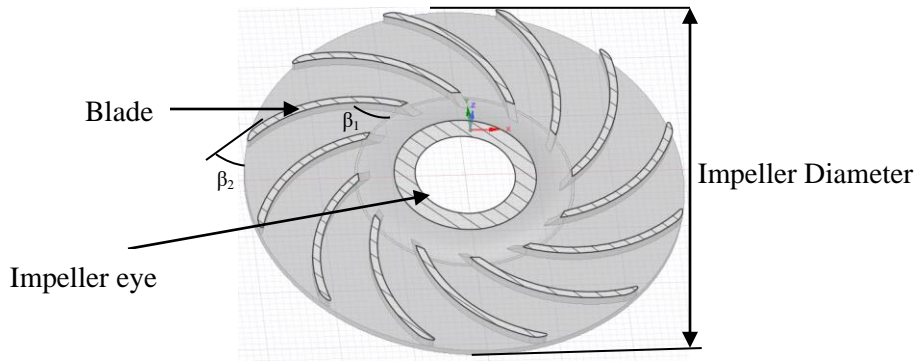


Figure 2.10: Centrifugal fan Impeller [15].

2.4.1.2 Impeller Diameter

To minimize hydraulic loss of the fan, the impeller diameter must be carefully selected. It can be used to size the fan from the fan law relationship between the impeller diameter and flow rate. By increasing the impeller diameter alone the flow rate becomes dependent on the impeller diameter which is given by the relation below.

$$\frac{Q_1}{Q_2} = \frac{D_1}{D_2} \quad (2.16)$$

where, Q_1 is flow rate at impeller diameter D_1 and Q_2 is flow rate at impeller diameter D_2 .

2.4.1.3 Impeller Width

The impeller width greatly affects the steepness of the fan performance curve. A blade with large diameter and narrow width is characterized by Steep performance curve whiles Small diameter and wide width results in flat performance curve. Also, it must be ensured that the blades do not overlap at the hub in order to prevent the choking of the flow [10].

2.4.1.4 Blade Number

In theoretical calculations, it is assumed that the air movement in fans follows the blade profile exactly. This can only be achieved if there is infinite blade number. However, in practical application, air movement by blades is not ideal due to finite number of blades. Therefore, it is difficult to predict the optimum number of blades using theoretical methods. Between 5 and 12 blades is said to be a good range for good design [10]. Other literatures suggest 8 to 12 blades for optimum design [17]. Using large number of blades may reduce the flow separation and inter-

blade circulation losses. However, large number of blades may cause the blades themselves to constrict the flow especially at the blade inlet, increase flow friction and thereby reducing fan performance.

2.4.1.5 Blade Spacing

One major impeller parameter that affects the operating conditions of fans is blade spacing. Irregular blade spacing affects the balance of the impeller and hence may contribute to the generation of noise during fan operation. Correctly designed impellers have good balance and operate at low noise. Irregular blade spacing makes the manufacture of the impeller more difficult especially from the balancing point of view resulting in an unsteady flow behaviour [19].

2.4.1.6 Fan Hub

One feature that may contribute to the operating noise level of the fan is the hub. This is because it interferes directly to the incoming air flow stream. To reduce noise levels, a careful design of the fan hub may contribute to high fan efficiency by reducing the noise to an acceptable level.

2.4.1.7 Roughness of Impeller

The roughness of the impeller may affect the performance of the fan. This roughness may arise from the technique used in manufacturing the impeller such as 3-D printing. Dvořák et al. [15] in their investigation, analyzed the effect of different 3-D printing methods such as Polyjet and Fused Deposition Modelling (FDM) as well as curing techniques on fan performance. It was observed that that high roughness of impeller surfaces ensures higher power transfer from impeller to fluid as well as reduces the leakage of air through the gap between inlet area of fan case and impeller.

2.4.2 Fan Casing Design Considerations

2.4.2.1 Fan Case Dimensions

The power requirement of the fan is somewhat dependent on the dimensions of the fan case such as the width and the outlet area. By increasing the width and outlet area of the fan, there is a reduction in pressure loss due to sudden expansion at the fan outlet. Usually, for backward

curved fans theoretical analysis suggests that the ratio of impeller width to fan case width should be of the order of 2.5 for backward curved fans for optimum performance.

2.4.2.2 Cut-off Clearance

There is a strong correlation between the noise level cut-off clearances of the fan [20]. Lyons L.A revealed [21] that usually, this noise levels are observed when blades pass the cut off region. The noise levels of the fan with a rounded cut-off are lower than for the fan with a sharp cut-off. Usually, rounded cut-off increases fan performance than sharp cut-off due to low noise. Therefore, the performance of the fan with rounded cut-off is increased for the same power requirements. Furthermore, the noise level can be slightly reduced by angling the cut-off.

2.4.2.3 Inlet Cone Clearance

One way of increasing the efficiency of fans is to have a good inlet cone design in order to ensure a smooth, streamlines flow into the fan. This will help in the reduction of energy loss since turbulence flow is minimized. Furthermore, the inlet cone increases the performance of a fan and also slightly reduces the maximum power requirements of the fan. At least a minimum of 2 mm clearance is acceptable to prevent catching between the inlet cone and the impeller.

2.4.3 Motor Design Considerations

2.4.3.1 Shaft Rotation Speed

Different rotation speeds of the motor shaft have an effect on the internal fluid flow in the impeller, thus affecting the volume flow. The fan law relates the fan rotation speed to the volume of fluid discharged at the fan outlet. With impeller diameter held constant, the shaft speed can be expressed as;

$$\frac{Q_1}{Q_2} = \frac{N_1}{N_2}, \quad (2.17)$$

where, Q_1 is flow rate at shaft rotation speed N_1 and Q_2 is flow rate at shaft rotation speed N_2 .

The shaft power can also be expressed in terms of the rotational speed as;

$$\frac{P_1}{P_2} = \left(\frac{N_1}{N_2}\right)^3, \quad (2.18)$$

where, P_1 is power at shaft rotation speed N_1 and P_2 is power at shaft rotation speed N_2 .

2.4.3.2 Impeller Positioning on Shaft

The research by Dvořák et al. [15] on fan performance also demonstrated how improper assembling of an impeller on the fan motor shaft may affect the fans performance. In their research, the impeller was positioned at different distances of the motor shaft. It was observed that there were different performance curves for different shaft positions, however, the difference between the curves were relatively insignificant.

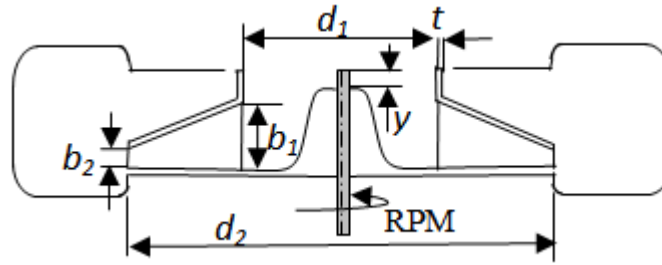


Figure 2.11: Schematic diagram of impeller in fan casing.

For the purpose of this work, parameters including blade inlet and outlet angles, number of blades, blade spacing, and roughness of impeller are considered for the impeller design features. Parameters such as shaft rotation speed and impeller positioning on shaft are considered for the shaft design features.

2.5 Measurement of Aerodynamic Parameters

2.5.1 Static Pressure Measurement

Generally, the pressure in a duct generated due to the operation of a fan has two components; dynamic pressure (p_v) and static pressure (p_s) [22]. The summation of the two pressures gives the total pressure;

$$p_T = p_s + p_v \quad (2.19)$$

The pressure that results from air movement is the dynamic pressure while the pressure due to the force exerted on the walls of the duct in both fan discharge and fan suction regions is the total pressure.

The total pressure can be expressed as;

$$p_T = p_{discharge} + p_{suction} \quad (2.20)$$

Static pressure measurement is significant for analyzing the performance of fan. It aids in investigating other flow parameters such as flow rate and flow velocity. The mass flow rate of air can be found by measuring static pressure difference. Static pressure is scalar and hence non directional, and it depicts molecular activities of a given fluid. The non-directional nature of this parameter makes it possible to use methods that require measurements that are stationary relative to fluid flow. Static pressure can be measured either at the free stream of air flow or at the duct wall. Static pressure at free stream can be measured with a static tube, and at the wall of the duct using wall tapping [5]. However, only wall tapping will be considered since pressure values will be taken from the walls of the duct.

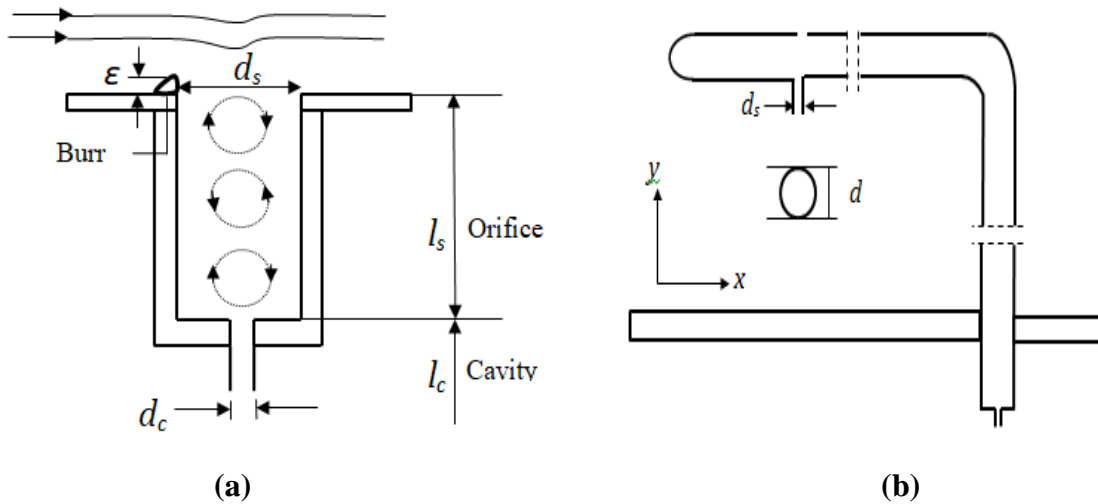


Figure 2.12: Static pressure measurement methods [5] (a) Wall tapping (b) Static probe.

The measured pressure at the wall of the duct can be expressed as;

$$p_{wm} = p_w + \Delta p_w, \quad (2.21)$$

where p_{wm} is the pressure measured at the wall, p_w is the actual pressure on the wall, and Δp_w is the error in the measured pressure.

According to Mckeon B.J and Smith A.J [23], one of the main sources of errors is due to eddies. Other forms are caused by fluid turbulence, varying Mach number. Also, depending on the orifice geometry, fluid stagnation may occur in holes. Therefore, care is taken in measuring high velocity flow when using the wall tapping method such as the case of the occurrence of eddies within the orifice cavity due to supersonic flows [5]. As a result, the recorded pressure at the wall may be greater than the actual value of pressure measured at the wall. However, since we will focus on flow below supersonic flow, the need to be conscious of this phenomenon is not required.

The change in Δp_w is a function of several variables which can be expressed as;

$$\frac{\Delta p_w}{T_w} = f \left(\frac{d_s u_\tau}{\nu}, \frac{d_s}{D}, M, \frac{l_s}{d_s}, \frac{d_c}{d_s}, \frac{\epsilon}{d_s} \right), \quad (2.22)$$

where d_s is the tapping diameter, $u_\tau = \sqrt{T_w/\rho}$ is the friction velocity, D is the pipe diameter, ρ is the density of fluid, M is the Mach number, l_s is the depth of the orifice, d_c is the diameter of the opening behind the orifice connecting to the pressure sensor, ϵ is height of the burrs on the tapping edge represented as the root-mean-square, ρ is the density of fluid, and ν is the kinematic viscosity.

Study by R. Shaw [24] revealed how the Δp_w varies relatively to the shear stress T_w at different values of l_s/d_s defined by d_s/ν and $\sqrt{T_w/\rho}$. The errors reach maximum at $l_s/d_s = 1.5$, and the effect is not significant when l_s/d_s is increased further. Also, for the diameter of the hole, there is an increase in static pressure error with increasing diameter of the hole and Mach number.

2.5.2 Methodologies of Mass Flow Measurement

For this work, it is expected that the fan moves air at a velocity less than that of sound. Therefore, flow is expected to remain subsonic throughout. The Flow rate measurement method is required to measure flow rate that can be based on pressure differential devices; according to ISO 5167:2003 [25].

Air flow is termed as closed conduit flow when pressure difference is the driving force causing the flow in a conduit. When flow is obstructed in a conduit, the pressure drop can be measured and thus the mass flow rate can be computed. The operating principle of the differential pressure flow meter is derived from Bernoulli equation, which expresses pressure drop in terms of the flow velocity. Fluid flow measurement in conduits is usually measured with devices that include orifice plates, Venturi tubes, and nozzles.

The Venturi may be appropriate for usage in applications where Turn Down Ratios are much higher. Measurement of flow rate by the Venturi tube is achieved by reducing the flow cross-sectional area in order to create a pressure difference.

Flow in nozzle is characterized by a high coefficient of discharge. However, compared to the orifice flow meter, the installation of a nozzle flow meter is difficult and also has a low pressure recovery.

The orifice plate basically consists of a flat circular plate with hole in in the middle section. The pressure difference is usually measured using pressure taps located at both upstream and downstream of flow near the orifice plate.

For the purpose of this study, the orifice method is considered and hence details of the orifice principle and construction is outlined according to ISO 5167; 2003.

2.5.2.1 Orifice Plate

The orifice plate method for mass flow rate measurement was chosen for this work. According to ISO 5167; 2003, the mass flow rate can be calculated if pressure difference across an orifice plate is known. To find the pressure difference across an orifice plate, the pressures before and after the plate are measured. The range of values for the ratio of diameter of the orifice bore and the diameter of pipe is given as $0.10 \leq \beta \leq 0.75$, where $\beta = d/D$.

The principle of the mass flow measurement is derived from the Bernoulli Equation. Assumptions such as the flow are incompressible and laminar is made to simplify the equation. At every instance, we expect that that the velocity of the flow is increased after flow through an obstruction hence upstream pressure is higher than downstream pressure. Considering a horizontal duct, the Bernoulli' Equation can be expressed as;

$$\frac{p_a}{\rho} + \frac{1}{2}v_a^2 = \frac{p_b}{\rho} + \frac{1}{2}v_b^2, \quad (2.23)$$

where p_a , p_b are the pressure upstream and downstream, v_a , v_b are velocity upstream and downstream, and ρ = density.

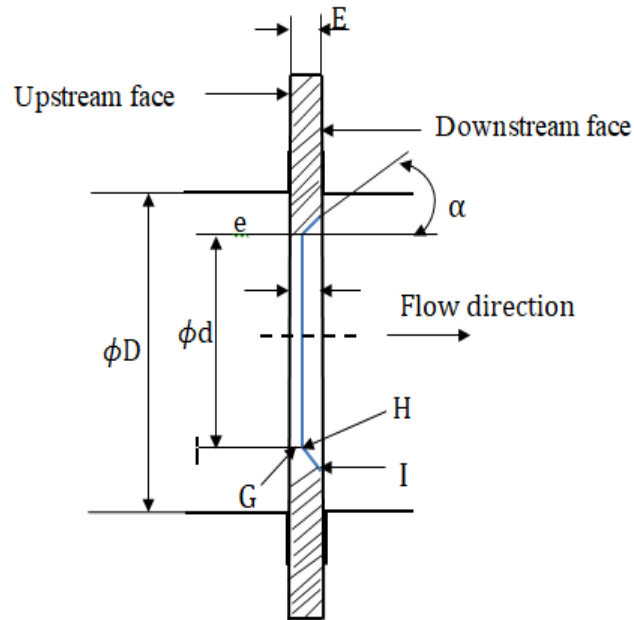


Figure 2.13: Orifice plate.

With the assumption that the velocity profiles in both upstream and downstream flow is uniform- the Continuity Equation is simplified as;

$$q = v_a \times A_a = v_b \times A_b, \quad (2.24)$$

where A_1 and A_2 represent the area upstream and downstream of the obstruction, and q is the volume flow rate.

The Bernoulli equation and continuity equation can be modified to compute the volume flow rate and is given by ISO 5167: 2003 as:

$$q_m = \varepsilon \frac{\pi}{4} D^2 \sqrt{2\Delta p \rho} \frac{C}{\sqrt{1-\beta^4}}, \quad (2.25)$$

D is the inside diameter of the pipe, $\beta = D/d$ diameter ratio, C is the discharge coefficient which depends on the Reynolds number and ε is the expansibility factor expressed as;

$$\varepsilon = 1 - (0.351 + 0.256d^4 + 0.93d^8) \left[1 - \left(\frac{p_2}{p_1} \right)^{\frac{1}{\kappa}} \right] \quad (2.26)$$

The Coefficient of discharge is calculated from the Reynolds number and A . The equations are expressed below;

$$\begin{aligned} C = & 0.5961 + 0.0261\beta^8 + 0.000521 \left(\frac{10^6 \beta}{Re_D} \right)^{0.7} \\ & + (0.0188 + 0.00063A)\beta^{3.5} \left(\frac{10^6}{Re_D} \right)^{0.3} \\ & + (0.043 + 0.080e^{-10l_1} - 0.123e^{-7l_1})(1 - 0.11A) \frac{\beta^4}{1 - \beta^4}, \end{aligned} \quad (2.27)$$

where Re_D is the Reynolds number calculated based on the pipe diameter D and $l_1 = 0$ for corner tapping.

$$Re = \frac{vD\rho}{\mu}, \quad (2.28)$$

$$A = \left(\frac{19000 \beta}{Re_D} \right)^{0.8}, \quad (2.29)$$

and κ is the Poisson's ratio

2.5.2.1.1 Parameter Description Based on ISO 5167-2:2003

2.5.2.1.1.1 Orifice Diameter d

The orifice bore is the surface between edges G and H in Figure 2.14 above. The shape of the orifice bore shall be cylindrical. The lowest diameter d shall be, in all cases, greater than 12.5

mm. Also, the diameter ratio, $\beta = d/D$, shall always be $0.10 \leq \beta \leq 0.75$. The maximum deviation from the mean diameter shall not exceed 0.05% of the mean diameter.

2.5.2.1.1.2 Angle of Bevel α

It is expected that the downstream side of the plate will be beveled. In the case when the thickness e of the orifice is less than thickness E of the plate exceeds the thickness e of the orifice. In addition, the angle of the bevel α shall be equal to $45^\circ \pm 15^\circ$.

2.5.2.1.1.3 Orifice Edge Quality, G,H,I

Proper geometry of, the edge g upstream of the flow as shown in figure 2.14 is necessary for good performance of the plate since it is in direct contact with the flow. It is required that the upstream edge labeled g in Figure 3.15 shall be sharp and square with edge radius not greater than $0.0004d$ for the edge to be considered as sharp and the angle between the orifice bore and the upstream face should be set to $90^\circ \pm 0.3^\circ$ to be considered square. Visual inspection of the edge radius is sufficient for orifice with diameter $d \geq 25$ mm. The H and I edges however, fall in the range of flow region that are separated hence, not much emphasis will be placed on these edges.

2.5.2.1.1.4 Flatness

The flatness of the plate plays an important role in minimizing errors in the values of discharge coefficient. If the plate is manufactured poorly, the plate may bend, and the centre may not coincide with the duct centre. This will affect the differential pressure measured across it. The flatness may therefore be measured as the offset between the plate and line drawn across the plate diameter. Furthermore, the equation for the measurement of the plate flatness is a function of the orifice diameter (d) and the pipe diameter (D). The flatness is such that the maximum offset should be less than $0.0005 (D - d) / 2$.

2.5.2.1.1.5 Roughness of Plate

The surface roughness of the upstream plate, R_a is expected to be $R_a < 10^{-4}d$. A case where R_a does not correspond to the specified surface quality criterion during normal operation, re-polishing or cleaning the surface within the diameter of at least D is used to correct it. Unless

reverse flow is to be measured, the surface quality of the downstream plate is not very strict. Therefore, sometimes visual inspection is enough like in this case.

2.5.2.1.1.6 Plate Thickness

The thickness, e of the orifice plate shall be $0.005D < e < 0.02$. However, it is expected that the difference between e values measured at any two points within the plate shall not exceed $0.001D$. Also, it is expected that thickness of the plate E shall be $e < E < 0.05D$. Considering pipe diameters of range $50\text{mm} \leq D \leq 64\text{mm}$, up to 3.2 mm orifice plate thickness E is considered. For pipe diameters $D \geq 200$ mm, the difference of measured E between two points within the plate shall not be greater than $0.001D$. For pipe diameters $D < 200$ mm, the difference of measured E between two points within the plate shall not be greater than 0.2 mm.

2.5.2.1.1.7 Positioning of the Plate

The Plate will be installed into two flanges. This method simplifies mounting and the dismounting of the orifice plate.

2.5.2.1.1.8 Material

Material considered for the manufacturing of the orifice plate should be suitable and maintain its properties such as strength during the measurement processes.

2.5.2.2 Pressure Tapping

Pressure taps are usually installed before and after the orifice plate for pressure and mass flow measurements. It is required that at least one pressure tap each is installed at the upstream and downstream side of the orifice plate. Based on ISO 5167-2:2003, there are three main choices for tapping: flange tapping, D and $D/2$ tapping and corner tapping. Flange tapping method is characterized by tappins positioned in the flanges at a distance of 25.4 mm at both upstream and downstream faces. It is simple to manufacture and install. However, because they are not geometrically similar, the discharge coefficient is complex. For D and $D/2$ tapping, the tappings are located $1D$ upstream and $D/2$ downstream with reference measurements taken from the upstream face of the orifice plate. Corner Tapping is characterised by the location of taps at the region between the orifice plate and the wall of the pipe. The tappings may be either single

tappings or with annular slots. For the purpose of this work, corner tapping with annular slot will be considered.

2.5.2.2.1 Corner Tapping with Annular Slot

In the design of corner tapping with annular slot, the taps can be located in the flange. Specific requirements of design are required to minimize errors and ensure proper functioning of the corner tapping. Generally, it is required that the pressure tapping hole should be circular with a diameter less than $0.13D$ and less than 13 mm with equal upstream and downstream diameters [26]. In order for good dynamic performance of the tapping, the minimum diameter of the pressure tapping should be small enough to prevent accidental blockage. Measuring from the inner wall of the pipe, it is also required that the depth of the hole shall be at least 2.5 times the pressure tapping diameter. Figure 2.14 below shows the schematic for the corner tapping. Also, a summary of the design requirements for the design of the corner tapping with annular slots is shown in Table 2-1 below.

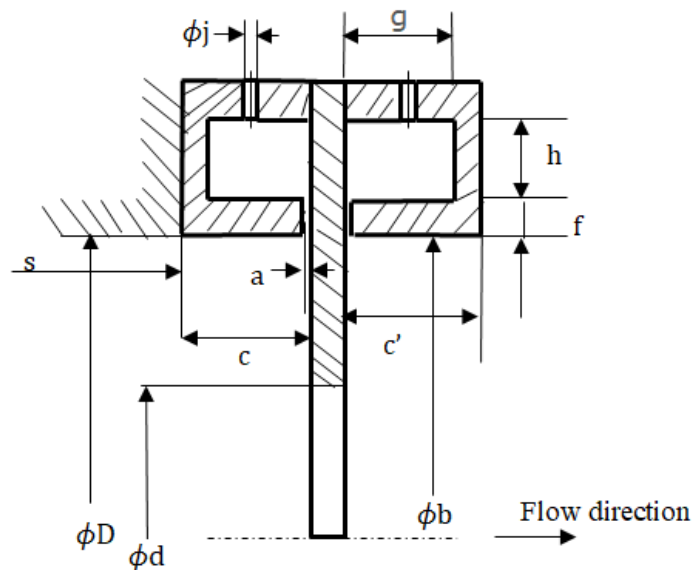


Figure 2.14: Corner tapping with annular slot.

Table 2-1: Orifice plate design requirements

Parameters	Recommended Values
Width of slot, a	<p>The width of the slot is given according to the diameter of the pipe, for a pipe with $D < 100\text{mm}$ a value of up to 2mm is accepted.</p> <p>An area of at least 12 mm^2 is required for each slot if four opening slots are used.</p>
Internal Diameter of carrier rings, b	<p>$b \leq 1.04D$ is accepted and should be strictly ensured that no protrusion of the pipe into the slot occurs.</p>
Length of upstream and downstream ring c/c'	<p>$c, c' \leq 0.5D$ is accepted.. Also the equation must be satisfied.</p>
Thickness of slot, f	<p>$f \geq 2a$ is accepted</p>
Annular slot Dimension, gh	<p>$gh \geq \frac{af}{2}$ is accepted</p>
Diameter of pressure tapping, j	<p>$j \leq 10 \text{ mm}$</p>

3 Test Stand Design

3.1 Details of Design

The test stand was design following ISO 5167; 2003 standard. The proposed design and sections are described in this section. The sections can be grouped into fan attachment section, flow pipes, test section, and backpressure control. Requirements necessary for the construction of the test stand are outlined. Furthermore, the detailed drawings for manufacturing and installation are discussed.

3.1.1 Fan Attachment Section

The fan inlet section will be connected to the fan outlet, and this will lead the air flow from the fan into the pipe. The inlet section is supposed to be air tight in order to prevent air leakage before the air enters the main pipe. In addition, the inlet section connection should be able to withstand the vibrations during the fan operation. Also, it should be able to hold the inlet section of the duct very tight to prevent air leakage, and at the same time the fan is able to detach itself from the inlet section to allow room for different fans to be tested.

3.1.2 Upstream and Downstream Duct

For upstream and downstream ducts, the duct length is very important. Hence, the upstream duct shall be long enough to allow the flow from the fan attachment section to be fully developed before it enters the test section. To reduce errors in measurement, the downstream pipe shall be long enough to prevent the fluctuations that arise from controlling the back pressure. In addition, the duct shall offer minimum resistance to air flow. The design shall allow the attachment of the test section to the ducts.

3.1.3 Test Section

The back pressure and mass flow rate section serves as the test region where measurements shall be conducted. It is attached to the upstream and the downstream pipes with the aid of flanges. It shall allow room for the attachment of pressure sensors for backpressure and mass flow rate to be measured.

3.1.4 Backpressure Control

The back pressure control shall regulate the flow through the test section in order to measure the different values of mass flow rates and their corresponding back pressures. The device shall be sensitive enough to allow gradual increment of mass flow rate. Also, it allows choking of the fluid in pipe when it is fully closed as well as prevent obstruction of air from the outlet of the pipe when it is fully open.

3.2 Proposed Design

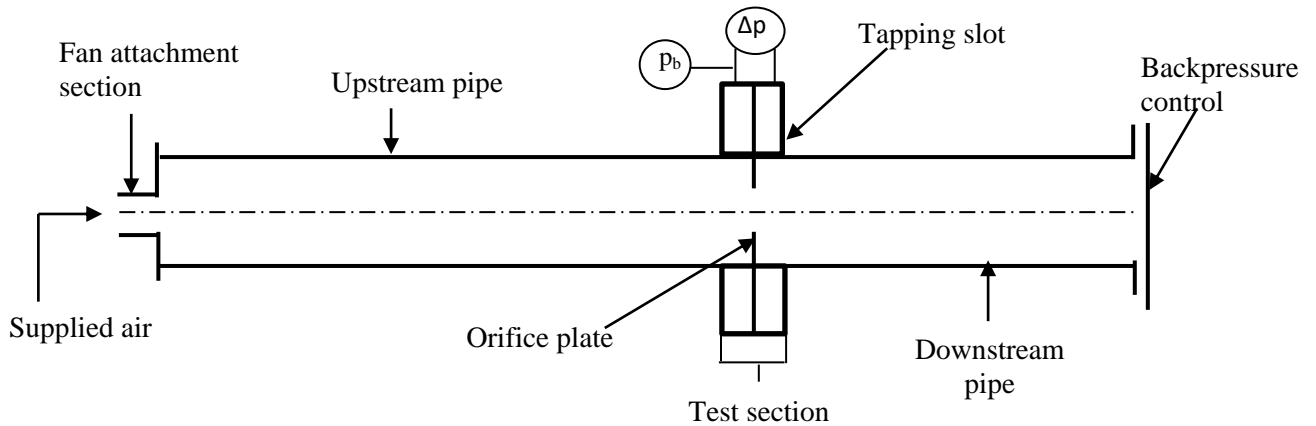


Figure 3.1: Schematic diagram illustrating the proposed design.

Air from the centrifugal fan outlet is supplied to the test stand at the fan attachment section. The air is then moved along the upstream pipe. The upstream pipe is long enough to allow for a steady flow to be achieved before the air enters the test section. The backpressure control device is used to obstruct the flow at the outlet of the downstream pipe in order for different mass flow rate and back pressure to be recorded at the test section. Chocking of the flow is expected in the tube when the outlet of the downstream pipe is fully closed. The highest mass flow rate is recorded when the outlet is fully opened. The mass flow rate is computed from values of the pressure difference measured across the orifice plate. Back pressure as well as the pressure difference across the orifice is measured at the test section using pressure sensors.

3.3 Design Evaluation

Table 3-1: Evaluation of solution based on requirements for fan attachment, upstream and downstream ducts

Design Requirement	Proposed Solution
Fan Attachment Section	
i. Allow attachment and detachment of fan	Plastic flange with an extended neck which has a threaded area is used to link the fan outlet to inlet of the upstream pipe. The flange allows for easy attachment and detachment of the fan outlet.
ii. Prevent air leakage of the air before entering pipe	Space in between the attachment of flange and the main piping is filled with silicone about 4 mm thick to ensure that its air tight.
iii. Should be able to withstand vibrations from the fan during fan operation	The flange is attached to the pipe with the aid of screws in order to prevent part movement at the inlet section.
Upstream and Downstream Ducts	
i. Ensure minimum resistance to airflow through the pipe	The pressure drop in the pipe was calculated using estimated diameter and length of the pipe. The total pressure drop in the pipe, p_l , was calculated using the Darcy-Weisbach equation given as $p_l = \frac{\lambda L}{D} \rho \frac{v_a^2}{2}$, where L is the total length of the pipe, v_a is the velocity of air flow, D is the diameter of the pipe, ρ is the density of the air, and λ is the friction coefficient.
ii. Flow is fully developed at upstream and straightened before it enters the test section	A stainless steel pipe of thickness 2 mm is used for the upstream pipe whose length is estimated in terms of the pipe diameter, D . The length is estimated as $20D$. The length is long enough to avoid swirling in the test section which may affect the reading of the back pressure and pressure

	difference across the orifice. This also ensures that flow is fully developed before it enters the test section.
iii. Downstream pipe prevent fluctuations at the test section due to back pressure control	A stainless steel pipe of thickness 2 mm is used for the downstream pipe whose length is estimated in terms of the pipe diameter, D . The length is estimated as $10D$, and it is long enough to prevent unsteady flow of air at the test section due to the regulation of the backpressure.
iv. Allow the attachment of the test section	The outlet area of the upstream pipe is welded to a flange as well as the inlet area of the downstream pipe to allow for easy assembly of the test section. The flange also provides rigidity of the test section.

Table 3-2: Evaluation of solution based on requirements for test section

Design Requirement	Proposed Solution
Test section	
i. Measurement of mass flow rate	The orifice plate is designed to allow the obstruction of flow which creates a pressure difference across the orifice. This difference is measured using pressure tapping, and the mass flow is computed using equation (2.25).
ii. Hold the orifice in place	Two annular slots hold the orifice in place such that the centre of the inner diameter of the orifice coincides with the centre of the pipe. This is also necessary for minimizing errors during measurements. Also, during installation, care is taking to ensure that the beveled area of the orifice plate is placed in the downstream side to minimize the plate's contact with the flowing air.

iii. Measurement of back pressure	An annular slot is designed to also measure the backpressure. The pressure is measured before the orifice plate with the aid of pressure tappings.
-----------------------------------	--

Table 3-3: Evaluation of solution based on requirements for back pressure control

Design Requirement	Proposed Solution
Back pressure control	
i. Regulate the flow across the test section	A plate is installed at the end of the downstream pipe outlet. This plate is gradually moved towards the outlet of the downstream pipe, and gradually away from it to create different flow regimes at the test section.
ii. Sensitive and rigid enough to allow pressure change	An M6 screw is attached to the control plate. The small pitch diameter of the screw ensures gradual change in pressure across the orifice plate when moved. The setup for the back pressure control is firmly attached to the main test stand with the aid of flanges.
iii. Flow choking	The outlet is fully closed to ensure that choking can occur within the pipe. When the plate is moved by the screw to totally close the outlet of the downstream pipe, the flow velocity is increased in the test stand enabling it to equal speed of sound.

4.2.2 Sectional View of the Design

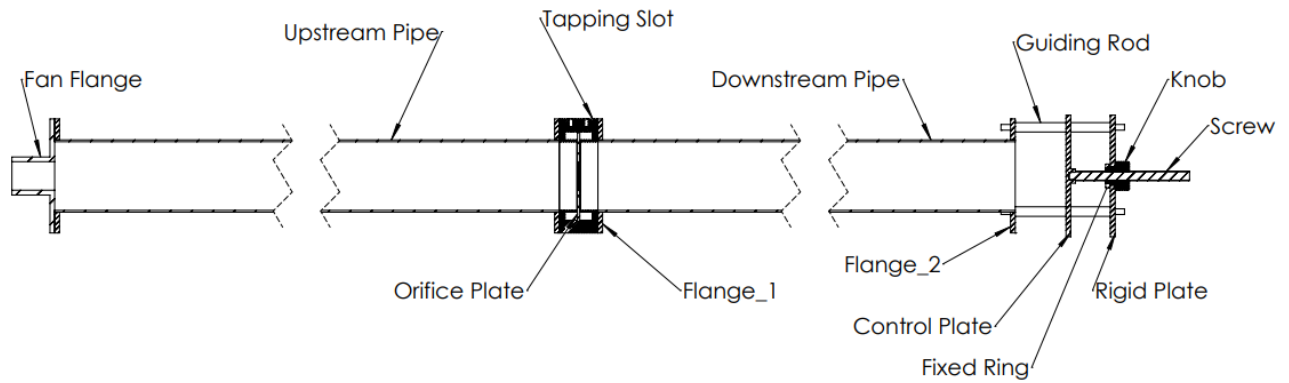


Figure 3.2: Test Stand.

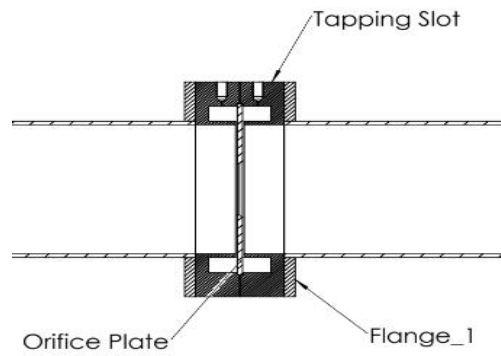


Figure 3.3: Test section.

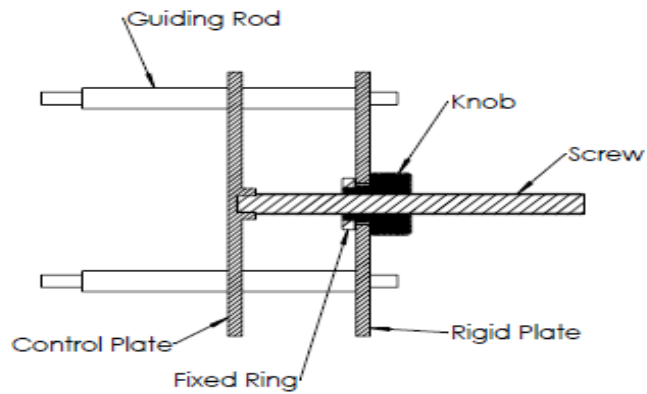


Figure 3.4: Backpressure control.

Figure 3.2 shows the section view of the main part of the test stand that comprises of the fan attachment section, the upstream and downstream pipes, the test section, and the back pressure control section. The test section consists of the Tapping slot, and the Orifice plate as shown in Figure 3.3. The back pressure control section consists mainly of the Movable plate, Guiding rods, Movable screw as shown in Figure 3.4. The backpressure control setup is rigidly attached to the outlet of the downstream pipe with M6 stud bolts. This also allows easy removal for different set up of backpressure control to be installed. Appendix contains part and assembly drawings.

4 Experimental Setup

4.1 Set-up Description

Figure 4.1 shows how the test stand was set-up for experiment. A brushless DC motor (3) was used to electrically propel the impeller. The fan motor was supplied with a voltage of 15V. The motor is also connected to a PC (6) where the RPM of the motor shaft can be regulated. The taps (4) of the tapping slot is connected to the PC where the values for the backpressure and the pressure difference across the orifice are displayed.

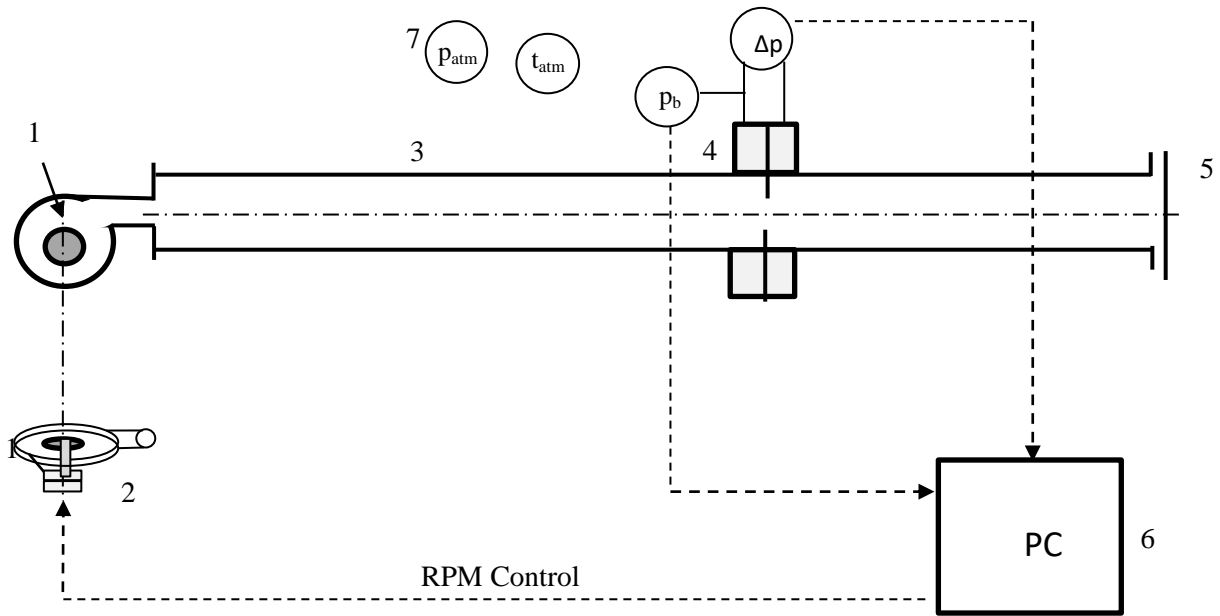


Figure 4.1: Schematic of the experimental setup.

Testing stand: 1- fan impeller, 2 – Motor, 3 – testing pipe 4 – Backpressure measuring (Δp_b) and differential pressure (Δp_m) measuring, 5 – Backpressure control (chocking), 6 – RPM control and pressure reading, 7 – measuring of atmospheric pressure and temperature.

4.2 Experimented Impellers

Initially, the test stand was tested for different fan motor speed that is 11000, 9000, and 6000 revolutions per minute, RPM. These measurements were done on a reference fan which was an impeller with 12 backward curved blades. Also, the reference fan was measured with a combined

ABEP-R filter in order to determine the design point of the fan. The position of the impeller on the motor shaft was also varied between 0.3 and 2.3 mm so that the effect of misalignment in fan assembly can be examined. Furthermore, 6 different impellers with different roughness were investigated in order to verify the effect of different impeller surfaces on fan performance. The impellers were manufactured with different 3-D printer technologies and materials. The different technologies, materials, and their resulting impeller parameters are summarized in Table 4-1 below.

Table 4-1: 3-D printing techniques and thickness layer.

3-D printer technology / material	Thickness of 3D Print layer (mm)	Blade dimension, $d_2 \times b_2$ (mm x mm)
Injection / plastic	-	60.0 x 3.86
PolyJet / VeroClear	0.014	60.0 x 4.17
PolyJet / VeroBlack	0.014	60.05 x 4.14
PolyJet / VeroGrey	0.016	60.1 x 4.12
PolyJet / ABS-like	0.03	59.95 x 4.1
FDM / ABS-M30	0.127	59.95 x 4.21

4.2.1 Impellers without Modification

More than 20 fan impellers with straight and backward curved blades were investigated. Three parameters of the impellers: number of blades, inlet blade angle, β_1 and outlet blade angle, β_2 were varied at 11000 RPM. In addition to maintaining constant RPM, the axial position of the impeller on the shaft was kept constant at about 1.5 mm for all samples during the testing. The working pressure for the fan was regulated and the corresponding pressure difference across the orifice plate was recorded in order to calculate the mass flow rate.

4.2.1.1 Impellers with Straight Blades

This group of impellers had a total of 9 different impellers with straight blades. Out of these 9 impellers, two sets of impellers had 4 impellers with each having 8 and 12 blades, respectively. These sets of impellers, in addition to the last impeller which had 16 blades, were tested. The

inlet blade angles for the radial blades were varied at 90°, 80°, 60° and 40°, and the outlet blade angle was varied at 90°, 80°, 76° and 78° Figure 4.2 below shows how the inlet blade angles were measured.

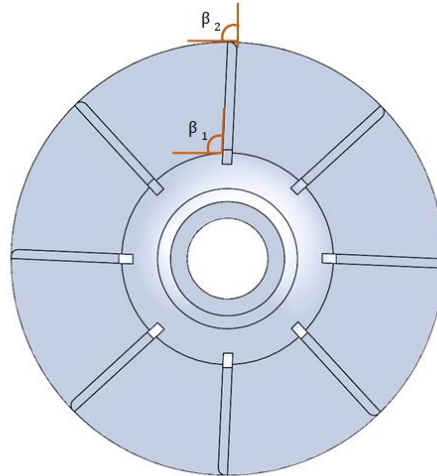


Figure 4.2: Impeller with straight blades.

Before the experiments were conducted, the impellers were sub divided into two groups: impellers with the same blade angles β_1 , β_2 and impellers with the same number of blades. Initially, the impellers with the same β_1 , β_2 were tested in order to investigate the effect of different number of blades on fan performance. The parameters of these impellers are given in Table 4-2 below.

Table 4-2: Tested impellers with straight blades having same blade angle and varied number of blades.

Impeller Name/ Parameters	A	B	C	G	D	H	E	I	F
Blade inlet angle, β_1 [°]	90			80		60		40	
Outlet blade angle, β_2 [°]	90			85		76		68	
Number of blades, [-]	8	12	16	8	12	8	12	8	12

For the second part of this experiment, the effect of inlet and outlet blade angle on fan performance was investigated. In this test, the number of impeller blades was kept constant and

β_1 , β_2 were varied. However, the impeller with 16 blades was not tested since it was the only impeller with that number of blades. Table 4-3 summarises the parameters for this set of impellers.

Table 4-3: Tested impellers with straight blades having same number of blades and varied blade angles

Impeller Name/ Parameters	A	G	H	I	B	D	E	F
Number of blades [-]	8				12			
Blade inlet angle, β_1 [°]	90	80	60	40	90	80	60	40
Outlet blade angle, β_2 [°]	90	85	76	68	90	85	76	68

4.2.1.2 Impellers with Backward Curved Blades

For the impellers with backward curved blades, a total of 8 impellers were experimented. The 8 impellers had 4 of its impellers with 8 blades and the other 4 with 12 blades. Three parameters of the impellers that were varied for this experiment include inlet blade angle, outlet blade angle and number of blades. Figure 4.3 describes the blade geometry.

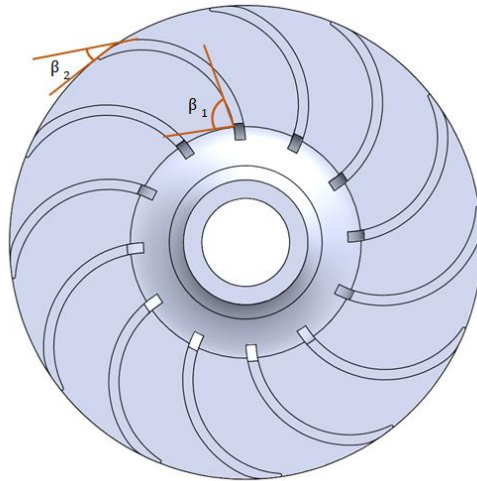


Figure 4.3: Impeller with backward curved blades showing the blade angles.

The impellers were initially compared for the same number of blades but different blade angles. The outlet blade angle was varied at 20° and 50°, and the inlet blade angle was varied at 80° and

50°. The impellers were also tested at constant β_1 and β_2 and varying number of blades. Table 4-4 and Table 4-5 below show the summary of the different Impeller parameters.

Table 4-4: Tested impellers with backward curved blades for varied number blades.

Impeller Name/ Parameters	J	N	K	O	L	P	M	Q
Blade inlet and outlet angles, β_1 [°] and β_2 [°]	80 and 50		80 and 20		40 and 50		40 and 20	
Number of blades [-]	8	12	8	12	8	12	8	12

Table 4-5: Tested Impellers with backward curved blades, varying inlet and outlet blade angles, and constant number of blades

Impeller Name/ Parameters	J	K	L	M	N	O	P	Q
Number of blades [-]	8				12			
Blade inlet angle, β_1 [°]	80		40		80		40	
Blade outlet angle, β_2 [°]	50	20	50	20	50	20	50	20

4.2.2 Modified Impellers with Backward Curved Blades

Modifications were done to other groups of impellers with backward curved blades, and their fan performances were investigated. The modifications were grouped into three: impellers with short blade between main impeller blades, impellers with narrow channels at the impeller outlet area, and impellers with different blade pitch angles.

4.2.2.1 Impellers with Short Blades

This type of impellers has 6 short blades in addition to 6 main impeller blades. The distance between the radii of the short blade and the main blade is 4 mm. In addition, the blades are spaced evenly. Figure 4.4 shows the arrangement of the short blades, and how the angles of the main blades were measured.

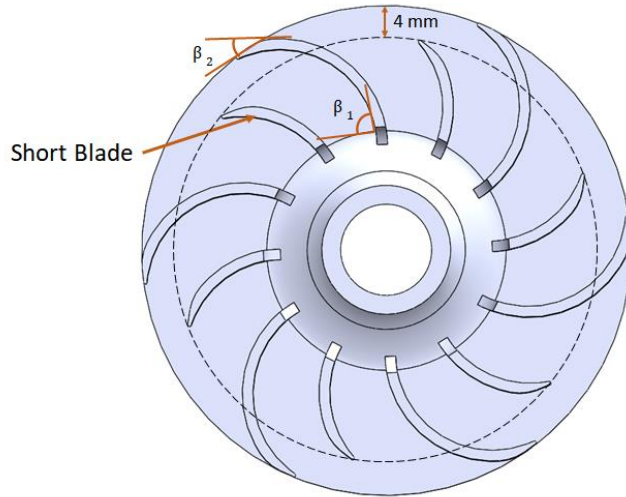


Figure 4.4: Impeller with short blades.

All the impellers had the same number of short and main blades. In all, a total of 4 impellers were tested at varying β_1 and β_2 . The parameters of this group of impellers are summarized in Table 4-6 below.

Table 4-6: Backward curved blades with shorter blades

Impeller Name/ Parameters	II	JJ	KK	LL
Blade inlet angle, β_1 [°]	80		40	
Blade outlet angle, β_2 [°]	50	20	50	20

4.2.2.2 Impellers with Large Number of Blades

This group of impellers had a total of 24 blades: 12 main blades and 12 blades positioned close to the impeller outlet area. These narrow channels are expected to increase the flow velocity of the air when it is discharged from the impeller. Figure 4.5 shows the narrow channels in the impeller and how the blade angles were measured.

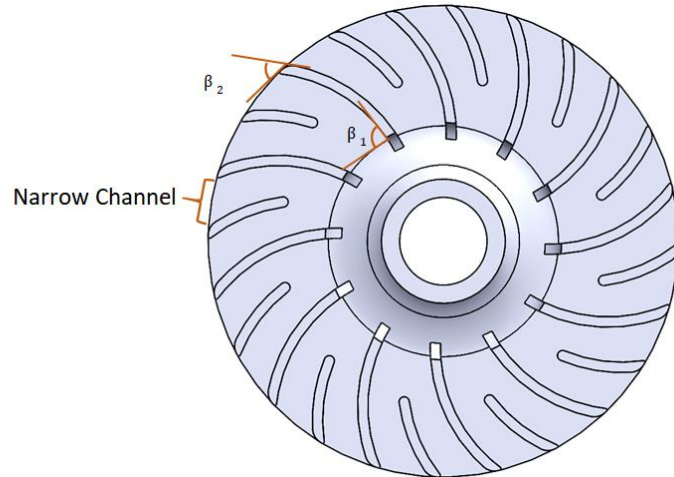


Figure 4.5: Impeller with narrow outlet channel.

The impellers were tested for varying β_1 and β_2 . The number of blades, 12 is the same for all the tested impellers. Also, the area between the channels depends on blade outlet angle. The parameters of this group of impellers are summarized in Table 4-7 below.

Table 4-7: Backward curved blades with narrow outlet channel

Impeller Name/ Parameters	R	S	T	U
Blade inlet angle, β_1 [°]	80		40	
Blade outlet angle, β_2 [°]	50	20	50	20

4.2.2.3 Impellers with Different Blade Pitch Angle

The last group of impellers was designed in order to test the effect of irregular blade spacing on fan performance. There were 8 impellers designed to have the same number of blades, but different blade pitch angles. Each impeller has two pitch angles, γ_1 and γ_2 . The difference between the pitch angles, $\Delta\gamma = |\gamma_1 - \gamma_2|$, is used to describe the impellers. Out of the 8 impellers, 4 has $\Delta\gamma = 2^\circ$ and the other 4 has $\Delta\gamma = 4^\circ$. Figure 4.6 shows how the blade pitch angles were measured. The parameters of the different impellers are summarised in Table 4-8 below.

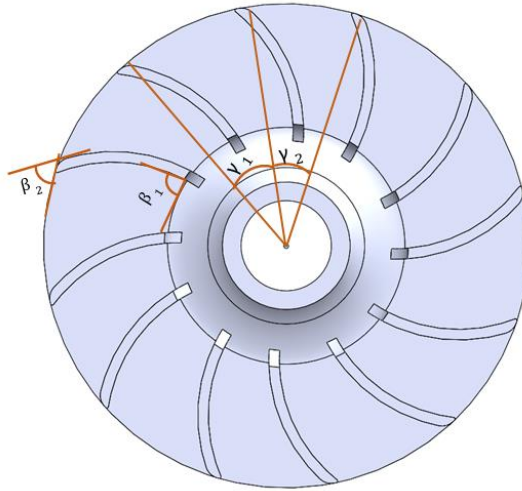


Figure 4.6: Impeller with varying blade pitch angle.

Table 4-8: Backward curved blades with angled blades

Impeller Name/ Parameters	AA	CC	EE	GG	BB	DD	FF	HH
Blade inlet angle, β_1 [°]	80		40		80		40	
Blade outlet angle, β_2 [°]	50	20	50	20	50	20	50	20
Difference in pitch angle [°]	2				4			

4.3 Representation of Results

After the experiment, the volume flow rates were calculated using equation (2.25) by substituting the measured pressure difference across the orifice. The measured total pressure was used to compute the pressure coefficient. The computed mass flow rate was also used to calculate the flow coefficient. These were calculated as:

$$\text{Pressure coefficient, } \psi = \frac{\Delta p_b}{\rho \frac{u_2^2}{2}} \quad (5.1)$$

$$\text{Flow coefficient, } \varphi = \frac{Q}{\pi d_2 b_2 u_2} \quad (5.2)$$

The atmospheric pressure and temperature in the laboratory were measured and were considered in the calculation for the air density.

Table 4-9 is the summary of the dimensions that were common to all the impellers that were measured.

Table 4-9: Basic Impeller dimensions

Outer blade diameter, d_1 (mm)	60
Impeller eye diameter, d_e (mm)	30
Outer blade width, b_2 (mm)	6
Inlet blade width, b_1 (mm)	4
Thickness of blade, (mm)	1

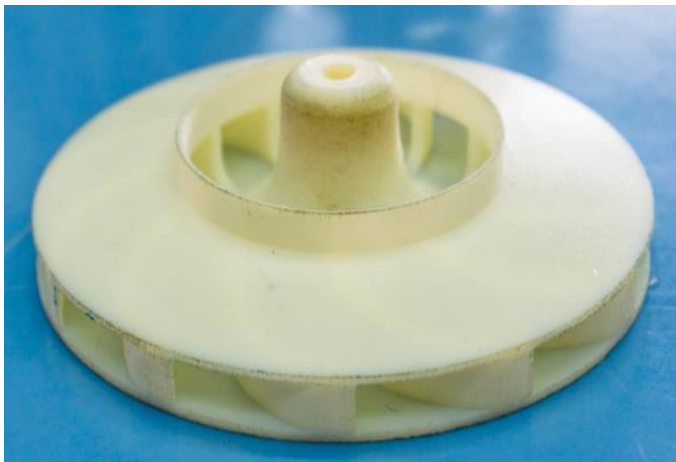


Figure 4.7: Sample of experimented impeller.



Figure 4.8: Impeller casing.

5 Analytical solution – One dimensional

5.1 Deviation from the Linear Relation

In practical situations, the performance curve obtained deviates from the ideal curves shown in Figure 3.9 above. This is due to losses associated with the flow. Therefore, the Euler pressure calculated using equation 2.14 above is only for ideal situations. For practical cases, the Euler pressure is reduced due to losses associated with the fan design. Depending on the parameters of the fan design features, the Euler pressure may reduce significantly.

5.1.1 Inter-Blade Circulation Loss

In the derivation of the Euler equation, it was assumed that the air follows the path of the blade profiles exactly. This phenomenon is only possible if the impeller consists of an infinite number of blades. However, this is not possible for practical design. The loss can be accounted for by calculating the effective radius. This is somewhat difficult to calculate. It is generally calculated as half of the perpendicular distance between the periphery of the blade the tangent of the blade.

The effective radius can be expressed as [18];

$$r = \frac{\pi d_2 \sin \beta_2}{2z}, \quad (5.1)$$

where z is the number of blades

The angular velocity of the blade can be deduced as:

$$\omega = \frac{2u_2}{d_2}, \quad (5.2)$$

Inter-blade circulation loss can therefore be expressed in terms of the effective radius and the angular velocity

$$p_c = \rho(u_2)r\omega, \quad (5.3)$$

By substituting equation (5.1) and (5.2) into equation (5.3),

$$p_c = \rho(u_2) \frac{\pi d_2 \sin \beta_2}{2n} \frac{2u_2}{d_2}, \quad (5.4)$$

$$p_c = \rho(u_2)^2 \frac{\pi \sin \beta_2}{2}, \quad (5.5)$$

5.1.2 Impeller Loss

This pressure loss is associated with the separation of fluid stream in the impeller as the fluid flow through the blade. There is a change in the relative velocity components of the fluid [18].

Impeller pressure loss is given as:

$$\Delta p_{imp} = k_{imp} \frac{\rho}{2} (w_1 - w_2)^2 \quad (5.6)$$

Using the trigonometry functions

$$\sin \beta_1 = \frac{c_{m1}}{w_1} \quad (5.7)$$

$$\sin \beta_2 = \frac{c_{m2}}{w_2} \quad (5.8)$$

Substituting into equation (5.6)

$$w_1 = \frac{Q}{\sin \beta_1 \cdot \pi \cdot d_1 \cdot b_1} \quad (5.9)$$

$$w_2 = \frac{Q}{\sin \beta_2 \cdot \pi \cdot d_2 \cdot b_2} \quad (5.10)$$

This gives an overall equation expressed as;

$$\Delta p_{imp} = k_{imp} \frac{\rho}{2} Q^2 \left(\frac{1}{\sin \beta_1 \cdot \pi \cdot d_1 \cdot b_1} - \frac{1}{\sin \beta_2 \cdot \pi \cdot d_2 \cdot b_2} \right)^2 \quad (5.11)$$

where k_{imp} is described as the loss factor which is often in the order of 0.2 to 0.3 for sheet metal blades. This factor is less for blades in the with aerofoil profile.

5.1.3 Outlet Pressure Loss

This loss occurs due to free vortex conditions occurring in fan casing. In practice this phenomenon is difficult to prevent. Consequently, there is a reduction of the velocity of the flow due to eddy formation. Up to 2.5 times increase of flow area is expected as fluid moves from the

blade to the volute casing. To compare flow under such phenomenon to flow through a normal pipe flow which suddenly enlarges. The resulting outlet velocity triangle is shown in Figure 5.1 below.

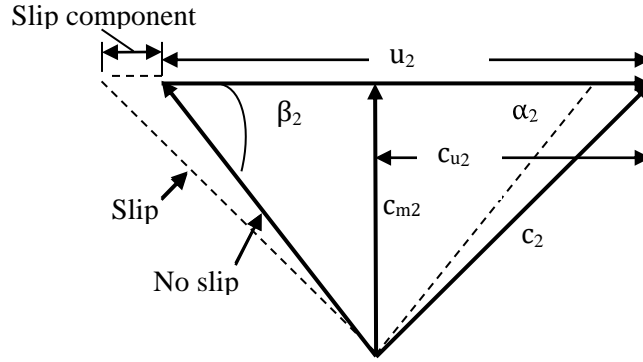


Figure 5.1: Outlet velocity showing slip condition.

The pressure loss from the casing can therefore be expressed as [18];

$$p_{out} = k_{out} \frac{\rho}{2} (c_2' - c_3)^2 \quad (5.12)$$

The average fan velocity c_3 is given as:

$$c_3 = \frac{Q}{A_{out}}, \quad (5.13)$$

where, c_3 is the outlet velocity and A_{out} is the fan outlet area

$$c_2' = \sqrt{(u_2)^2 + \left(\frac{c_{m2}}{\sin \beta_2}\right)^2 - \left(\frac{2u_2 c_{m2}}{\tan \beta_2}\right)} \quad (5.14)$$

$$P_{out} = k_{out} \frac{\rho}{2} \left[\sqrt{(u_2)^2 + \left(\frac{c_{m2}}{\sin \beta_2}\right)^2 - \left(\frac{2u_2 c_{m2}}{\tan \beta_2}\right)} - \frac{Q}{A_{out}} \right]^2, \quad (5.15)$$

k_{out} is the loss factor of the order of 0.4.

5.1.4 Inlet Loss

According to Hunter [18], the inlet losses based on the factors causing these losses may be divided into two: loss due to air expansion and loss due to swirl .

5.1.4.1 Loss due to the Expansion of Air

This loss occurs due to the expansion of air as a result of sudden change of air flow direction. After air passes through the eye of the inlet cone into the impeller the flow direction is changed from axial to straight flow, hence, resulting in pressure loss due to the turning of the flow. This inlet loss can be calculated as follows [18];

$$p_{in1} = k_{in1} \frac{\rho}{2} v_e^2, \quad (5.16)$$

where the inlet eye velocity is expressed as,

$$v_e = \frac{Q}{A_e} \quad (5.17)$$

The inlet eye area is expressed in terms of the inlet eye diameter

$$A_e = \frac{\pi d_e^2}{4} \quad (5.18)$$

$$p_{in1} = k_{in1} \frac{\rho}{2} \left(\frac{4Q}{\pi d_e^2} \right)^2 \quad (5.19)$$

5.1.4.2 Pre-swirl Loss

When the air turns as a result of entering the passage of the blades, there is the tendency of pre-swirl of the flow. The pre-swirl is critical at an angle of 45 degrees. In order to remove swirls, vane diffusers can be use [27]. This pre-swirl loss can be calculated as follows [18]:

$$p_{in2} = k_{in2} \frac{\rho}{2} (v_e - w_1)^2 \quad (5.20)$$

From the velocity triangle the relative velocity can be expressed as;

$$w_1 = \sqrt{c_{m1}^2 + (u_1 - c_{m1} \tan \beta_s)^2} \quad (5.21)$$

$$p_{in2} = k_{in2} \frac{\rho}{2} \left[\left(\frac{4Q}{\pi d_e^2} \right) - \sqrt{c_{m1}^2 + (u_1 - c_{m1} \tan \beta_s)^2} \right]^2, \quad (5.22)$$

where k_{in1} and k_{in2} are in the order 0.7 to 1.1 for sheet blades. However, k_{in2} of 7 to predict the flow pattern due to very high inlet loss associated with the fan that was investigated.

5.1.5 Internal Volumetric Leakage

Internal volumetric leakage may occur in the instance when the motor shaft enters the volute casing. Also, it may also occur, when there is leakage of flow between the impeller eye and the inlet cone. The most significant loss is the leakage loss between the impeller eye and the inlet cone. This can be calculated by assuming flow through the orifice.

Leakage volume can be expressed as [18];

$$Q_L = C_d A \sqrt{2 \frac{p_s}{\rho}}, \quad (5.23)$$

where C_d is the Discharge Coefficient and p_s is the Static pressure difference across clearance

Leakage area

$$A = \pi d_1 \alpha, \quad (5.24)$$

where α Inlet clearance.

By substitution the leakage volume can be expressed as;

$$Q_L = C_d \pi d_1 \alpha \sqrt{2 \frac{p_s}{\rho}} \quad (5.25)$$

If the edge of the gap is sharp, it is reasonable to assume that the value of C_d will be of the order of 0.6.

Figure 5.2 shows the effect of the losses on the theoretical pressure of a backward curved blade fan predicted by the Euler equation.

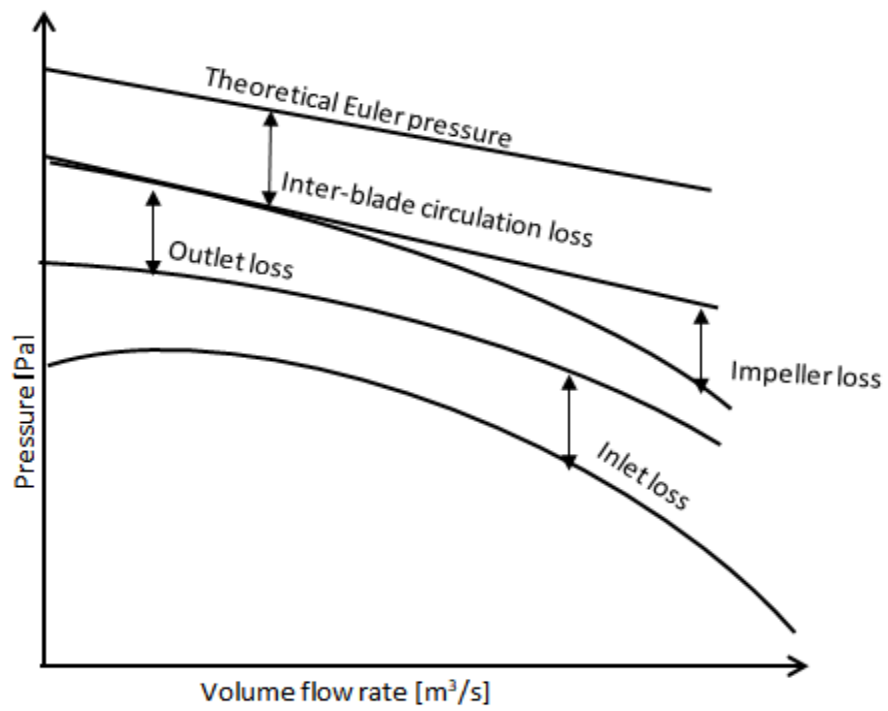


Figure 5.2: Loss curves [18].

6 Results and Discussion

6.1 Manufactured Parts and Assembly

Based on the specifications required for the test stand design the model, together with detailed 2D drawings, were submitted for manufacturing. The following figures show photos of the manufactured test stand assembly and the components of the assembly. The details 2D drawings of the individual components are shown in Appendix.



Figure 6.1: Test stand assembly.



Figure 6.2: Fan Inlet Section.



Figure 6.3: Test section assembly.



Figure 6.4: Backpressure control assembly.



Figure 6.5: Upstream pipe.



Figure 6.6: Downstream Pipe.



Figure 6.7: Guiding rod.



Figure 6.8: Control plate welded with screw



Figure 6.9: Rigid plate welded with ring and handle



Figure 6.10: Tapping slot.

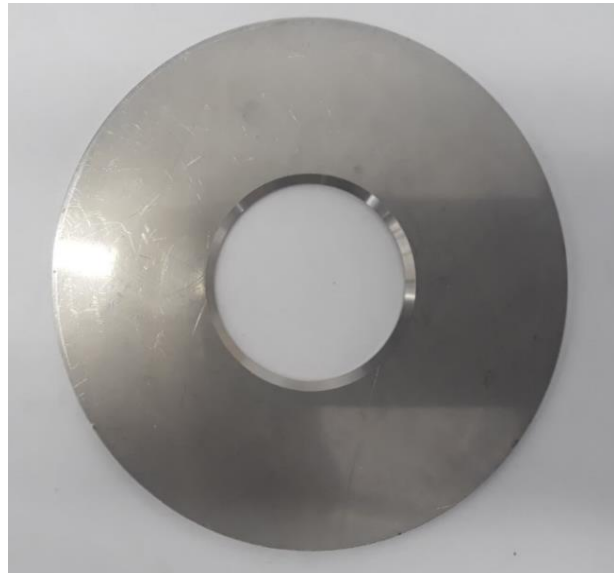


Figure 6.11: Orifice plate.

6.2 Experimental and Analytical Results

6.2.1 Results for Testing of Test Stand and Fan

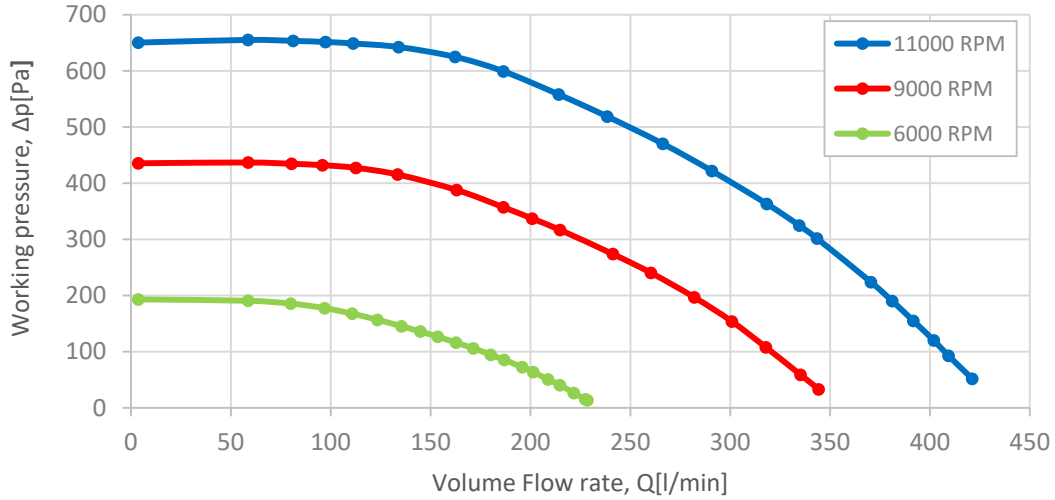


Figure 6.12: Fan output for different motor speed.

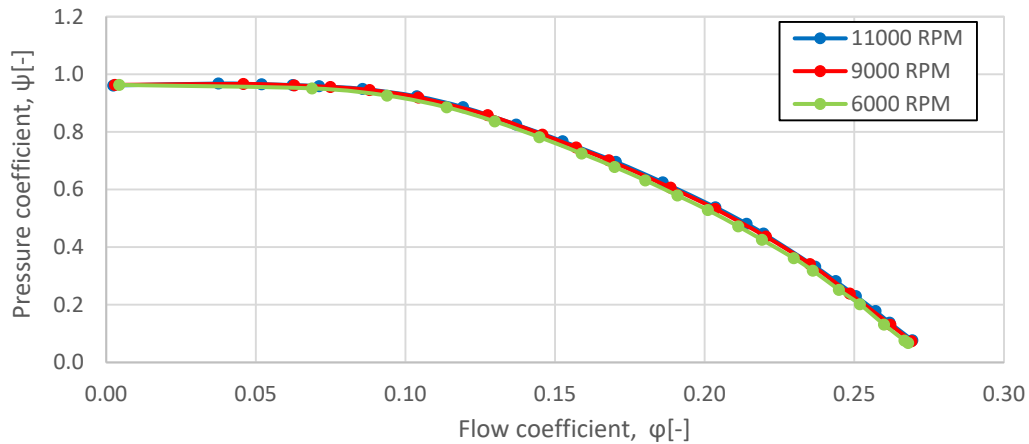


Figure 6.13: Fan output for different motor speed by comparing dimensionless numbers.

Before the test stand can be used to experiment on the designed impellers, it is necessary to investigate if it is reliable and repeatable. Therefore, it was used to experiment on a reference fan which was operated at different speeds: 11000, 9000 and 6000 RPM. A comparison was first made between the change in back pressure and the volume flow rate. This is shown in Figure 6.12 below. The highest working pressure of a fan is obtained when the outlet of the test stand is

completely closed, resulting in chocking of the flow. This means that no pressure difference is recorded across the orifice plate hence, no air flow. From the graph, the highest working pressure is observed at 650 Pa, 440 Pa, and 200 Pa for 11000, 9000 and 6000 RPM, respectively. The decrease in working pressure with rotation speed is because of the decrease in the power transmitted to the impeller by the shaft [28]. This power is termed as the shaft power. According to the fan laws, the shaft power is proportional to the cubic power of the fan rotational speed. Therefore, a decrease in rotation speed results in a decrease in shaft power and vice versa. It can also be observed from the graph that the pressure decreases with increasing volume flow rate irrespective of the rotational speed. This is because as the flow increases, the velocity of air passing through the orifice plate increases, resulting in a decrease in working pressure. When the fan was operated at 6000 RPM, it reached its lowest working pressure at a volume flow rate of 230 l/min. The highest flow rate was recorded by the fan operated at 11000 RPM which was observed to be 420 l/min. This is expected because the volume flow rate according to the fan law is proportional to the rotation speed hence as the rotation speed increases the volume flow rate is expected to increase.

In order to show that the results obtained after measuring with the manufactured test stand are repeatable, the working pressure and the volume flow rate were converted to dimensionless quantities. The working pressure is converted to pressure coefficient, and the volume flow rate is converted to flow coefficient. It is expected that for good repeatability of this test stand, the three curves must follow the same curve. As shown in Figure 6.13, it can be seen that the performance curve for the three different RPMs follow the same curve. This observations agrees with results by Dvořák et al. [15] who experimented on similar design. Therefore, the test stand can be said to be reliable and can be used for the experiment.

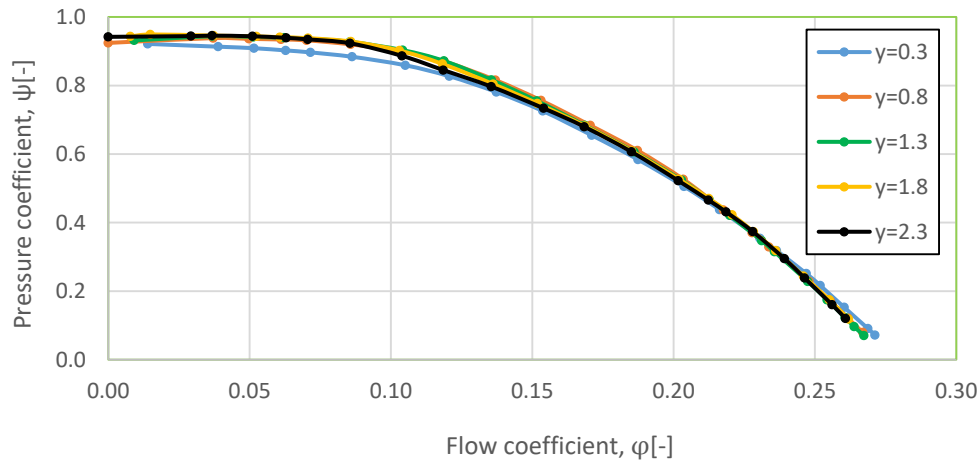


Figure 6.14: Fan output for various mutual positions of impeller and motor shaft.

This test was aimed at identifying the effect the impellers will have on fan performance if its mutual position with the motor shaft is changed. Figure 6.14 shows the results after the distance between impeller and mutual position of the motor shaft was varied. When the fan was measured at 11000 RPM for all values of y , it was observed that the lowest maximum working pressure is observed at $y=0.3$. At flow coefficient range of 0.10 and 0.15, rate, it can be noticed that as the distance of y decreases, there is a very little rise in working pressure. Similar trend was observed by Dvořák et. al when similar experiment was conducted at 9000 RPM [15]. This was explained as due to the additional suction pressure generated in the gap between the impeller eye and the diffuser of the fan. Nevertheless, the effect of improper assembly for this design is not conspicuous. The difference in pressure difference y has varied is not significant.

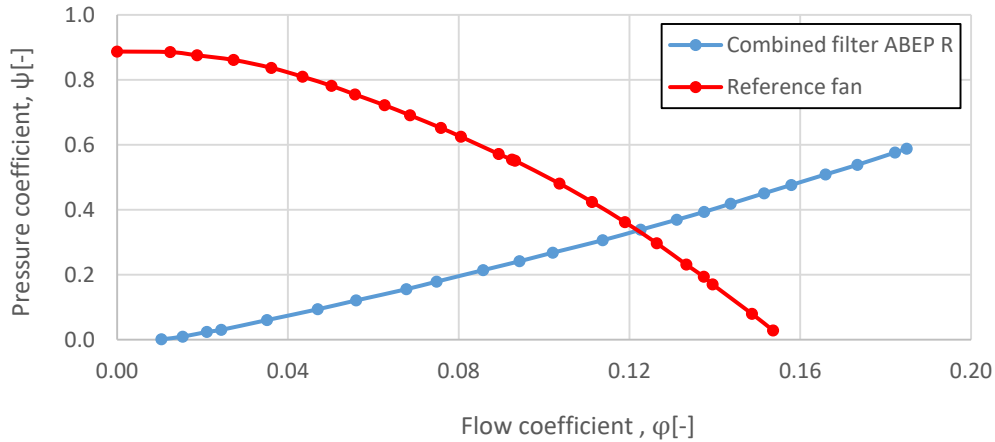


Figure 6.15: Measuring of fan with ABEP-R filter at 11000 RPM motor speed.

Measuring the reference fan with a combined filter ABEP-R resulted in the graph shown in Figure 6.15 above. The point of intersection between the system resistance curves caused by the use of filters with the fan, and the fan performance point is the operating point of the fan. This is observed at flow coefficient of about 0.12 and a pressure coefficient of about 0.35.

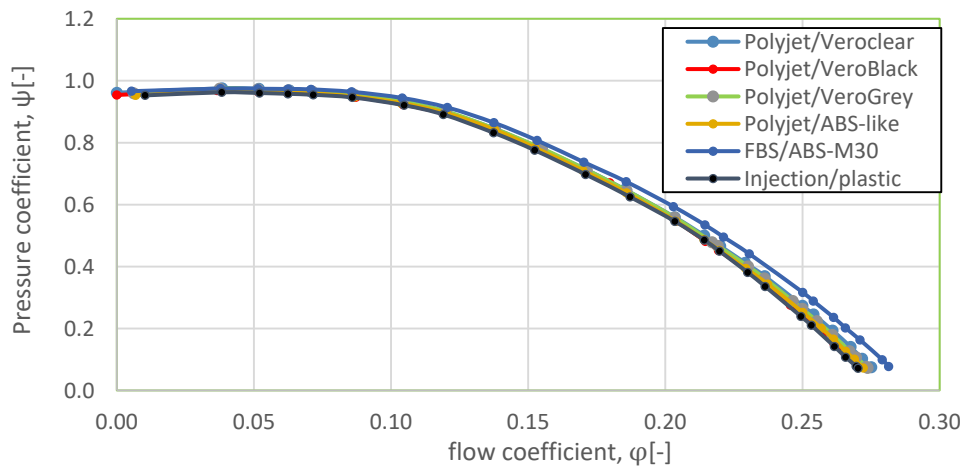


Figure 6.16: Fan output for different 3D printed impellers at 11000 RPM motor speed.

In Figure 6.16, high pressure coefficient is observed in the performance curve of the FBS/ABS-M30 mainly at high volume flow rate. The lowest flow rate was provided by the plastic impeller. With reference to Table 4-1, the impeller manufactured using FBS/ABS- M30 has the highest surface roughness due to high thickness of the material layer during printing. At very low flow rate, no significant change in working pressure was observed. The impeller by injection

technology had a smooth surface. It recorded the lowest flow rate. The Rest of the impellers that were printed with Polyjet, had their performance curve between the impellers printed by FBS/ABS- M30 and the injection/plastic. This means that the working pressure increased with increasing blade thickness. Therefore, Surface roughness of the impeller may increase the power transferred to fluid by the impeller, and also reduce losses at the impeller inlet section [15]. Therefore, the air leakage between the hub and the impeller is minimized. Since this effect is significant at low flow rate, it may be sufficient to say that the surface roughness of impeller affects fan performance at low flow rate. However, it was observed by Toshio mashimo [29] that surface roughness affects the efficiency of the impeller. He observed that when the impeller roughness is increased, there is high friction between adjacent blades resulting in high friction loss. This reduced the efficiency of the impellers especially at high flow coefficient. This means that efficiency increases with smooth blade surface.

6.2.2 Results for Impellers with Straights Blades

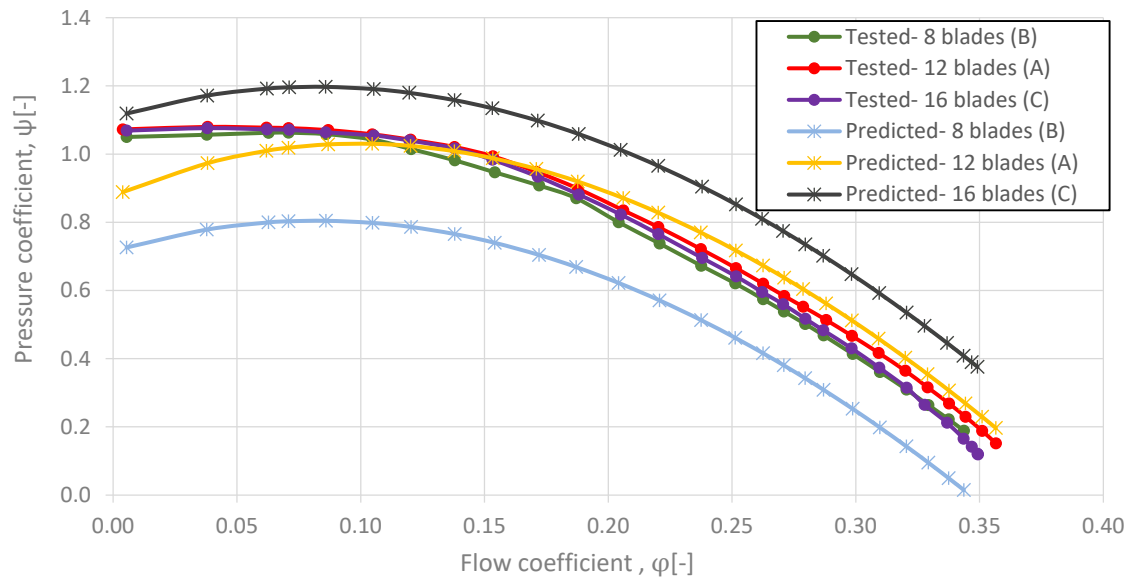


Figure 6.17: Impellers with 8, 12 and 16 straight blades, $\beta_1 = \beta_2 = 90^\circ$.

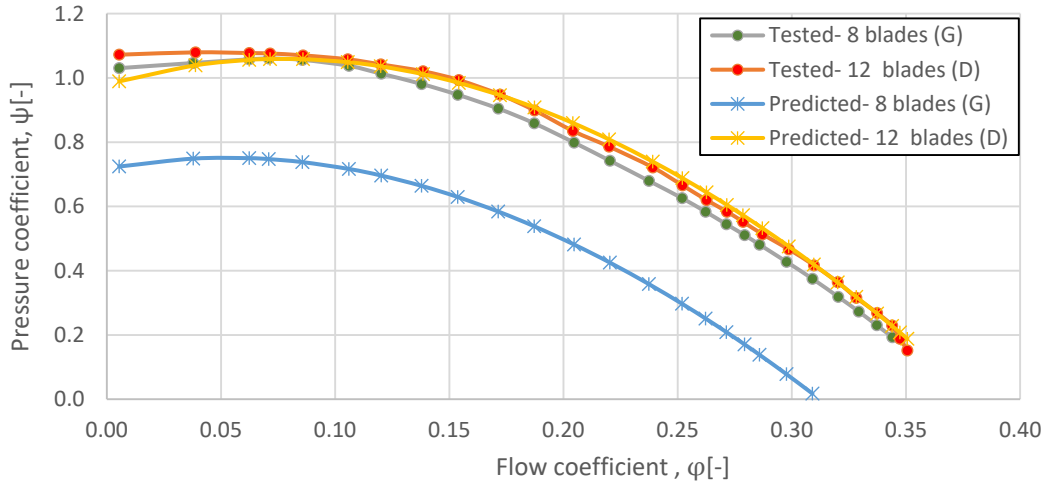


Figure 6.18: Impellers with 8 and 12 straight blades, $\beta_1=80^\circ$, $\beta_1=85^\circ$.

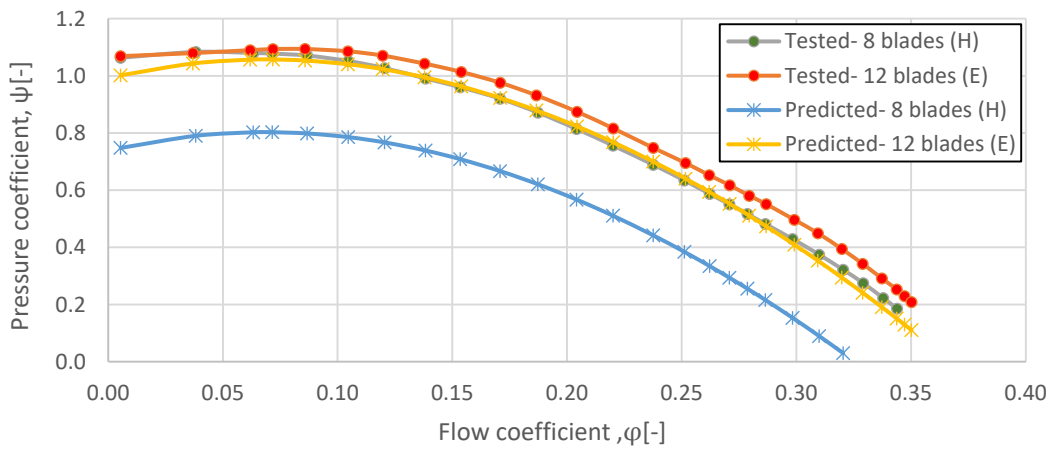


Figure 6.19: Impellers with 8 and 12 straight blades, $\beta_1=60^\circ$, $\beta_1=76^\circ$.

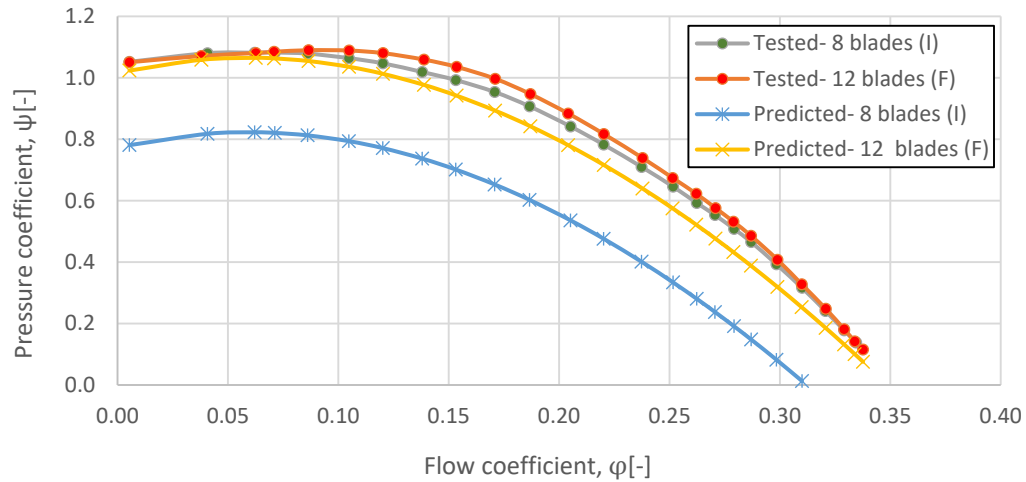


Figure 6.20: Impellers with 8 and 12 straight blades, $\beta_1=40^\circ$, $\beta_2=68^\circ$.

Figure 6.16 to Figure 6.19 revealed how impellers with different number of blades affect fan performance. From the tested results, it was observed in all the graphs that the performance curves of the tested impellers, A, D, E and F, all having 12 blades, are able to generate higher pressure than their corresponding impellers with 8 blades, namely, B, G, H and I. This is because as the number of blades increases, the pressure loss due to flow separation decreases. Therefore, this results in an increase in the pressure of the fan. However as shown in Figure 6.16, at low flow coefficient values, it was observed that impeller C having 16 blades is able to generate lower pressure than impeller A. As the flow increases, the pressure of impeller C drops below the pressure of impeller B. This means that the impeller C has unstable operation. This could be due to high blade friction loss resulting from high number of blades causing the narrowing of the flow area. Furthermore, when the curves of the test results were compared with the curves predicted by analytical calculations, it was noticed that the analytical calculations were able to quite predict the curves for the 12 blade impellers than for the 8 blade impellers. The pressure coefficient values predicted by the analytical solution for the 8 blade impellers were higher than the tested values. Mwinuka [9] also analysed the effect of blade number on fan performance. He recorded an increase in the working pressure of fan at high number of blades. Several researchers including Amjadimanesh et al. [30] have reported an increase in pressure of fans with increasing blade number. However, there is always an optimum number of blades depending on the fan design. This is because large number of blades may result to high flow friction between the blades. Frank P. Bleier [10] reported that optimum range may be from 5 to 12 blades.

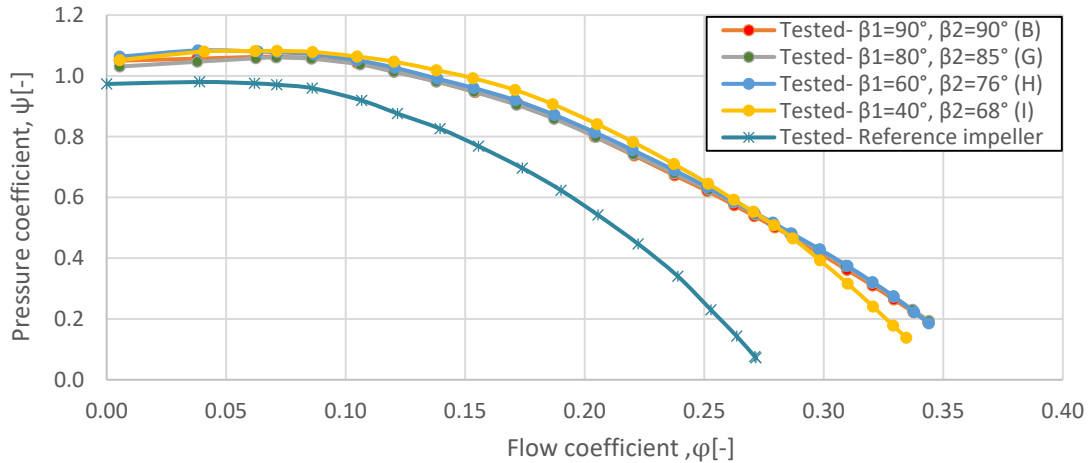


Figure 6.21: Comparison between reference impeller and impellers with 8 straight blades having different blade angles.

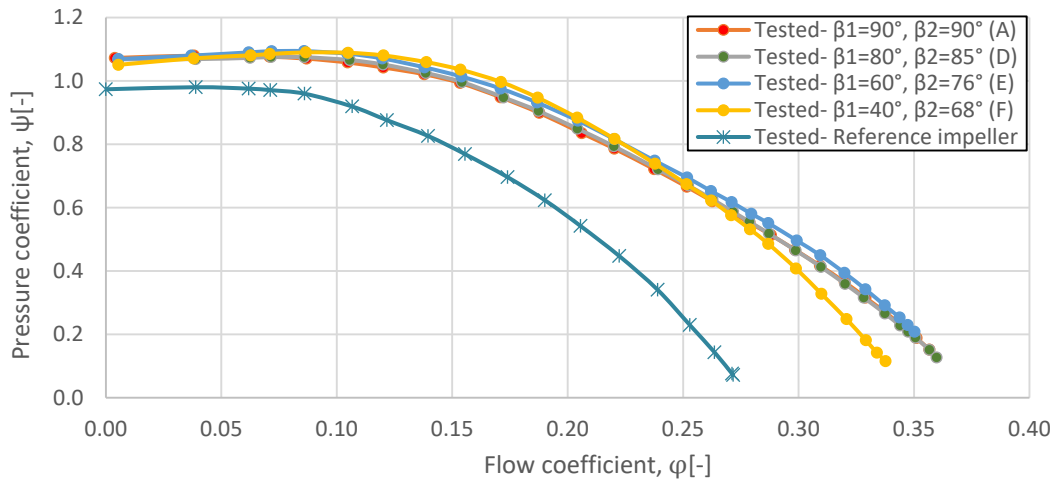


Figure 6.22: Comparison between reference impeller and impellers with 12 straight blades having different blade angles.

In Figure 6.20 and Figure 6.21, the inlet blade angle, β_1 , was varied for the same number of blades. The results were compared with the reference impeller. It is evident from the two graphs above that the impellers with straight blades are able to generate higher pressure than the reference fan. In addition, they are able to reach very high flow rate. Therefore, these may not be suitable for this application.

Comparing the different inlet blade angles, $\beta_1 = 90^\circ, 80^\circ, 60^\circ,$ and 40° , it was observed that the varied inlet angles had no significant effect on the performance of the fan. However, the impeller with $\beta_1 = 40^\circ$ was observed to drop in pressure at higher flow. Experiment conducted by Meng et

al. [18] on the effect of inlet blade angle on centrifugal fan revealed that the flow curve for centrifugal fans with varying inlet blade angle affects the shaft power. This results in a decrease in pressure head of the fan. This was observed at low flow rate for inlet blade angle, $\beta_1=40^\circ$ corresponding to impellers I and F. Meanwhile, impellers with inlet blade angles 90° , 80° and 40° had their performance curves almost undistinguishable.

6.2.3 Results for Impellers with Backward Curved Blades

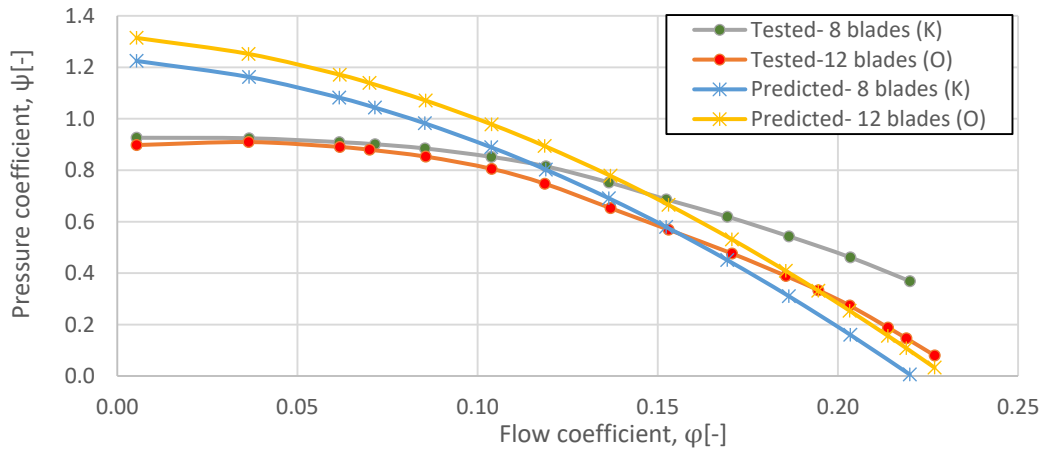


Figure 6.23: Impellers with 8 and 12 backward curved blades, $\beta_1=80^\circ$, $\beta_2=20^\circ$.

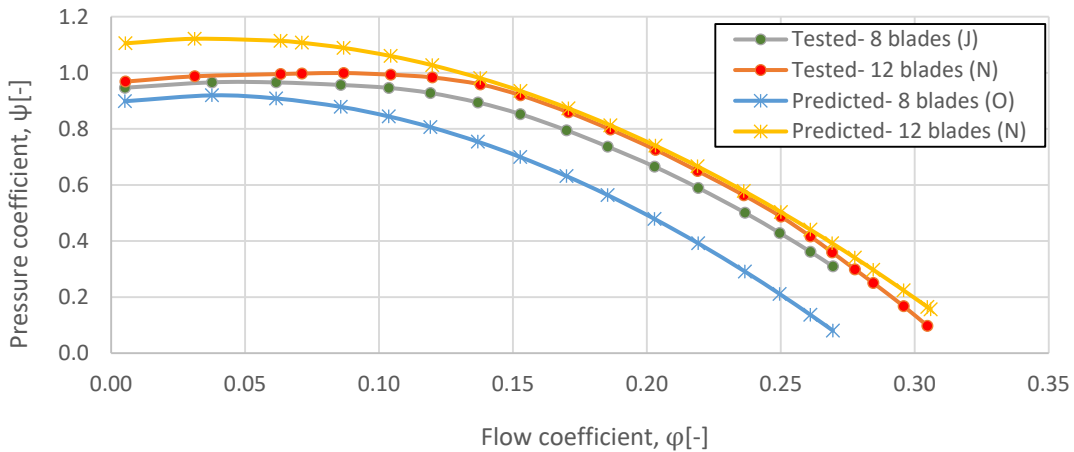


Figure 6.24: Impellers with 8 and 12 backward curved blades, $\beta_1=80^\circ$, $\beta_2=50^\circ$.

For this group of impellers, comparison was made at constant blade angles, β_1 and β_2 , but with varied number of blades. It is evident in Figure 6.23 that the analytical calculation could not predict the performance curves for the entire flow coefficient values irrespective of the

impeller's blade number. For impeller N having 12 blades, $\beta_1=80^\circ$ and $\beta_2=50^\circ$, the curve from the analytical calculation followed closely the curve of the experimentally tested impeller at middle and higher flow rates. However, for impeller J having 8 blades, the analytical solution was not able to predict the performance curve at higher flow rates. In Figure 6.24 the predicted curve only followed closely the curve for tested impeller O at higher flow. The predicted curve for impeller K deviates greatly.

Furthermore, comparing the number of blades for the same β_1 and β_2 shows that at high flow, the number of blades required for high fan performance for $\beta_1=80^\circ$ and $\beta_2=20^\circ$ is 8 blades. This is very significant at high flow coefficient values as seen in Figure 6.23. Conversely, in Figure 6.24, the number of impeller blades required for higher fan performance for $\beta_1=80^\circ$ and $\beta_2=50^\circ$ is 12 blades. This means that increasing the number of impeller blades does not necessarily translate into high fan performance. Other parameters such as the blade geometry may also influence the fan performance.

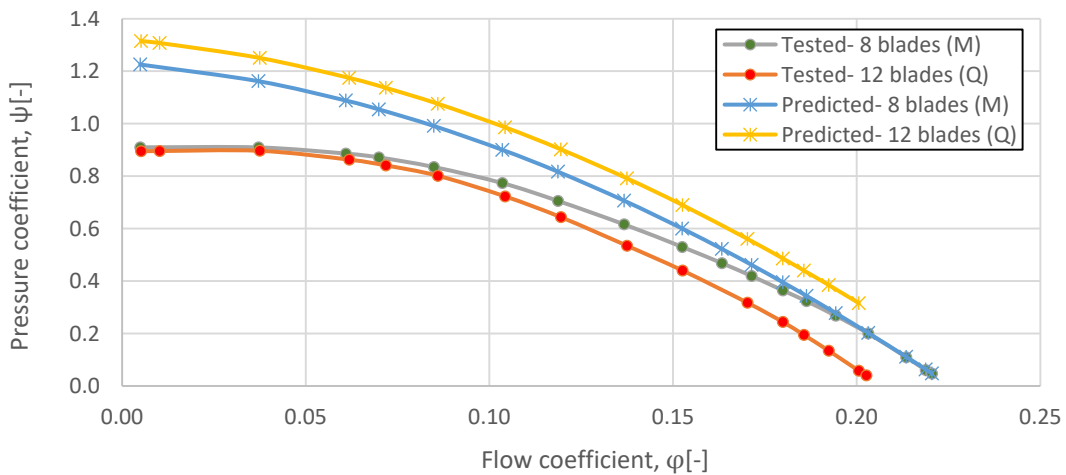


Figure 6.25: Impellers with 8 and 12 backward curved blades, $\beta_1=40^\circ$, $\beta_2=20^\circ$.

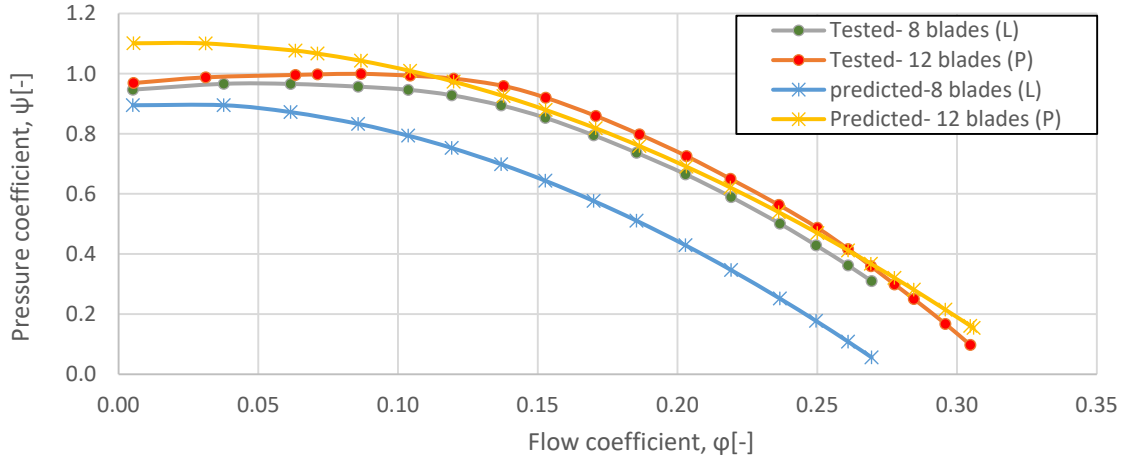


Figure 6.26: Impellers with 8 and 12 backward curved blades, $\beta_1=40^\circ$, $\beta_2=50^\circ$.

It can be noticed in Figure 6.25 that the number of blades required for high fan performance for $\beta_1=40^\circ$, $\beta_2=20^\circ$ is 8 blades. Conversely, in Figure 6.26, the number of impeller blades required for higher fan performance for $\beta_1=80^\circ$ and $\beta_2=20^\circ$ is 12 blades. Hence, this somehow confirms that there is an optimum blade number depending on the blade construction and fan design required to achieve high pressure at increasing blade number as indicated by Bleier [10] in his book.

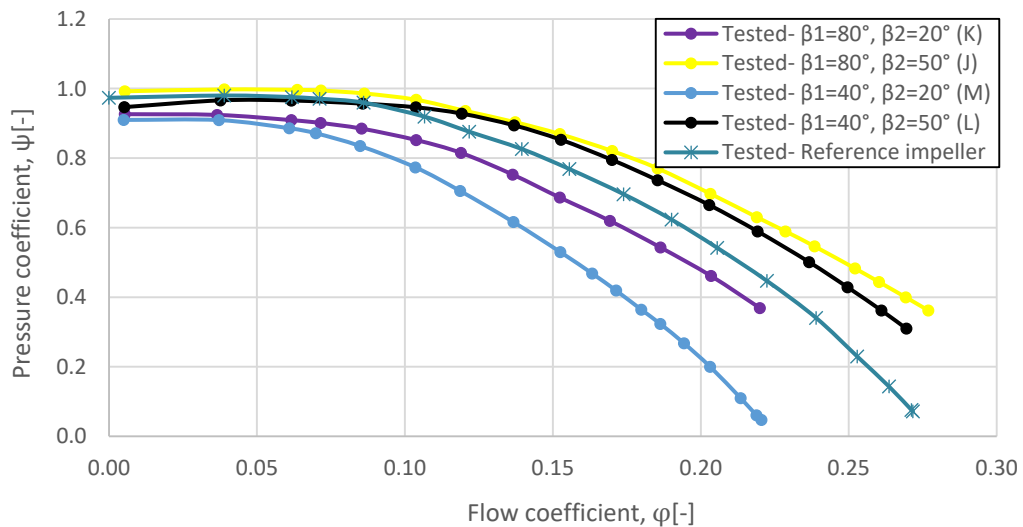


Figure 6.27: Comparison between the reference impeller and impellers with 8 backward curved blades and varying β_1 , β_2 .

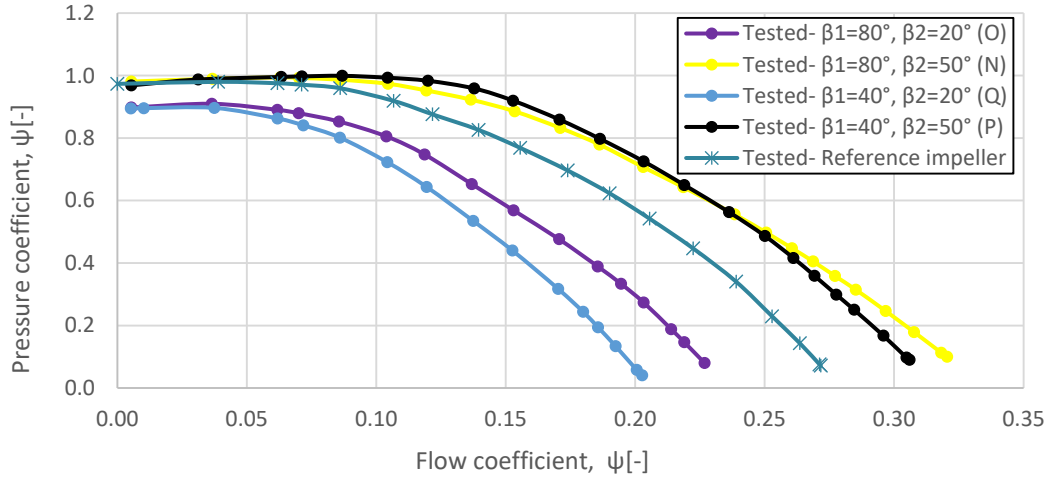


Figure 6.28: Comparison between the reference impeller and impellers with 12 backward curved blades and varying β_1 , β_2 .

Figure 6.27 and Figure 6.28 demonstrate the effects of varying β_1 and β_2 on fan performance. Comparing impellers K with M, and N with Q, it can be observed that at $\beta_2=20^\circ$, impellers with $\beta_1=80^\circ$ are able to generate higher pressure at lower flow rate than the impellers with $\beta_1=40^\circ$. However, there is no significant difference in the performance curves of the impellers with $\beta_2=50^\circ$ because their performance curves did not vary irrespective of the blade inlet angles.

However, considering impellers with the same blade number and blade inlet angle, there is a very significant difference between the performance curves at varying outlet blade angles. From theory, an increase in β_2 leads to a decrease in $\cot(\beta_2)$, hence leading to an increase in pressure head. This result agrees with results obtained by Chen-Kang Huang and Mu-En Hsieh [17], who also observed an increase in pressure at higher flow rate when β_2 was increased from 40° to 50° . This effect is seen by comparing impeller K with J and N with Q Figure 6.26. Similar trend is observed when N is compared with O, and Q with P as shown in Figure 6.28.

The blades were also compared with the reference blades. It can be observed from the two figures above that the performance curve of the reference fan lies between the two outlet blade angles. Therefore the performance of the reference fan can be obtained by modifying the blade geometry. This may be achieved if the outlet angle is chosen between 20° and 50° .

6.2.4 Results for Modified Backward Curved Impellers

6.2.4.1 Impellers with Large Number of Blades

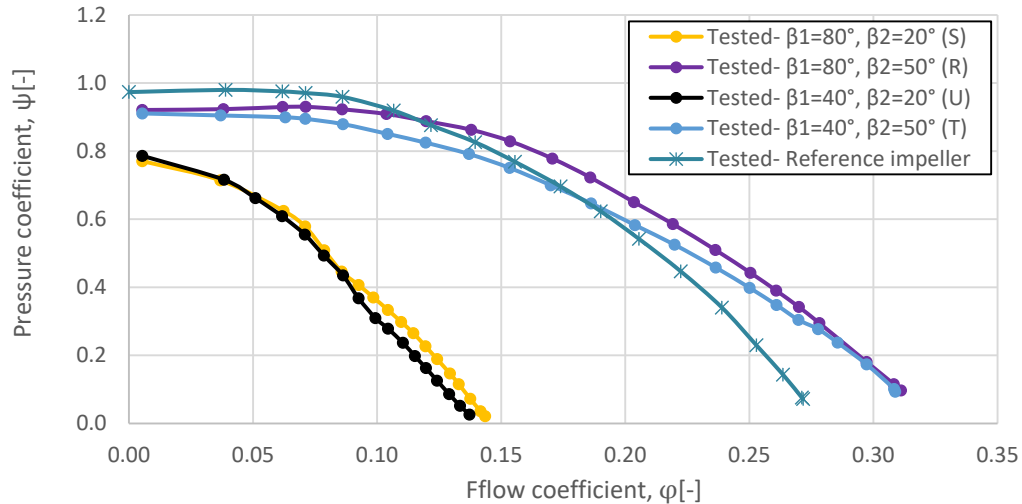


Figure 6.29: Impellers with 24 backward curved blades, and varying blade angles compared with reference impeller

In Figure 6.29 the effect of having large number of blades on fan performance was investigated. This was tested for varying blade angles. For the same β_2 , the performance curves were very close as observed in the curves for impellers S and U, and impellers R and T. However, the impellers with $\beta_1=80^\circ$ generate a higher pressure as the flow increases. The change in pressure was very prominent at constant inlet blade angle and varying outlet blade angle. When the curves of the fan with impellers S and R, and U and T are compared, the performance curves of R and T are observed generate a higher pressure than their corresponding impellers S and U. Therefore, the outlet blade angle for this type of impellers has significant effect on fan performance than the inlet blade angles.

It is also observed that the performance curves of impellers R and T are much closer to the performance curve of the reference impeller. Unlike impellers N and P in Figure 6.28 which were characterised by higher pressure at increasing flow, the pressures at high flow for impellers R and T were less. It can be said that the extra number of blades decreased the flow area at the impeller outlet. This resulted in an increase in flow velocity, thereby, resulting in a decrease in the fan working pressure.

6.2.4.2 Impellers with Short Blades

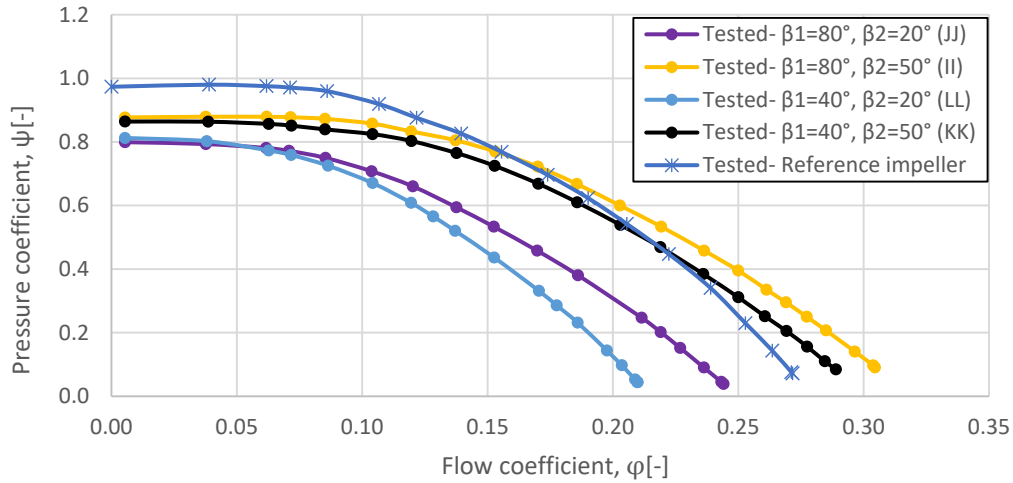


Figure 6.30: Impellers with short blades and varying blade angles compared with reference impeller

In Figure 6.30 the effect of having short impellers within main impeller blades were analyzed. This was also tested for varying blade angles. It is observed that for the same outlet blade angle, increasing the inlet blade angle resulted in an increase in pressure at higher flow. This was observed when the curves for impellers JJ and II are compared with impellers LL and KK, respectively.

The effect of varying the outlet blade angle resulted in significant difference between the performance curves for the same inlet blade angle. This is observed when impeller JJ is compared with II and when LL is compared with KK. Therefore, this type of modification is suitable when the impellers operate at $\beta_2 = 50^\circ$.

It is also observed that the performance curves of impellers II and LL are much closer to the performance curve of the reference impeller than KK and JJ. However, it can be observed from the graph that the impellers II and LL are not able to reach higher pressure at low flow. This is because the short blades increase the friction at the inlet of the impeller causing reduction of the energy transmitted to the air.

6.2.4.3 Impellers with Varying Blade Pitch Angle

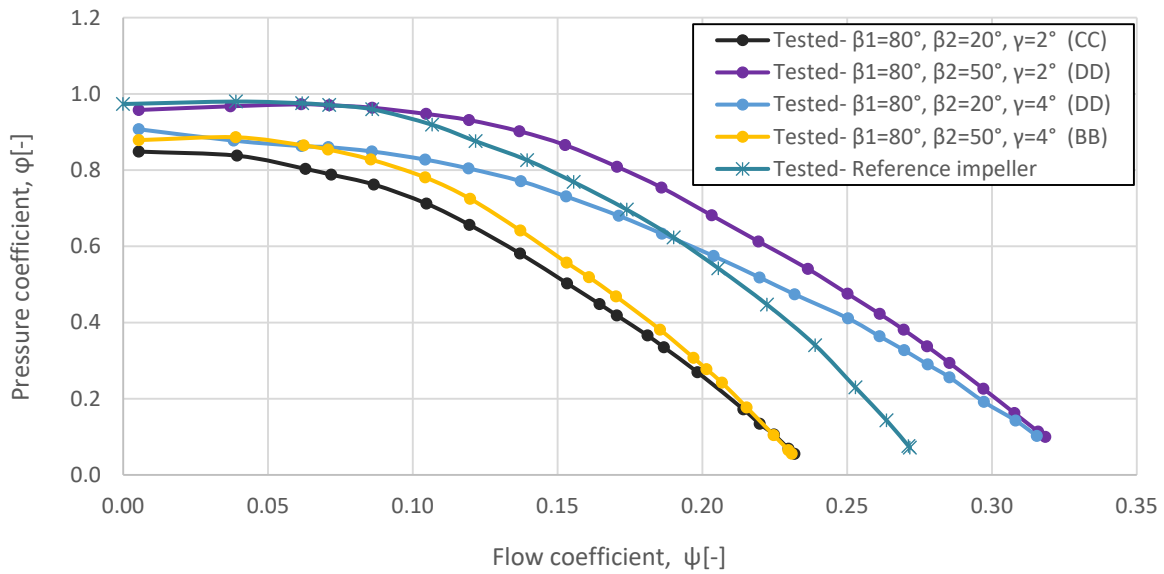


Figure 6.31: Impellers with 12 backward curved blades, 2° and 4° pitch difference, $\beta_1=80^\circ$ compared with reference impeller.

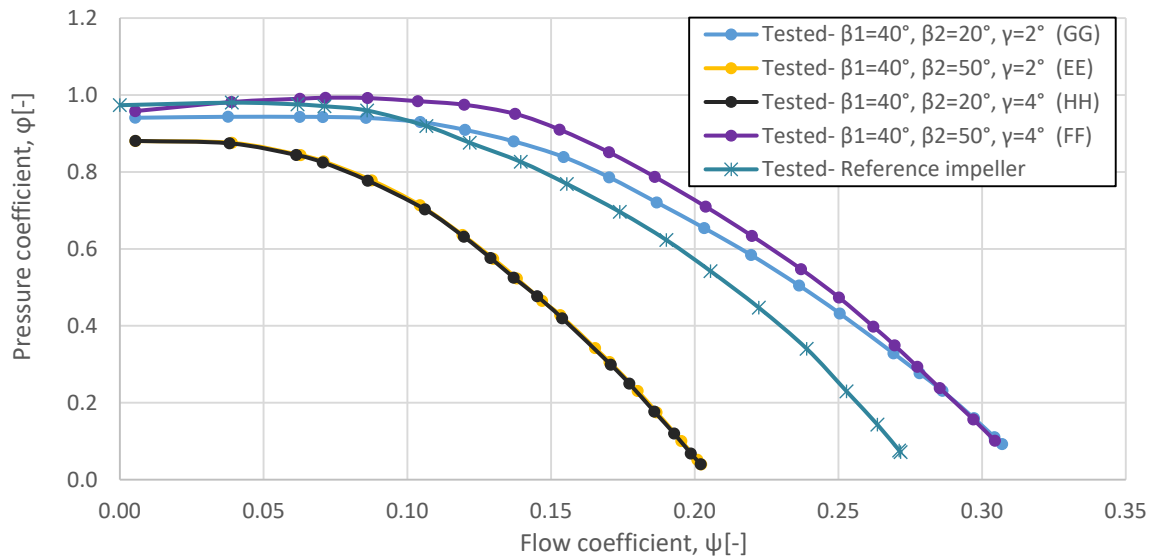


Figure 6.32: Impellers with 12 backward curved blades, 2° and 4° pitch difference, $\beta_1=40^\circ$ compared with reference impeller.

These groups of impellers were designed in order to investigate the effect of different blade pitch angles on the fan performance. Initially, the impellers were compared when the blade inlet angle was constant. It is evident from Figures 6.31 and 6.32 that the inlet blade angle has no

significant effect on the fan at high flow rate. In fact, at $\beta_1 = 40^\circ$, the performance curve for $\beta_2 = 50^\circ$ and $\beta_2 = 20^\circ$ are almost undistinguishable. For the same blade angles, varying the difference in blade pitch angle, γ , only results in a difference in performance curve at low flow rate. It can be observed from Figure 6.31 that the impeller with $\gamma = 4^\circ$ generates higher pressure than the impeller with $\gamma = 2^\circ$. This is also evident in Figure 6.32 when the performance curves of impellers EE and FF are compared. Also, the same phenomenon is observed when impellers GG and HH are compared. As revealed by Lyons [21] on his research on blowers, noise frequencies are produced as blades go pass fan volute cut off regions. It can be explained that for impellers having different blade pitch angles, the frequency of the noise increases. However, from the graph it can also be seen that as γ increases the intensity of the noise increases thereby reducing the working pressure of the fan. Lonkar [20] revealed that increasing the distance between the blade and the cutoff leads to a favourable aerodynamic environment, therefore, leading to minimum occurrence of flow resonance frequency. Therefore, for this group of impeller modification, blades operating at $\gamma = 4^\circ$ gives better performance than for $\gamma = 2^\circ$.

When the impellers were compared with the reference impeller, it was observed that the performance curves of impellers GG and DD are much closer to the performance curve of the reference impeller at low flow. Therefore, this group of impellers is more suitable at low air flow.

7 Conclusion

The main objective of this work is to investigate the performance of different impellers of fans used in air-purifying ventilation system. Firstly, literatures were reviewed to understand the various fan design methods, and fan measurement techniques. The fan investigation was completed in three sections: designing a test stand that will be used for experimental measurement, testing the fan impellers, and performing one dimensional fan performance calculations to predict tested results. Results obtained from both analytical calculations and experiments are compared.

The test stand was designed based on set requirements, such as ability to choke the air flow and measure aerodynamic parameters of the fan. The model for the test stand design was proposed and parts were manufactured. Experiments were carried out to first verify the repeatability and dependability of the test stand by operating a typical air-respirator fan having a standard impeller known as the reference impeller. The test stand was verified to have good repeatability after testing the reference impeller at different RPMs: 1100, 900 and 6000 RPM. It was also observed that the impeller position on the motor shaft did not have significant effect on the fan performance after testing for different shaft impeller positions. In addition, the reference fan was operated with a typical air-mask filter and the design point of the fan was noted after testing with an ABEP-R Filter.

Furthermore, measurements were done on impellers with straight and backward curved blades with varying impeller design parameters including blade number, blade inlet and outlet angle. Also, measurements were done on backward curved blade impellers with certain modifications such as addition of short blades to main blades, increasing the number of blades, and varying the blade pitch angle. The results were compared with analytical results. The analytical results were obtained by accounting for the losses which were not accounted for in the ideal flow proposed by the Euler pressure model. Losses such as inter-blade circulation loss, outlet blade loss, inlet blade loss, impeller loss, and volume leakage were considered.

Comparing the various test results and analytical results, it was observed the analytical model was not able to predict very accurately the performance curve for the 8 blade impeller

irrespective of the blade angle. However, the model was able to predict performance curve for the impellers with 12 blades for some blade geometry. Modification of the slip factor loss calculation may aid in better prediction of the performance. The impellers with outlet blade angles 20° have a steeper curve than those impellers with 50° outlet blade angle. Therefore, 50° blade angle is able to reach very high flow compared with the 20° . However, the blade inlet angle did not have significant effect compared to the outlet blade angle. Impellers with short backward curved blades were characterized by low pressure coefficient due to high flow separation at the inlet of the blade. It was also revealed that reducing the flow area caused by increasing the number of impeller blades increased the velocity of air at the outlet. Therefore this resulted in low pressure. Also, varying the blade pitch angles had significant effect on performance such that blades with 4° difference in pitch angle generated higher pressure than those with 2° difference.

The investigation also revealed that at blade outlet angle of 50° , the performance curves for the non-modified impellers showed higher deviation from the reference impeller. However, the curves for the modified impellers having short blades and larger number of blades deviates slightly at blade outlet angle of 50° .

It is recommended that for better prediction of the performance curve, the loss coefficient be examined carefully in order to accurately account for the losses. Also, a vanned diffuser or stator blades can be used to reduce the loss due to swirling. However, care must be taken in the addition of vanes to the diffuser since vanes are known to increase friction losses. If this modification does not produce reasonable results, the inlet section of the design of the volute design must be reconsidered.

8 Reference

- [1] A. Revel and B. P. Huynh, “Characterising Roof Ventilators,” *Australas. Fluid Mech. Conf.*, pp. 1–4, 2007.
- [2] A. C. of G. I. Hygienists, *ACGIH: Industrial Ventilation Manual*, vol. 552. 1998.
- [3] A. Kumar, A. Duvvuru, and I. Patel, “Development and Evaluation of a Software for Design of Industrial Ventilation System,” vol. 20, no. 1, 2000.
- [4] D. Brzezinska and M. Sompolinski, “The accuracy of mapping the airstream of jet fan ventilators by fire dynamics simulator,” *Sci. Technol. Built Environ.*, vol. 4731, 2017.
- [5] C. Tropea, A. L. Yarin, and J. F. Foss, *Springer handbook of experimental fluid mechanics*, no. 1. 2007.
- [6] D. A. Harnish *et al.*, “Challenge of N95 Filtering Facepiece Respirators with Viable H1N1 Influenza Aerosols,” *Infect. Control Hosp. Epidemiol.*, vol. 34, no. 05, pp. 494–499, 2013.
- [7] S. G. Rayhans and B. H. Pathak, *Practical guide to respirator usage in industry*. Elsevier, 2002.
- [8] A. W. Richardson, J. P. Eshbaugh, and K. C. Hofacre, “Respirator filter efficiency testing against particulate and biological aerosols under moderate to high flow rates,” *Battelle Meml. Inst. Columbus*, 2006.
- [9] T. Mwinuka, “Experimental Determination of the Effect of Number of Impeller Blades on the Air Flow Rate and Power Consumption of Centrifugal Blowers,” *Am. Sci. Res. J. Eng. Technol. Sci.*, vol. 17(1), pp. 81–88, 2016.
- [10] F. P. Bleier, *Fan Handbook: Selection, Application, and Design*. McGraw-Hill Education, New York, 1998.
- [11] D. J. Gingery, *How to Design and Build Centrifugal Fans for the Home Shops*. Lindsay Publication, Inc, 1987.
- [12] E. L. Upp and P. J. LaNasa, *Fluid flow measurement: A practical guide to accurate flow measurement*, vol. 1, no. 4. Butterworth—Heinemann, 1990.

- [13] M. Pierce, “Fans and Blowers,” *Energy*, pp. 93–112, 1997.
- [14] J. S. Hunter, “A design philosophy for centrifugal fans,” Laoughborough University Institutional Repository, 1996.
- [15] V. Dvořák, R. Votrubec, J. Šafka, and J. Kracík, “Experimental investigation of centrifugal fans for personal protection equipment – effect of used 3D printing technologies,” *EPJ Web Conf.*, vol. 180, no. January, p. 02023, 2018.
- [16] E. Korkmaz, M. Golcü, and C. Kurbanoğlu, “Effects of blade discharge angle, blade number and splitter blade length on deep well pump performance,” *J. Appl. Fluid Mech.*, vol. 10, no. 2, pp. 529–540, 2017.
- [17] C. K. Huang and M. E. Hsieh, “Performance analysis and optimized design of Backward-Curved airfoil centrifugal blowers,” *HVAC R Res.*, vol. 15, no. 3, pp. 461–488, 2009.
- [18] F.-N. MENG, L.-W. WANG, G.-Z. XIE, F. ZHAO, D.-H. ZHANG, and W.-L. DU, “Effects of Blade Inlet Angle on Flow Field of Centrifugal Fan,” *DEStech Trans. Eng. Technol. Res.*, no. icmecca, pp. 138–144, 2018.
- [19] M. Younsi, F. Bakir, S. Kouidri, and R. Rey, “Influence of impeller geometry on the unsteady flow in a centrifugal fan: Numerical and experimental analyses,” *Int. J. Rotating Mach.*, vol. 2007, 2007.
- [20] P. P. Lonkar, “Effect of cutoff clearance on centrifugal blowernoise : A Review,” *Int. J. Adv. Mech. Civ. Eng.*, vol. 2, no. 4, pp. 16–18, 2015.
- [21] L. A. Lyons, “Effect of Cutoff Configuration on Pure Tones Generated by Small Centrifugal Blowers,” *J. Acoust. Soc. Am.*, vol. 35, 1996.
- [22] S. C. Sugarman, *HVAC Fundamentals*, vol. 53, no. 9. The Fairmont Press, 2005.
- [23] B. J. Mckeon and A. J. Smits, “Static pressure correction in high Reynolds number fully developed turbulent pipe flow,” *Meas. Sci. Technol.*, vol. 13, pp. 1608–1614, 2002.
- [24] R. Shaw, “The influence of the hole dimension on static pressure measurements,” *J. Fluid Mech.*, vol. 7, no. 4, pp. 550–564, 1960.

- [25] I. O. F. STANDARDIZATION, "Measurement of fluid flow by means of pressure differential devices inserted in circular-cross section conduits running full. ISO 5167-2:2003," *Geneva Int. Organ. Stand.*, 2003.
- [26] M. Reader-Harris, *Orifice Plates and Venturi Tubes*. Springer International Publishing, 2015.
- [27] T. Turunen-saaresti, *Computational and experimental analysis of flow field in the diffusers of centrifugal compressors* /, no. February. 2014.
- [28] R. S. R. Gorla and A. A. SKhan, *Turbomachinery*. Marcel Decker, New York, 2003.
- [29] T. Mashimo, "Effect of Surface Roughness of Impeller Channel in Centrifugal Compressor on Its Performance," *SAE Tech. Pap. Ser.*, vol. 1, 2010.
- [30] A. Amjadimanesh, H. Ajam, and A. H. Nezhad, "Numerical Study of Blade Number Effect on the Performance of a 3D FC Centrifugal Fan," *Int. J. Mechatronics, Electr. Comput. Technol.*, vol. 5, no. 15, pp. 2109–2119, 2015.

Appendix
Assembly and part drawings

1 2 3 4

A

A

B

B

C

C

D

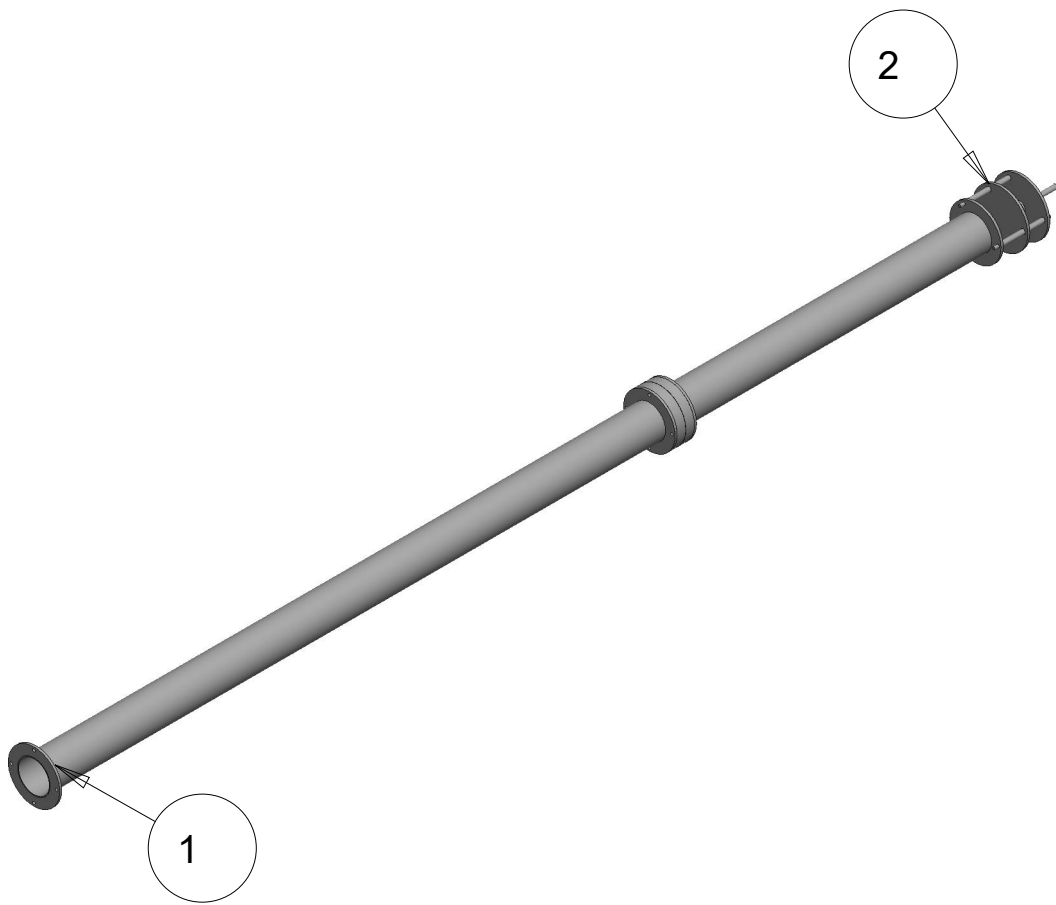
D

E

E

F

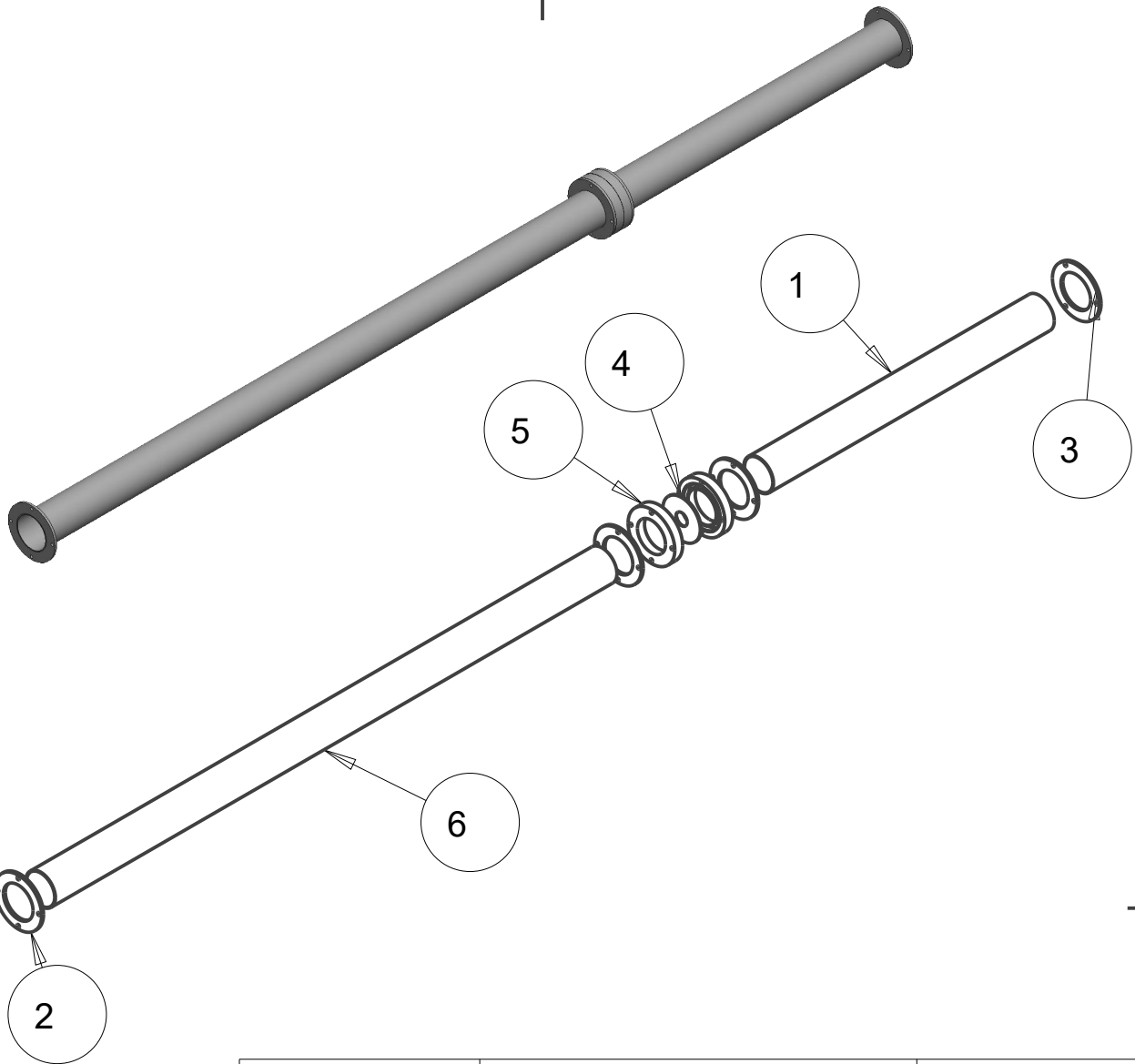
F



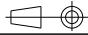

S NO.	SUB ASSEMBLY
1	MEASUREMENT_ASSEMBLY
2	PRESSURE_CONTROL_ASSEMBLY

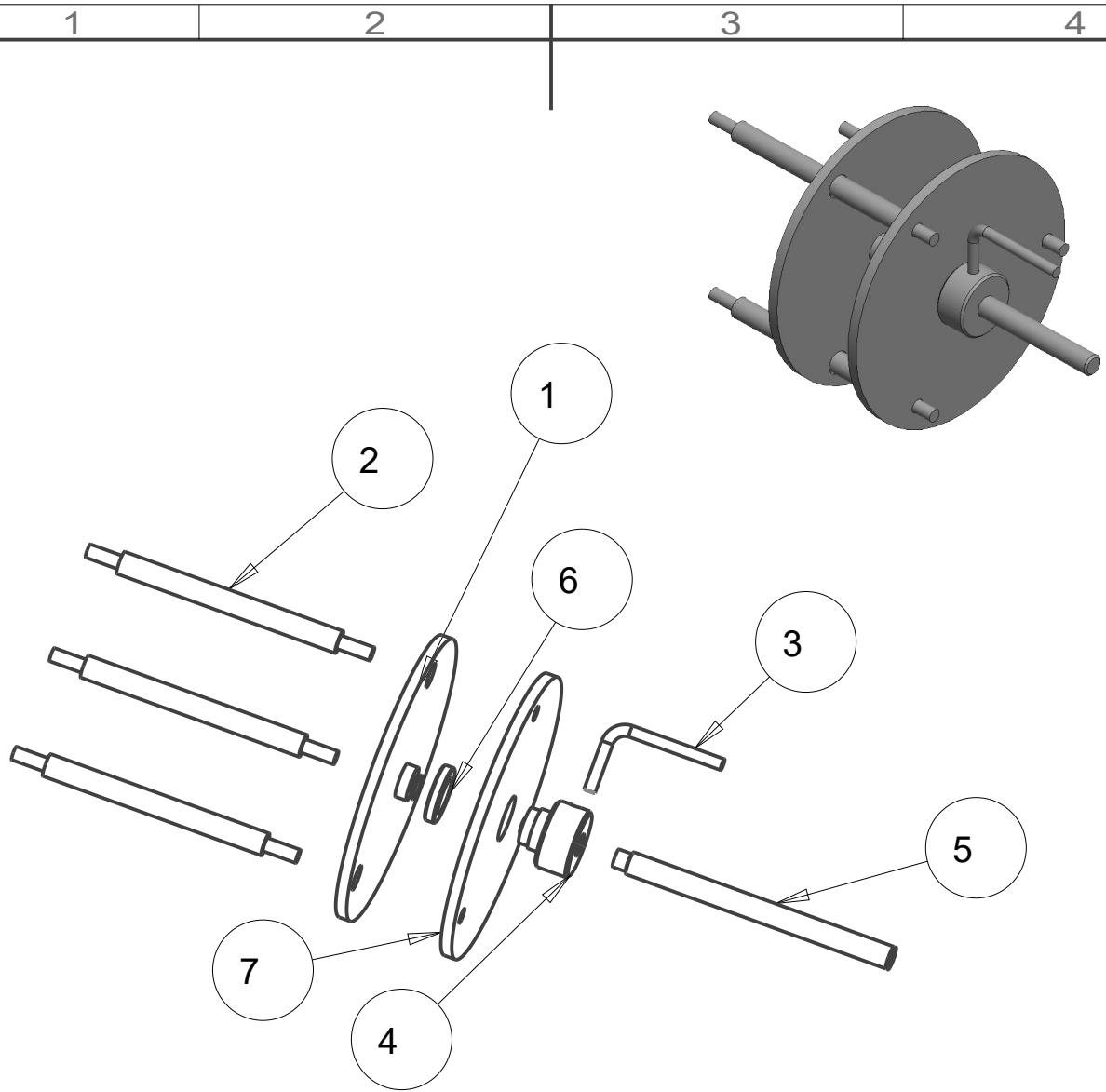
Roz. -Polot.		mm				Presnost Tolerovani		
		c)	Mater.	STAINLESS STEEL	Tr. odp			
		b)	C. hm	Hr. hm.				
		a)						
Zmena		Datum	Index	Podpisy	TECHNICKÁ UNIVERZITA V LIBERCI www.tul.cz			
Meritko	Pozn.	Navrhl						Nazev TEST STAND ASSEMBLY
0.080		Kreslil	GAFARU MORO		Cis. vykresu			
C. seznamu		Prezkousel						list 1 listu 1
C. sestavy		Technolog						
Stary vykr.		Normaliz.						
Novy vykr.		Schválil						
		Datum	Apr-24-19					

1 2 3 4



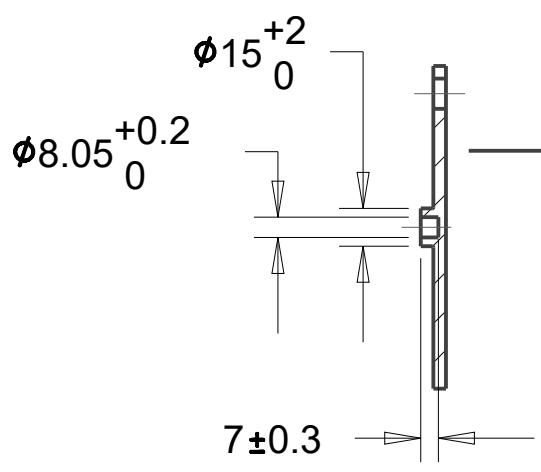
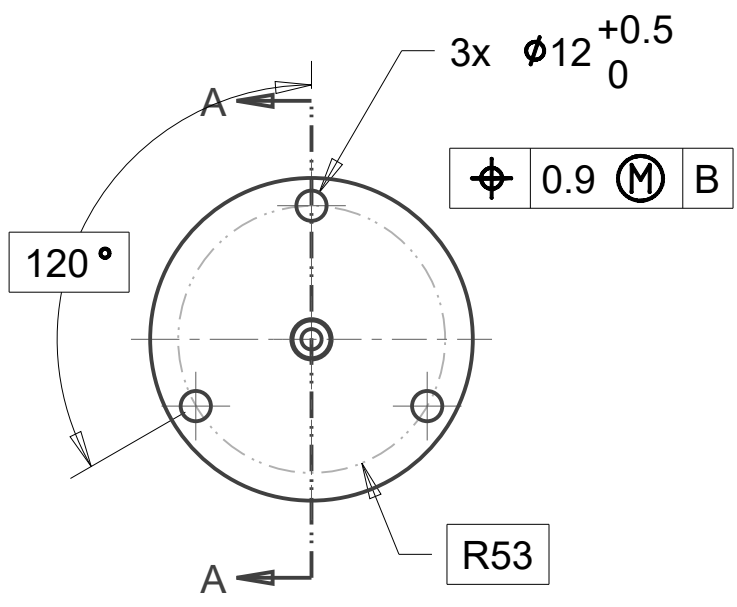
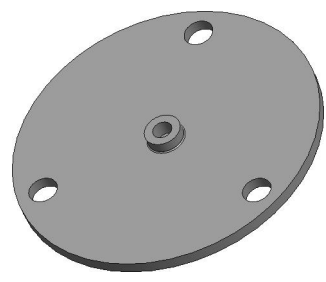
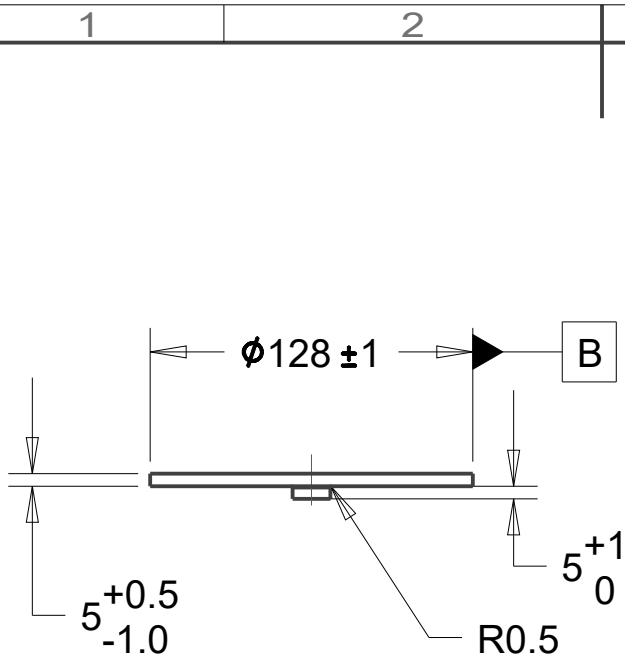
S.No.	PART NAME	QUANTITY
1	DOWNSTREAM_PIPE	1
2	FLANGE_1	3
3	FLANGE_2	1
4	ORIFICE_PLATE	1
5	TAPPING_SLOT	2
6	UPSTREAM_PIPE	1

Roz. -Polot.		mm				Presnost	
		c)	Mater.	STAINLESS STEEL	Tr. odp	Tolerovani	
		b)	C. hm		Hr. hm.		
		a)					
Zmena		Datum	Index	Podpisy			
Meritko	Pozn.	Navrhl					
0.080		Kreslil	GAFARU MORO				
C. seznamu		Prezkousel					
C. sestavy		Technolog					
Stary vykr.		Normaliz.					
Novy vykr.		Schvalil					
		Datum	Apr-24-19				
				 TECHNICKÁ UNIVERZITA V LIBERCI www.tul.cz			
				Nazev MEASUREMENT ASSEMBLY			
				Cis. vykresu			
				list 1			
				listu1			



S.No,	PART NAME	QUANTITY
1	CONTROL_PLATE	1
2	GUIDING_ROD	3
3	HANDLE	1
4	KNOB	1
5	MOVING_SCREW	1
6	RETAINING_RING	1
7	RIGID_PLATE	1

Roz. -Polot.		mm				Presnost	
		c)	Mater.	STAINLESS STEEL	Tr. odp	Tolerovani	
		b)	C. hm	Hr. hm.			
		a)					
Zmena		Datum	Index	Podpisy			
Meritko	Pozn.	Navrhl					
0.333		Kreslil	GAFARU MORO				
C. seznamu		Prezkousel					
C. sestavy		Technolog					
Stary vykr.		Normaliz.					
Novy vykr.		Schvalil					
		Datum	Apr-24-19				
				TECHNICKÁ UNIVERZITA V LIBERCI www.tul.cz			
				Nazev BACKPRESSURE CONROL ASSEMBLY			
				Cis. vykresu			
				list 1 listu1			



SECTION A-A

NOTES:

1. BREAK SHARP EDGES.
2. ALL CORNER FILLET R0.4 MAX
3. SURFACE FINISH 3.2 um

Roz. -Polot.		mm				Presnost		
		c)	Mater.	STAINLESS STEEL	Tr. odp	Tolerovani		
		b)	C. hm	Hr. hm.				
		a)			TECHNICKÁ UNIVERZITA V LIBERCI www.tul.cz			
Zmena		Datum	Index	Podpisy				
Meritko	Pozn.	Navrhl						
0.333		Kreslil	GAFARU MORO					
		Prezkousel						
C. seznamu		Technolog			Nazev	CONTROL PLATE		
C. sestavy		Normaliz.						
Stary vykr.		Schvallil			Cis. vykresu	list 1 listu 1		
Novy vykr.		Datum	Apr-23-19					

1

2

3

4

A

A

B

B

C

C

D

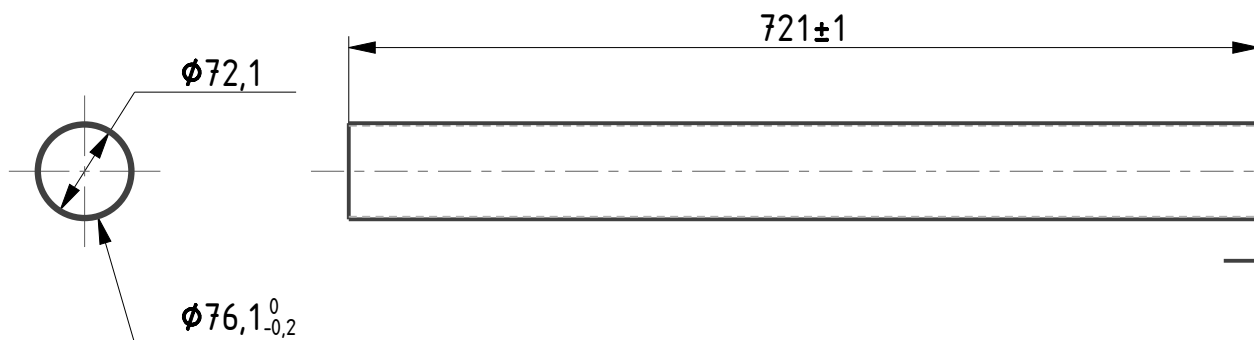
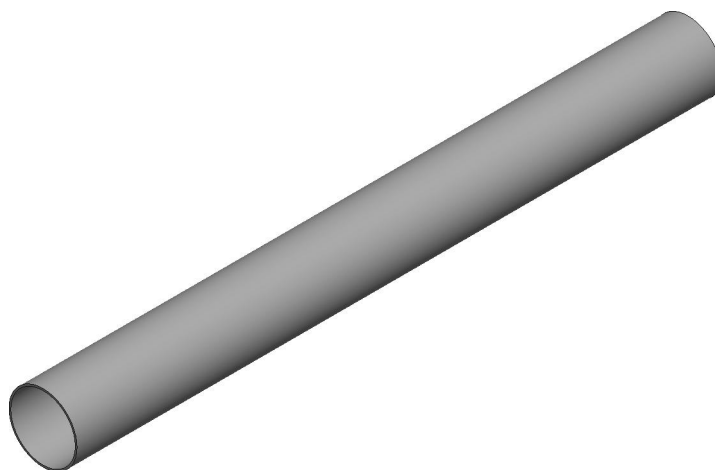
D

E

E

F

F



NOTES:

1. BREAK SHARP EDGES.
2. SURFACE FINISH 3.2 μm

Roz. - Polot.		mm						Presnost Tolerovani	
		c)	Mater.		STAINLESS STEEL	Tr. odp			
		b)	C. hm		Hr. hm.				
		a)							
Zmena		Datum	Index	Podpisy	TECHNICKÁ UNIVERZITA V LIBERCI www.tul.cz				
Meritko	Pozn.	Navrhl							
0,167		Kreslil	GAFARU MORO		Nazev DOWNSTREAM PIPE				
C. seznamu		Prezkoušel							
C. sestavy		Technolog			Cis. vykresu				
Stary vykr.		Schválil							
Novy vykr.		Datum	Apr-24-19		list 1 listu 1				

1

2

3

4

1

2

3

4

A

A

B

B

C

C

D

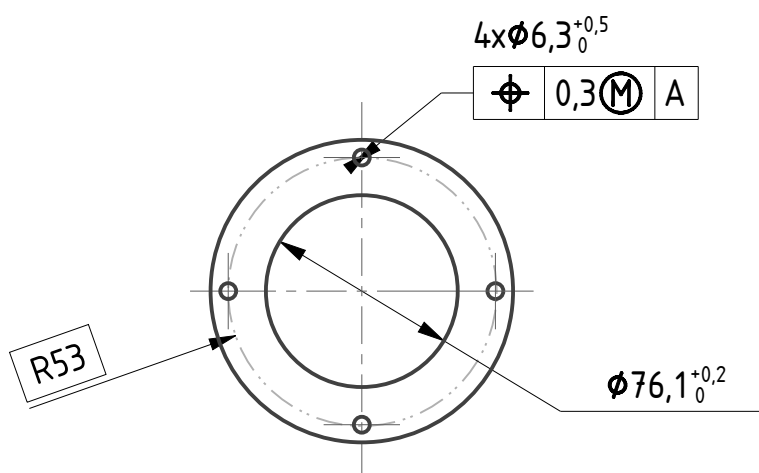
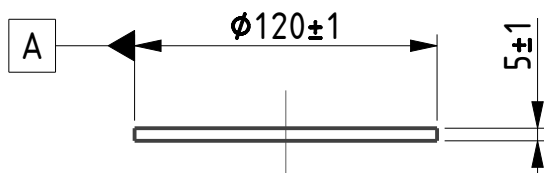
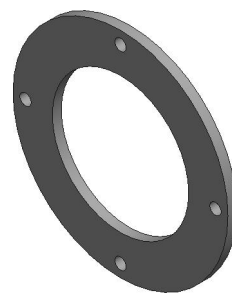
D

E

E

F

F



NOTES:

1. BREAK SHARP EDGES.
2. ALL CORNER FILLET R0.4 MAX
3. SURFACE FINISH 3.2 μm

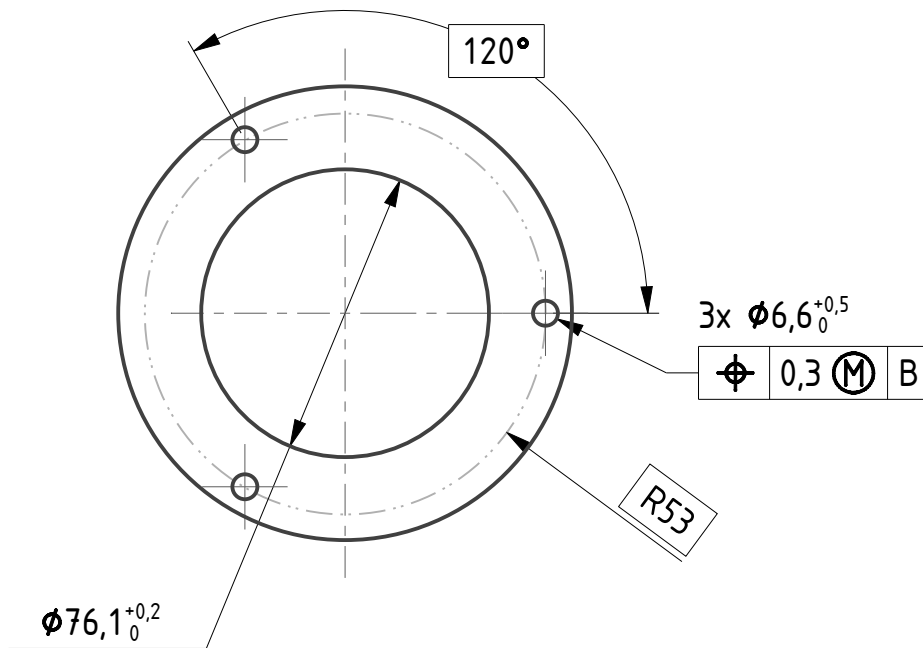
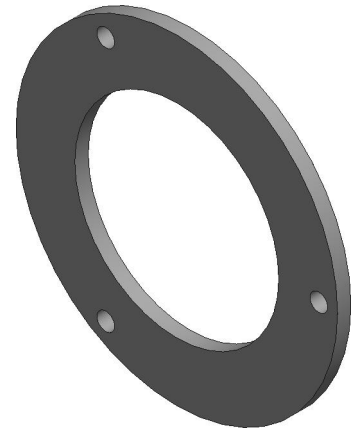
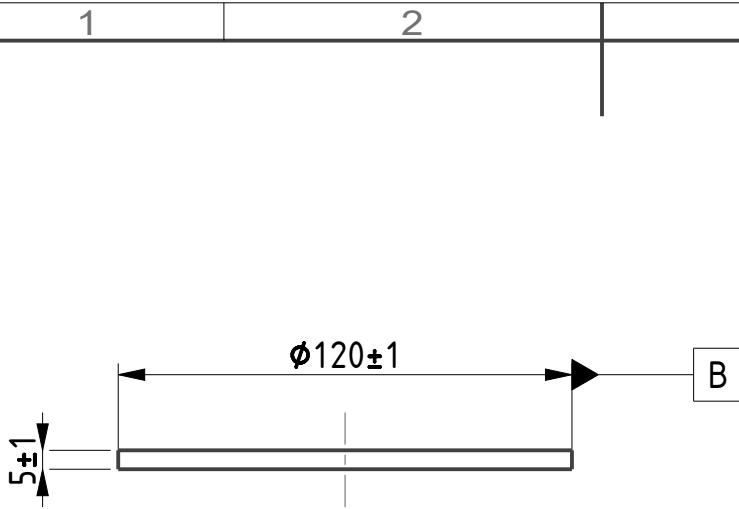
Roz. - Polot.		mm						Presnost Tolerovani	
		c)		Mater.	STAINLESS STEEL	Tr. odp			
		b)		C. hm		Hr. hm.			
		a)							
Zmena		Datum	Index	Podpisy	TECHNICKÁ UNIVERZITA V LIBERCI www.tul.cz				
Meritko	Pozn.	Navrhl							
0,333		Kreslil	GAFARU MORO		Nazev FLANGE 1				
C. seznamu		Prezkousel							
C. sestavy		Technolog			Cis. vykresu				
Stary vykr.		Schvalil							
Novy vykr.		Datum	Apr-24-19		list 1 listu 1				

1

2

3

4



NOTES:

1. BREAK SHARP EDGES.
2. ALL CORNER FILLET R0.4 MAX
3. SURFACE FINISH 3.2 μ m

Roz. - Polot.		mm				Presnost Tolerovani	
		c)		Mater.	STAINLESS STEEL	Tr. odp	
		b)		C. hm		Hr. hm.	
		a)					
Zmena		Datum	Index	Podpisy	TECHNICKÁ UNIVERZITA V LIBERCI www.tul.cz		
Meritko	Pozn.	Navrhl					
0,500		Kreslil	GAFARU MORO		Nazev FLANGE 2		
C. seznamu		Prezkousel					
C. sestavy		Technolog			Cis. vykresu		
Stary vykr.		Normaliz.					
Novy vykr.		Schvalil			list 1 listu 1		
		Datum	Apr-24-19				

1

2

3

4

A

A

B

B

C

C

D

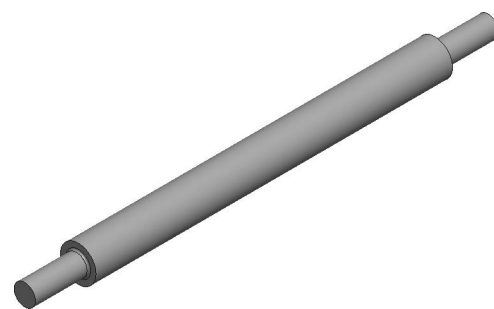
D

E

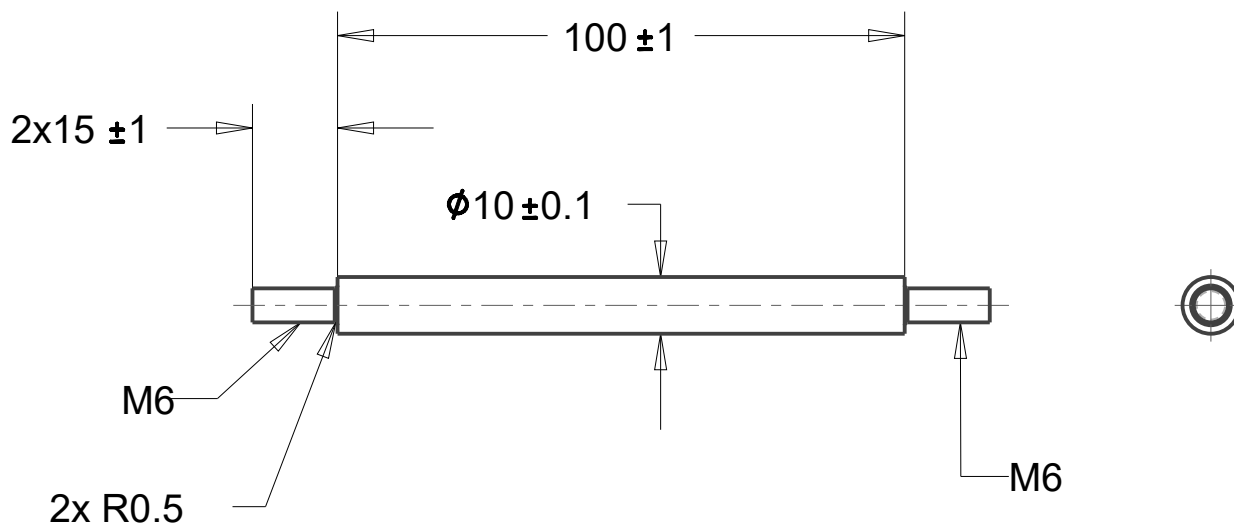
E

F

F




SCALE 0.667



NOTES:

1. BREAK SHARP EDGES.
2. ALL CORNER FILLET R0.4 MAX
3. SURFACE FINISH 3.2 μm

Roz. -Polot.		mm						Přesnost Tolerovani	
		c)		Mater.	STAINLESS STEEL	Tr. odp			
		b)		C. hm		Hr. hm.			
		a)		 TECHNICKÁ UNIVERZITA V LIBERCI www.tul.cz					
Zmena		Datum	Index						
Meritko	Pozn.	Navrhl			Nazev GUIDING ROD				
0.750		Kreslil	GAFARU MORO						
C. seznamu		Technolog			Cis. vykresu				
C. sestavy		Normaliz.							
Stary vykr.		Schválil			list 1 listu 1				
Novy vykr.		Datum	Apr-24-19						

1

2

3

4

1

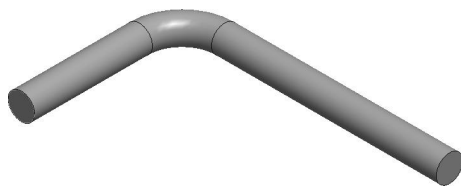
2

3

4

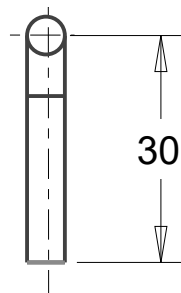
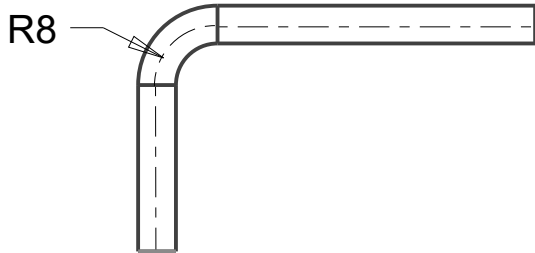
A

A



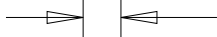
B

B



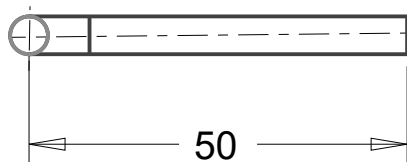
C

C

 $\varnothing 5 \begin{matrix} 0 \\ -0.2 \end{matrix}$


D

D



NOTES:

1. BREAK SHARP EDGES.
2. ALL CORNER FILLET R0.4 MAX
3. SURFACE FINISH 3.2 μ m

E

E

Roz. -Polot.		mm						Presnost Tolerovani	
		c)		Mater.	STAINLESS STEEL	Tr. odp			
		b)		C. hm		Hr. hm.			
		a)							
Zmena		Datum	Index	Podpisy	TECHNICKÁ UNIVERZITA V LIBERCI www.tul.cz				
Meritko	Pozn.	Navrhl							
1.000		Kreslil	GAFARU MORO		Nazev HANDLE				
C. seznamu		Prezkousel							
C. sestavy		Technolog			Cis. vykresu				
Stary vykr.		Schválil							
Novy vykr.		Datum	Apr-24-19		list 1 listu 1				

F

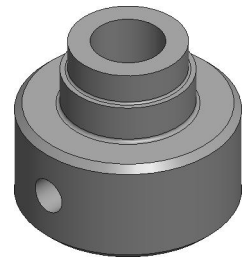
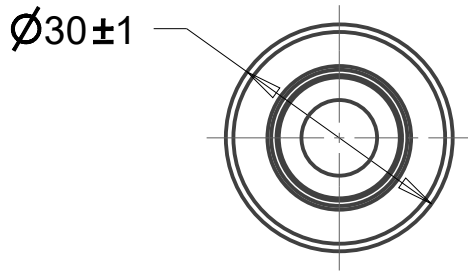
F

1

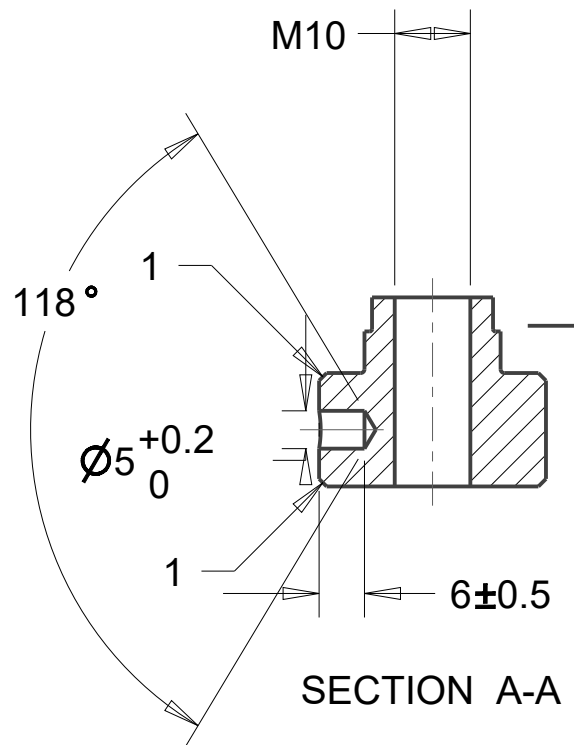
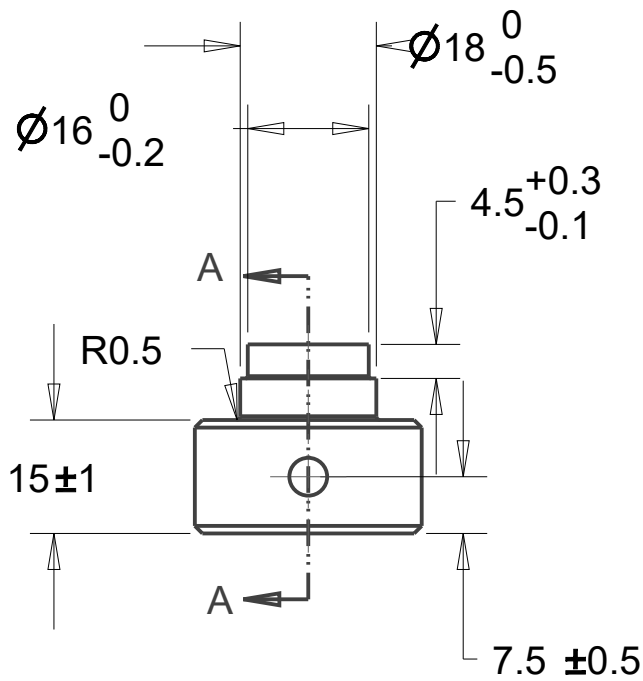
2

3

4



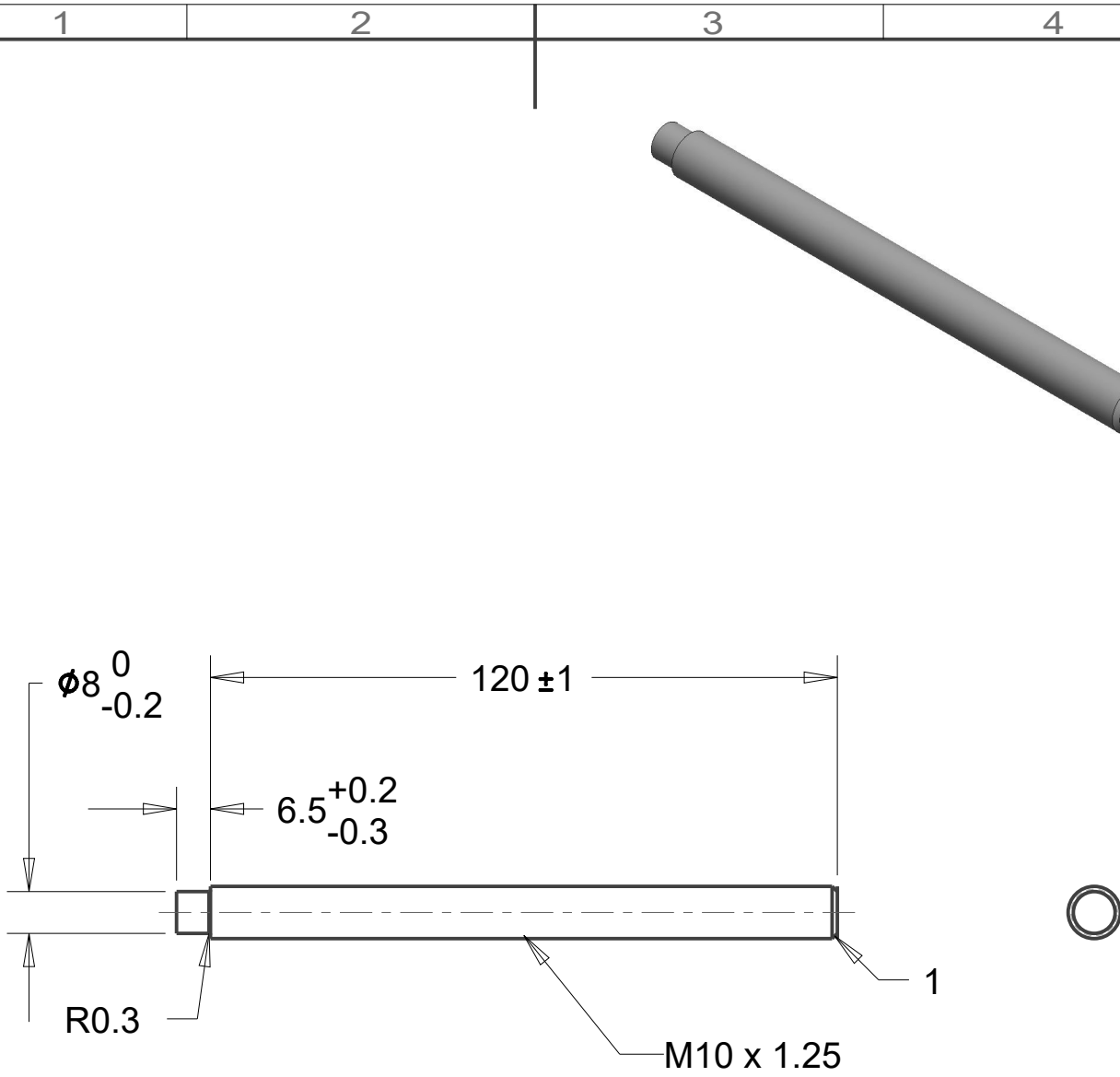
SCALE 1.000



NOTES:

1. BREAK SHARP EDGES.
2. ALL CORNER FILLET R0.4 MAX
3. SURFACE FINISH 3.2 μ m

Roz. -Polot.		mm				Presnost				
		c)	Mater.	STAINLESS STEEL	Tr. odp	Tolerovani				
		b)	C. hm	Hr. hm.						
		a)								
Zmena		Datum	Index	Podpisy	TECHNICKÁ UNIVERZITA V LIBERCI www.tul.cz					
Meritko	Pozn.	Navrhl	Kreslil						GAFARU MORO	
1.000		Prezkousel								
C. seznamu	Technolog									
C. sestavy	Normaliz.									
Stary vykr.	Schvalil									
Novy vykr.	Datum		Apr-24-19							
				Nazev		KNOB				
				Cis. vykresu						
						list 1 listu 1				

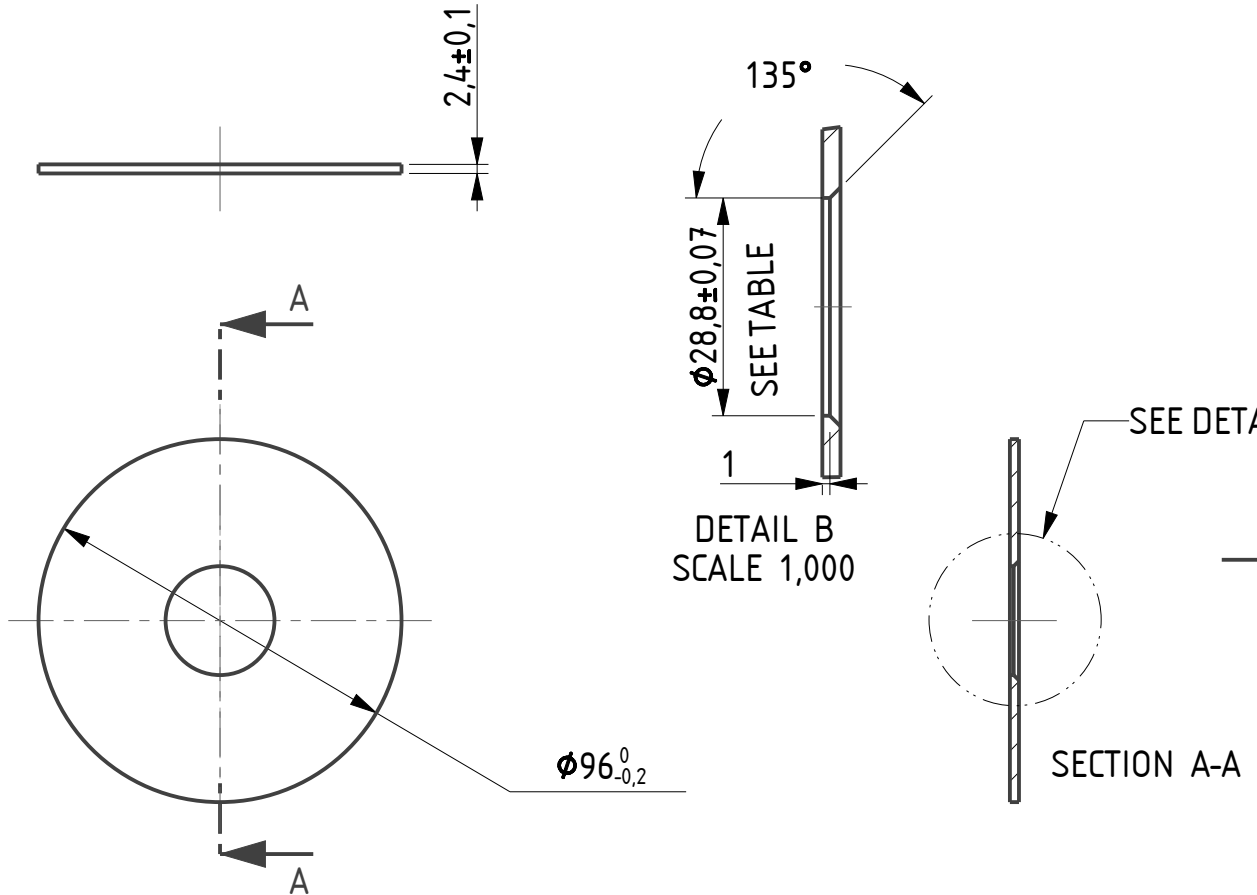
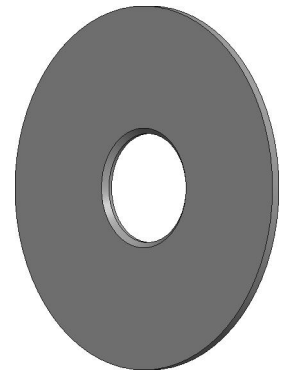


NOTES:

1. BREAK SHARP EDGES.
2. ALL CORNER FILLET R0.4 MAX
3. SURFACE FINISH 3.2 μ m

Roz. - Polot.		mm				Presnost	
		c)	Mater.	STAINLESS STEEL	Tr. odp	Tolerovani	
		b)	C. hm	Hr. hm.			
		a)					
Zmena		Datum	Index	Podpisy	TECHNICKÁ UNIVERZITA V LIBERCI www.tul.cz		
Meritko	Pozn.	Navrhl					
0.750		Kreslil	GAFARU MORO		Nazev MOVING SCREW		
C. seznamu		Prezkousel					
C. sestavy		Technolog			Cis. vykresu		
Stary vykr.		Normaliz.					
Novy vykr.		Schválil			list 1 listu 1		
		Datum	Apr-24-19				

PART NAME	INSIDE DIA.
ORIFICE - 28.8	28.8 ± 0.07
ORIFICE - 32.4	32.4 ± 0.1
ORIFICE - 36.1	36.1 ± 0.1



NOTES:

1. BREAK SHARP EDGES.
2. ALL CORNER FILLET R0.4 MAX
3. SURFACE FINISH $3.2 \mu\text{m}$

Roz. - Polot.		mm				Presnost Tolerovani	
		c)		Mater.	STAINLESS STEEL	Tr. odp	
		b)		C. hm		Hr. hm.	
		a)					
Zmena		Datum	Index	Podpisy	TECHNICKÁ UNIVERZITA V LIBERCI www.tul.cz		
Meritko	Pozn.	Navrhl					
0,500		Kreslil	GAFARU MORO		Nazev ORIFICE PLATE		
C. seznamu		Prezkousel					
C. sestavy		Technolog			Cis. vykresu		
Stary vykr.		Normaliz.					
Novy vykr.		Schvalil			list 1 listu 1		
		Datum	Apr-24-19				

1

2

3

4

A

A

B

B

C

C

D

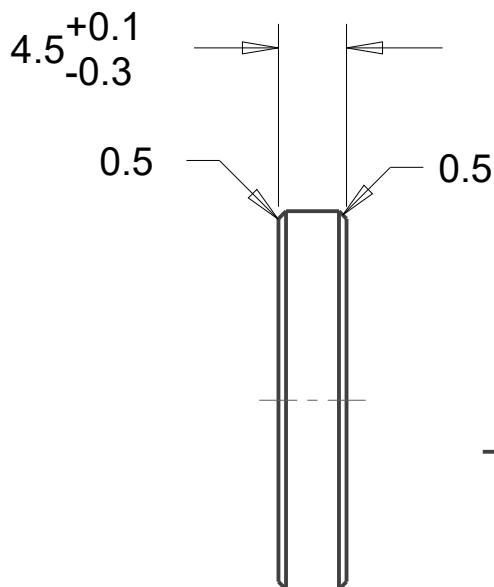
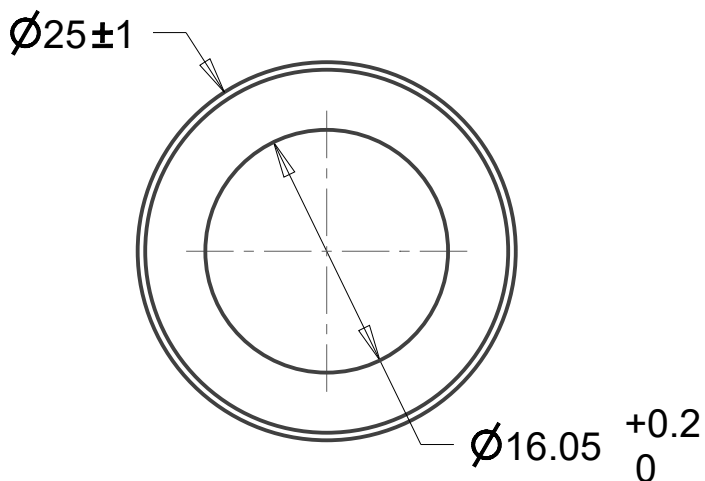
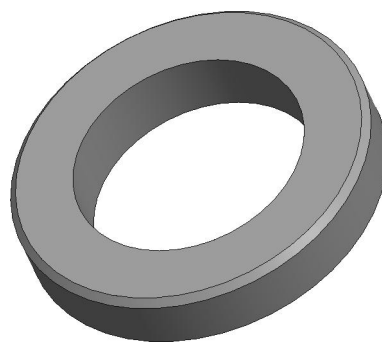
D

E

E


F

F



NOTES:

1. BREAK SHARP EDGES.
2. ALL CORNER FILLET R0.4 MAX
3. SURFACE FINISH 3.2 μm

Roz. -Polot.		mm						Přesnost Tolerovani	
		c)		Mater.	STAINLESS STEEL	Tr. odp			
		b)		C. hm		Hr. hm.			
		a)		 TECHNICKÁ UNIVERZITA V LIBERCI www.tul.cz					
Zmena		Datum	Index						
Meritko	Pozn.	Navrhl			Nazev RETAINING RING				
2.000		Kreslil	GAFARU MORO						
C. seznamu		Prezkoušel			Cis. vykresu				
C. sestavy		Technolog							
Stary vykr.		Normaliz.			list 1 listu 1				
Novy vykr.		Schválil							
		Datum	Apr-24-19						

1

2

3

4

1

2

3

4

A

A

B

B

C

C

D

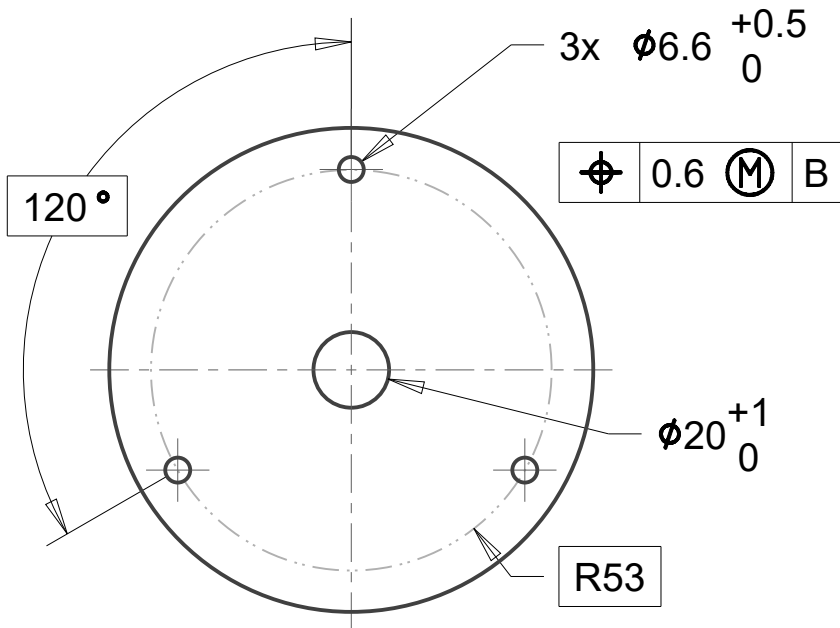
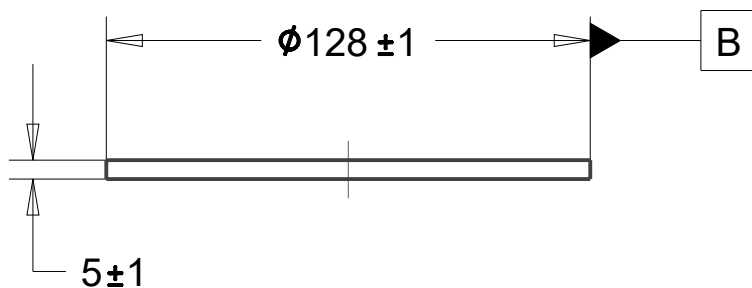
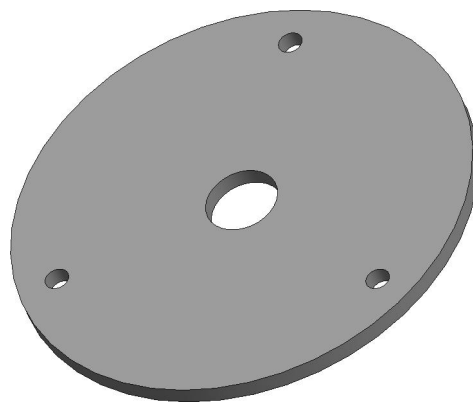
D

E

E

F

F



NOTES:

1. BREAK SHARP EDGES.
2. ALL CORNER FILLET R0.4 MAX
3. SURFACE FINISH 3.2 μm

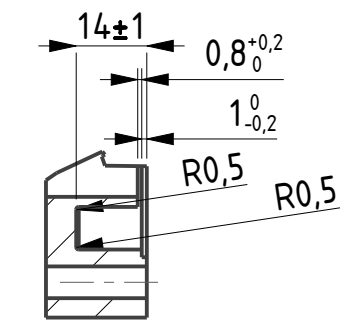
Roz. -Polot.		mm				Přesnost Tolerovani		
		c)	Mater.	STAINLESS STEEL	Tr. odp			
		b)	C. hm	Hr. hm.				
		a)						
Zmena		Datum	Index	Podpisy	TECHNICKÁ UNIVERZITA V LIBERCI www.tul.cz			
Meritko	Pozn.	Navrhl						
0.500		Kreslil	GAFARU MORO					
C. seznamu		Prezkousel						
C. sestavy		Technolog						
Stary vykr.		Normaliz.			Nazev	RIGID PLATE		
Novy vykr.		Schválil			Cis. vykresu			
		Datum	Apr-24-19			list 1 listu 1		

1

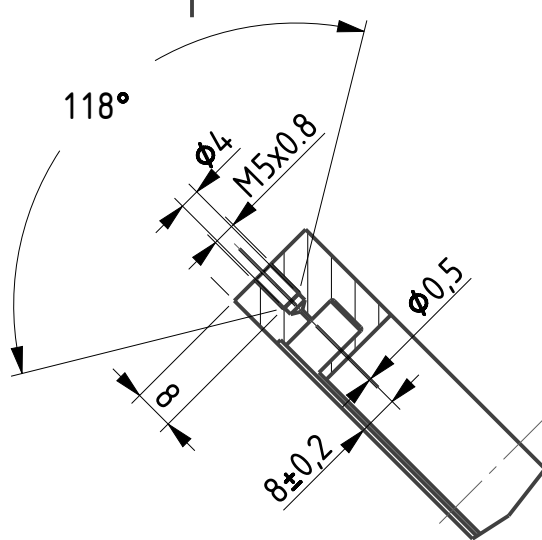
2

3

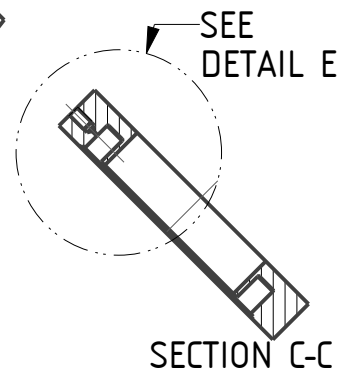
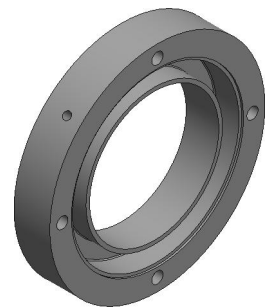
4



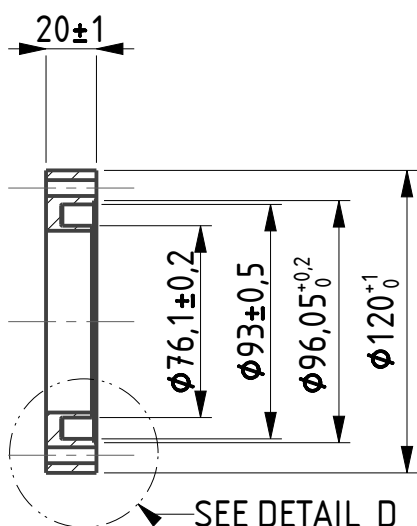
DETAIL D
SCALE 0,667



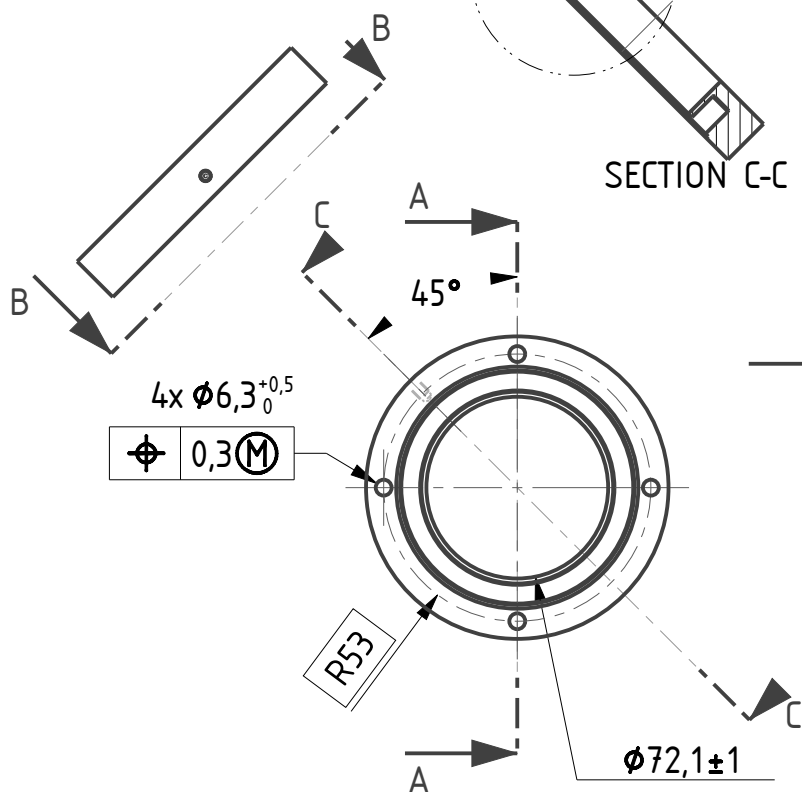
DETAIL E
SCALE 0,667



SECTION C-C



SECTION A-A



NOTES:

1. BREAK SHARP EDGES.
2. ALL CORNER FILLET R0.4 MAX
3. SURFACE FINISH 3.2 μ m

Roz. - Polot.		mm				Presnost Tolerovani	
		c)	Mater.	STAINLESS STEEL	Tr. odp		
		b)	C. hm	Hr. hm.			
Zmena		a)			TECHNICKÁ UNIVERZITA V LIBERCI www.tul.cz		
Meritko	Pozn.	Navrhl					
0,333		Kreslil	GAFARU MORO				
C. seznamu		Prezkousel					
C. sestavy		Technolog					
Stary vykr.		Normaliz.			Nazev	TAPPING SLOT	
Novy vykr.		Schválil			Cis. vykresu		
		Datum	Apr-24-19			list 1	listu 1

1

2

3

4

A

A

B

B

C

C

D

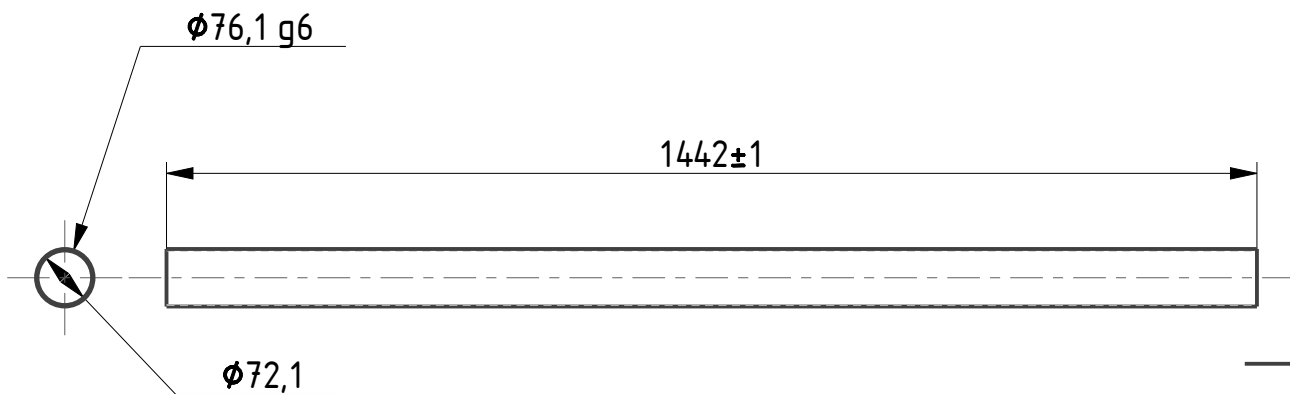
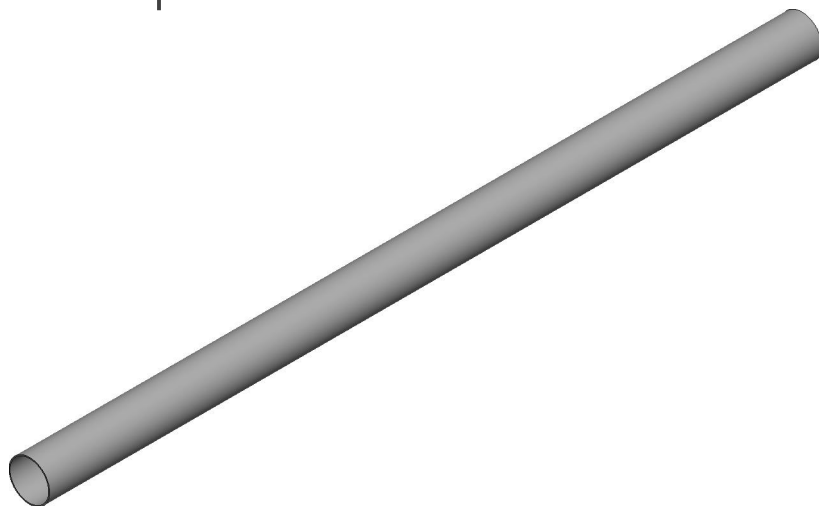
D

E

E

F

F



NOTES:

1. BREAK ALL SHARP EDGES.
2. SURFACE FINISH 3.2 μm

Roz. - Polot.		mm						Presnost	
		c)		Mater.	STAINLESS STEEL	Tr. odp	Tolerovani		
		b)		C. hm		Hr. hm.			
		a)							
Zmena		Datum	Index	Podpisy	TECHNICKÁ UNIVERZITA V LIBERCI www.tul.cz				
Meritko	Pozn.	Navrhl							
0,100		Kreslil	GAFARU MORO		Nazev UPSTREAM PIPE				
C. seznamu		Prezkousel							
C. sestavy		Technolog			Cis. vykresu				
Stary vykr.		Schválil							
Novy vykr.		Datum	Apr-24-19		list 1 listu 1				

1

2

3

4